IN SITU MEASUREMENT
OF THE COEFFICIENT OF MOLECULAR DIFFUSION
IN FINE GRAINED TILL

A Thesis Submitted to the College of

Graduate Studies and Research

In Partial Fulfillment of the Requirements

For the Degree of Master of Science

In the Department of Geological Sciences

University of Saskatchewan

Saskatoon

By

Laura Reifferscheid

Keywords: diffusion, *in situ*, clay, aquitard

Permission to Use

In presenting this thesis in partial fulfillment of the requirements for a Postgraduate degree from the University of Saskatchewan, I agree that the Libraries of this University may make it freely available for inspection. I further agree that permission for copying of this thesis in any manner, in whole or in part, for scholarly purposes may be granted by the professor or professors who supervised my thesis work or, in their absence, by the Head of the Department or the Dean of the College in which my thesis work was done. It is understood that any copying or publication or use of this thesis or parts thereof for financial gain shall not be allowed without my written permission. It is also understood that due recognition shall be given to me and to the University of Saskatchewan in any scholarly use which may be made of any material in my thesis.

Requests for permission to copy or to make other use of material in this thesis in whole or part should be addressed to:

Head of the Department of Geological Sciences

University of Saskatchewan

Saskatoon, Saskatchewan

S7N 5E2

ABSTRACT

Diffusion dominated systems, including naturally occurring aquitards and engineered barrier systems, are important components for long-term waste containment. Diffusive transport can be quantified using the effective coefficient of diffusion (D_e) and the effective porosity (n_e). These are empirical parameters that are commonly measured in a laboratory setting. The purpose of this research was to develop a field-based technique to perform *in situ* measurement of diffusive transport rates. Results from this measurement technique were evaluated by comparison with the results of conventional laboratory testing and back-analysis of a previously determined large-scale field diffusion profile.

In situ diffusion testing was performed on two wells completed in diffusion-dominated zone of a till aquitard. Laboratory diffusion cell tests were conducted on core samples obtained from the screened zones of the diffusion wells. Diffusion testing was completed using conservative isotopes of water as tracers.

A finite element model was used to back-analyze results of laboratory and field experiments to determine the D_e values that best describe each system. Comparison of the field results with the laboratory results obtained from this study as well as previous studies indicate the field system is a useful method for measurement of D_e.

Back-analysis of a previously determined large-scale field deuterium profile for this aquitard showed very precise measurement of D_e is not required for estimation of contaminant transport in thick till aquitard systems. More accurate measurement may be more useful for barrier systems such as clay liners or slurry walls, where the

characteristics of the diffusion-dominated zone are easier to define and the transport path is shorter relative to the transport time.

ACKNOWLEDGMENTS

First and foremost, I would like to acknowledge the support and assistance provided by my supervisors, Dr. Jim Hendry and Dr. Lee Barbour. Their knowledge, patience, and willingness to help was invaluable in the completion of this work.

I would also like to acknowledge the financial assistance provided by the Department of Geology.

A special thank you is extended to Brigitte Boldt-Leppin for her involvement and encouragement throughout this project. Thanks also to Ray Kirkland for facilitating the field portion of this research. The advice and camaraderie provided by my fellow grad students was greatly appreciated.

Finally, I would like to thank my family and friends, especially my husband Kurt, for their patience and understanding throughout this process.

TABLE OF CONTENTS

LIST OF TABLES

LIST OF FIGURES

LIST OF APPENDICES

CHAPTER 1 INTRODUCTION

1.1 Background

The ability of natural or engineered clay barriers to limit contaminant transport has been studied in great detail over the past two decades. Licensing of waste containment facilities which rely on the performance of these barriers requires accurate and long-term estimates of impacts on the environment, especially as the need to store hazardous and radioactive waste has grown.

It is well established that diffusion governs flow both through aquitards (Desaulniers et.al., 1981, 1989; Remenda et.al., 1996; Hendry and Wassenaar, 2000, among others) and through engineered clay liners (Goodall and Quigley, 1977; Crooks and Quigley, 1984; Quigley et.al., 1987; Johnson et.al., 1989). Therefore, understanding contaminant transport for these systems requires a thorough understanding and accurate measurement of the diffusion process. Knowledge of the diffusion process can also be used to evaluate the contamination history of a site (Ball et.al., 1997) as well as the geologic and paleoclimatic history of an area (Remenda et.al., 1996; Hendry and Wassenaar, 1999).

Diffusion rates are typically measured in laboratory tests and several different types of laboratory testing procedures have been developed. Because these test procedures are generally conducted on small samples (i.e. $<100\ cm^3$ (Hendry et.al., 2003)), minor uncertainties in measurements could have a major effect on the determination of diffusion rates. Also, the samples used in these laboratory procedures

are generally disturbed as a result of sampling and sample preparation. In a similar manner to hydraulic transport properties in aquitards such as hydraulic conductivity, it is expected that *in situ* measurements of diffusion would provide more accurate estimates of the diffusion coefficient.

Purpose-designed *in situ* tests to measure the coefficient of diffusion have been conducted in low permeability rock (Phalut et.al., 2003; Vilks et.al., 2003). These have been conducted in specialized facilities at high stress conditions. Application of *in situ* testing to a surficial diffusion-dominated system has not been attempted. A simple system using conventional field equipment would permit easy application to other diffusion dominated geologic media.

1.2 Research Objectives

The main objectives of this research were to (1) develop and apply a field-based method to measure the coefficient of molecular diffusion in a clay-rich aquitard and (2) evaluate the results obtained using this method via comparison to results obtained from conventional lab-scale testing and analysis of a previously obtained field-scale diffusion profile.

These objectives were met by:

1. Designing and executing an *in situ* diffusion test in a well-characterized clay aquitard system;
2. Interpreting the *in situ* diffusion test results and evaluating the impact of test conditions (installation and operation) on the estimates of the coefficient of molecular diffusion; and

3. Comparing the coefficients of diffusion obtained from the conventional laboratory diffusion tests and the *in situ* single reservoir diffusion tests, and evaluating these results through back-analysis of a field-scale profile.

1.3 Organization of Thesis

This thesis is divided into six chapters. Background on the theory of diffusive transport in fine-grained soil systems and a summary of relevant literature is provided in Chapter 2. The literature review focuses on methods used to measure the effective diffusion coefficient in both field and laboratory settings. A discussion of effective porosity as it relates to the effective diffusion coefficient is also included. Chapter 3 provides a description of the laboratory and *in situ* field experiments performed. This includes a description of the field site, the physical apparatuses used, and the procedures employed in conducting the experiments. A description of the numerical modelling program used and the method for determination of best-fit diffusion parameters are also included in this chapter. Presentation and interpretation of results obtained from both the laboratory and field experiments is completed in Chapter 4. Analysis of the laboratory and field data using the numerical modelling program is presented in Chapter 5, along with a discussion of the numerical modelling results. The laboratory and field results are also analyzed with respect to results from previous diffusion studies performed at this site, including a large-scale field profile. Chapter 6 includes a summary of the research, as well as conclusions that can be drawn from this work and recommendations for future work.

Results of an alternative *in situ* test are included in Appendix D, along with a brief description of the apparatus and methodology used.

CHAPTER 2 LITERATURE REVIEW

2.1 Introduction

Molecular diffusion is the dominant transport process in geologic materials where advective transport is limited by very low values of hydraulic conductivity. Diffusive movement is quantified by the effective coefficient of diffusion and the effective porosity. These are empirical parameters that are commonly measured in a laboratory setting. This chapter introduces the theory of diffusion in porous media, including the equations used to describe the diffusion of solutes in soil and the factors affecting diffusion coefficients. A summary of previous research on the measurement of diffusion is also included.

2.2 Transport Processes

2.2.1 Advection Dispersion Model

Evaluation and prediction of the migration of contaminants in groundwater is commonly performed using advection-dispersion dispersion based models. Mass flux is attributed to two physical processes, advection and hydrodynamic dispersion. Advection refers to the movement of the contaminant due to the bulk movement of water. Dispersion is the spreading of the contaminant front as a result of mixing with background groundwater. These processes are mathematically described in the advection-dispersion equation. The one-dimensional form of the advection-dispersion equation for non-reactive, dissolved constituents in saturated, homogeneous, isotropic media is:

$$n_e \frac{\delta C}{\delta t} = D_h n_e \frac{\delta^2 C}{\delta x^2} - v n_e \frac{\delta C}{\delta x} \quad [2.1]$$

where: n_e = effective porosity (L^3L^{-3}),
C = solute concentration in pore fluid (ML^{-3}),
t = time (T),
D_h = coefficient of hydrodynamic dispersion along the flow path (L^2T^{-1}),
x = distance along the flow path (L), and
v = average linear groundwater velocity (LT^{-1}).

In Eq.[2.1],

$$v = q / n_e \quad [2.2]$$

where: q = the Darcy velocity or flux (LT^{-1}).

Hydrodynamic dispersion is the combination of mechanical dispersion and molecular diffusion and can be expressed as:

$$D_h = \alpha_l v + D_e \quad [2.3]$$

where: α_l = dispersivity (L), and
D_e = coefficient of molecular diffusion of a solute in the porous media (L^2T^{-1}).

Mechanical dispersion is described as an 'apparent' spreading of the contaminant front that occurs during advective contaminant transport due to the different groundwater flow paths and velocity variation within and between pores. Molecular diffusion refers to further spreading of a contaminant front that is caused by concentration gradients.

2.2.2 Diffusion Dominated Transport

In the absence of advection, diffusion is often considered to be the dominant contaminant transport process. As advective flow becomes less significant, the average linear groundwater velocity approaches zero and D_h becomes dominated by D_e.

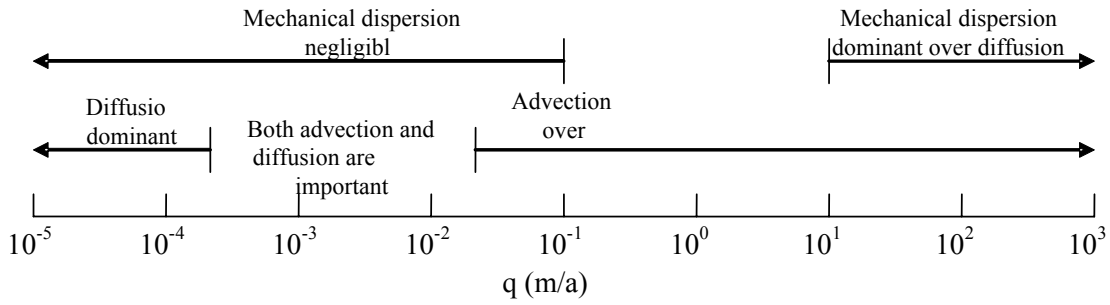

Figure 2-1 Range of Darcy velocities over which diffusion or mechanical dispersion control the coefficient of hydrodynamic dispersion (adapted from Rowe, 1987).

The relative contribution of diffusion and mechanical dispersion to the transport process is commonly expressed in terms of the dimensionless Peclet number (*Pe*).

$$Pe = \frac{vd}{D_e} \qquad [2.4]$$

where: d = characteristic length of the medium (L)

The characteristic length is generally taken as the mean grain-size diameter. At low *Pe* values, molecular diffusion will dominate, while at high *Pe* values mechanical dispersion (D_m) dominates.

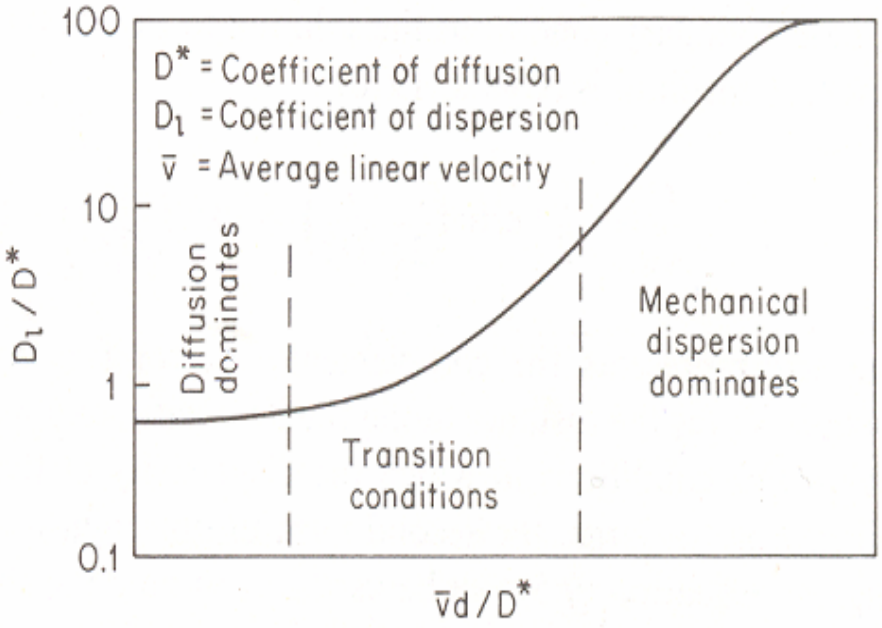

Figure 2-2. Graph of the dimensionless dispersion coefficient versus the Peclet number (adapted from Freeze and Cherry, 1979).

2.3 Theory of Diffusion

2.3.1 Molecular Diffusion

Molecular diffusion is a process whereby dissolved mass is transported from a higher chemical energy state to a lower chemical energy state through random molecular motion (Robinson and Stokes, 1959). Steady-state diffusion of a chemical or chemical species in free solution can be described empirically using Fick's first law (Crank, 1975):

$$J = -D_o \frac{\partial C}{\partial x} \qquad [2.5]$$

where: J = the solute mass flux ($ML^{-2}T^{-1}$),
D_o = the diffusion coefficient of the solute in water (L^2T^{-1}),
C = solution concentration (ML^{-3}),

x = the direction of transport (L), and
$\partial C/\partial x$ = concentration gradient ($ML^{-3}L^{-1}$).

The negative sign in Eq.[2.5] indicates that the net mass flux of contaminant is from areas of high concentration to areas of low concentration.

The rate of molecular diffusion is controlled in part by the frictional force between molecules in solution. Therefore the diffusion coefficient will vary with solution viscosity as well as the size and charge of the ion (Shackleford and Daniel, 1991). Solution viscosity is also dependent on the temperature; therefore diffusion processes are also temperature dependent. The diffusion coefficient of a molecule in solution can be calculated from using the Stokes-Einstein equation:

$$D_o = \frac{k_B T}{6\pi\eta a} \qquad [2.6]$$

where: k_B = Boltzmann constant (L^2MT^{-3}),
T = absolute temperature (^oK),
η = viscosity of the solution ($ML^{-1}T^{-1}$), and
a = hydrated radius of the ion (L).

2.3.2 Diffusion in Soil

Diffusion of a particular element or compound in groundwater requires consideration of the porous media. Solute diffusion is slower in soil than in free solution because the soil particles restrict the fluid filled cross-sectional area, the diffusion pathways for the solute are more tortuous, and other factors attributed to the presence of soil particles.

In a saturated soil system the reduced cross-sectional area for solute movement is accounted for by including the porosity of the medium in Fick's first law:

$$J = -nD_e \frac{\partial C}{\partial x} \qquad [2.7]$$

where: n = soil porosity (L^3L^{-3}), and
D_e = effective diffusion coefficient (L^2T^{-1}).

The partial differential equation describing one-dimensional transient diffusion in a homogeneous, saturated, porous media can be developed from Ficks' first law and conservation of mass. This equation is called Fick's second law and is written as follows:

$$\frac{\partial C}{\partial t} = D_e \frac{\partial^2 C}{\partial x^2} \qquad [2.8]$$

where: $\partial C/\partial t$ = change in concentration with time.

Development of this equation allows cancellation of porosity from the equation, on the assumption that porosity is constant with time and position. In other words, Fick's second law implies that the porosity available for flow and the porosity available for storage are the same, leaving only D_e to be considered. Pearson (1999) examined the relevancy of this assumption by distinguishing between area porosity (the porosity across which diffusion occurs or the porosity through contaminant flux occurs), and the volume porosity (the volume accessible for diffusion or storage porosity). Pearson also acknowledged that the difference between the two may only be relevant in fractured systems.

2.3.3 Effective Porosity

Effective porosity (n_e) is generally defined as the fraction of the total porosity that is accessible for solute movement. Factors such as isolated pores, very small interconnected pores and anion exclusion combine to reduce the pore volume available

for solute flow and storage. Meegoda and Gunasekera (1992) observed ratios of effective to total porosity that varied from 0.31 to 0.84 for different types of clay soils, with high plasticity clays having the lowest values and silty clays the highest. The n_e is considered to be dependent on characteristics of both the soil and the solute. This value varies with the nature of the soil matrix (mineralogy, particle size), the hydrodynamic radius and charge of the solute, as well as the soil/solute interactions. Effective porosity is more difficult to quantify than total porosity as it is not necessarily a singular value independent of solute concentration or speciation (Peyton et.al., 1985). Further, n_e is often assumed to equal total porosity because of the inability to measure the parameter independently, sometimes with disastrous results (Horton et.al., 1985).

Measurement of n_e has been attempted using both direct and indirect methods. Direct measurement methods include mercury porosimetry (Horton et.al., 1985) and steric exclusion chromatography (Peyton et. al, 1985). Indirect methods are more commonly and effectively used, allowing the calculation of n_e from field or laboratory tracer tests in conjunction with measurements of D_e (van der Kamp et.al, 1996; Meegoda and Gunasekera, 1992). In hydrogeology, it is common to estimate n_e based on available literature or personal experience (Stephens et.al., 1998).

For the stable isotopes of water, an n_e equal to the total soil porosity has been determined for clay till material (Hendry and Wassenaar, 1999; van der Kamp et.al., 1996).

2.3.4 Effective Diffusion Coefficient

The D_e is not consistently defined in literature (Shackelford, 1991). When obtaining diffusion values from the literature, it is often difficult to determine which

value is actually reported unless the form of Fick's first law being used is clearly stated. Some authors combine the porosity and D_e terms into the diffusion coefficient while others retain the separation as shown in Eq.[2.8].

In fine-textured materials, the diffusion coefficient can be affected by anion exclusion and the diffusion of ions in the adsorbed phase (Kemper, 1960; van Schaik et.al., 1966; van Schaik and Kemper, 1966). Various terms have been included in the definition of D_e to account for different factors assumed to influence diffusion in soil:

$$D_e = D_o \alpha \gamma \tau \qquad [2.9]$$

where: α = fluidity factor,
γ = the effect of anion exclusion, and
τ = tortuosity factor.

The fluidity factor, α, accounts for the increased viscosity of the water adjacent to the clay mineral surfaces relative to that of the bulk water. Anion exclusion, γ, can result when clay particles are squeezed so close together that the movement of anions between the negatively charged particles is restricted by electrostatic repulsion. Tortuosity, τ, refers to the fact that the actual distance a solute travels in a soil system is larger than the straight line travel distance, due to the presence of soil particles. None of these factors can be measured independently, making it necessary to specifically measure a diffusion coefficient for each new solute in each new soil system.

Shackelford and Daniel (1991) accounts for these soil characteristics by including an apparent tortuosity factor (τ_a) in the definition of D_e :

$$D_e = D_o \tau_a \qquad [2.10]$$

Typical values of τ_a are <1.

2.4 Measurement of the Effective Diffusion Coefficient

Numerous studies on diffusion have focused on the development and evaluation of laboratory tests and the examination of *in situ* diffusion profiles to determine diffusion parameters (D_e and n_e). These studies have considered a wide range of both organic and inorganic solutes.

2.4.1 Laboratory Methods

Laboratory test methods for the measurement of D_e are commonly of two types; transient and steady state. Common transient laboratory tests include half-cell methods, column tests with advection, and reservoir methods. Typically, the method of measurement is chosen based on what method best represents field conditions and the amount of information that is required (i.e. how many unknown parameters). The D_e is then back calculated from a best-fit curve generated using Fick's first law (for steady-state methods) or Fick's second law (for transient methods). Analytical (Shackleford, 1991), semi-analytical (POLLUTE, Rowe and Booker, 1997) and numerical solutions are available for these diffusion equations.

The half-cell method involves the preparation of two half-cells of soil. One of these half-cells is spiked with a solute and the half-cells are the pressed together and allowed to diffuse for some time (Figure 2-3). The cells are then separated and the soil is sectioned and the concentration of solute in each section is measured to provide a concentration profile within the soil (Li and Gregory, 1974). Adequate contact and ensuring uniform soil conditions (i.e. porosity, water content, density) in the two half cells may be difficult to achieve. Additional error may be introduced during core extraction and sectioning (van Reese, 1991).

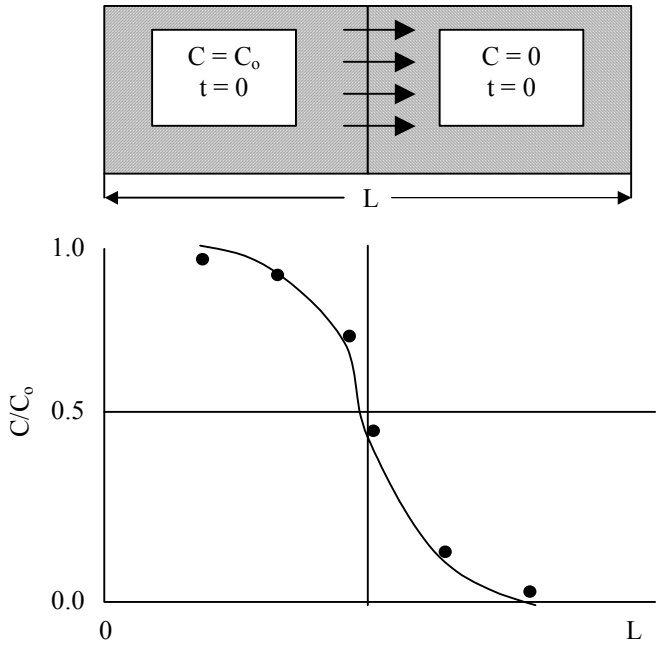

Figure 2-3 Schematic of half-cell method and example of soil concentration profile results. Arrows indicate direction of diffusion, circles represent measured data, line is theoretical fit of data (adapted from Shackelford, 1991).

Column methods involve establishing steady-state advective flow through a column of porous media. After steady-state flow has been established, the influent solution is spiked with the solute of interest. The concentration of the effluent solution is then monitored with time. These tests can be performed by either maintaining a constant influent concentration or by introducing only an initial spike to the source solution and allowing the concentration to decrease with time. Monitoring the decreasing source concentration with time results in the development of an additional independent set of data, which can be used to estimate one additional transport parameter such as porosity or the adsorption coefficient for retarded solutes. These tests are useful for representing field conditions where advective flow is expected. In low permeability clays, establishing steady-state advective flow may require a

considerable amount of time. Definition of the D_e from these tests requires knowledge of the soil mechanical dispersivity.

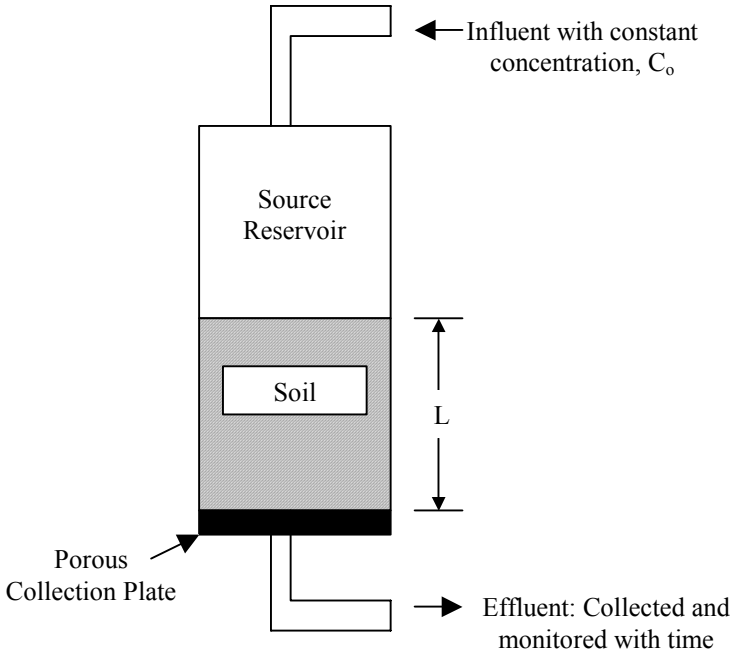

Figure 2-4 Schematic of column test with constant source concentration (adapted from Shackelford, 1991).

Reservoir methods do not require the establishment of steady-state conditions, making the tests relatively quick and easy to perform (Shackleford, 1991; Van Rees et.al., 1991). The design of a reservoir laboratory experiment varies with the number of reservoirs as well as the method of spiking. Single reservoir methods include a reservoir of water exposed to a column of soil. The reservoir of water is spiked and allowed to diffuse into the soil column. As in the column tests, the source reservoir can be maintained at a constant concentration or allowed to decrease with time. A variation of this method involves spiking the soil column and monitoring the diffusion of the

tracer from the soil into the water reservoir over time. The soil can be sectioned and the pore water analyzed upon completion of the test.

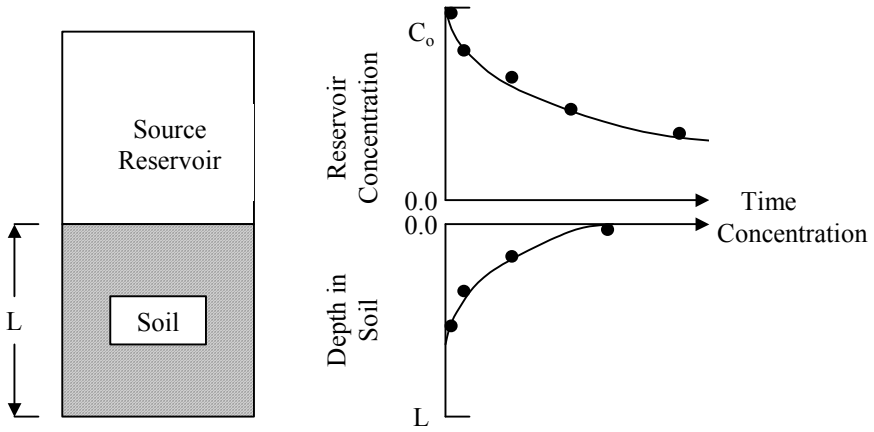

Figure 2-5 Schematic of single reservoir method with decreasing source concentration. Hypothetical graph shows measured (circles) and theoretical (solid line) concentrations in the source reservoir solution and soil (adapted from Shackelford, 1991).

A variation of the single reservoir method is the radial diffusion cell method (Novakowski and van der Kamp, 1996; van der Kamp et.al., 1996). This method involves drilling a hole along the axis of a cylindrical soil sample to create a central reservoir. The change of concentration in the reservoir with time is monitored. The D_e and n_e can then be determined by fitting a semi-analytical model to the measured data (Novakowski and van der Kamp, 1996).

This method minimizes the disturbance of the soil sample and provides for independent measured of the D_e and n_e without requiring sectioning of the soil sample at the completion of the experiment. Measurement of n_e requires equilibration of the reservoir with the pore water of the soil, but the geometry of the radial diffusion cell allows short equilibration times without the use of excessively small samples.

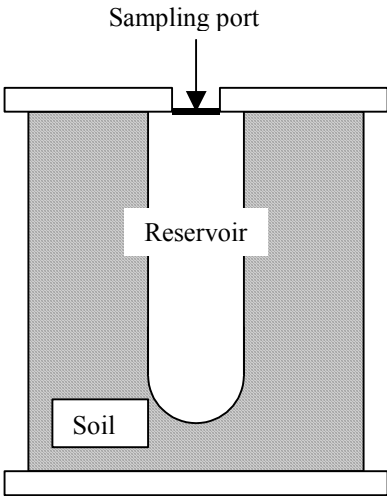

Figure 2-6 Schematic of radial diffusion cell (adapted from van der Kamp et.al., 1996).

The double reservoir diffusion test is essentially the same as the single reservoir diffusion test with the addition of a collection reservoir at the opposite end of the soil column to the source reservoir. The source solution concentration can be either maintained at constant or allowed to decrease with time. The concentration of the lower reservoir is monitored with time. The double reservoir diffusion test requires solute transport through the length of the soil column so may require more time than the single reservoir test, especially when considering retarded solutes. For conservative solutes, the double reservoir tests provide two independent concentration curves without requiring sectioning of the soil sample. If diffusion is allowed continued until the source and lower reservoir are at constant concentrations the effective porosity of the soil column can also be estimated from mass balance. Mixing of the reservoirs must be performed to prevent stratification over the course of the experiment.

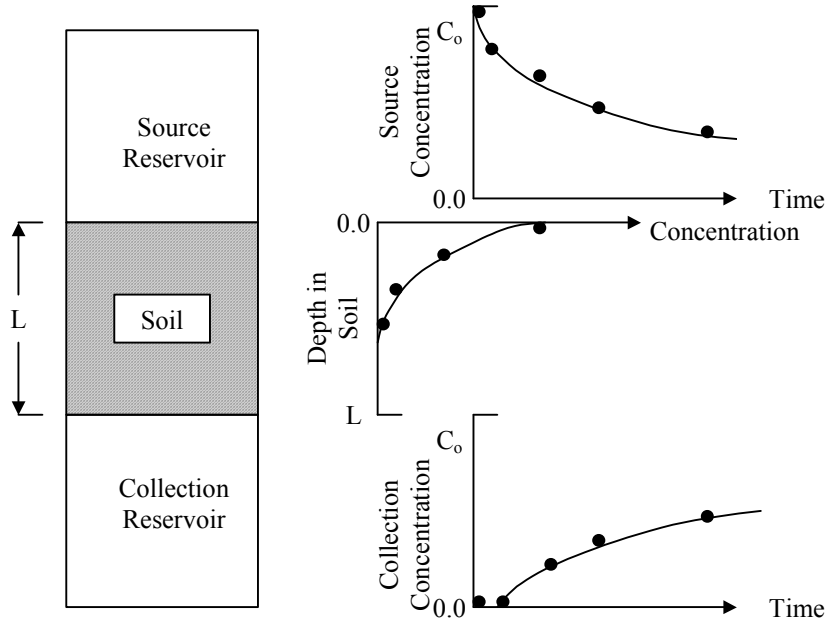

Figure 2-7 Schematic of double reservoir diffusion method with decreasing source concentration. Hypothetical graph shows measured (circles) and theoretical (solid line) concentrations in the reservoir solutions and soil (adapted from Shackelford, 1991).

In general, laboratory tests are conducted on relatively small specimens (i.e. approximately 400 cm^3 (Hendry and Wassenaar, 1999); <100 cm^3 (Hendry et.al., 2003)) for a short duration. Small uncertainties in the measurement of solute mass could have a significant effect on the determination of diffusion parameters. Other concerns with application of laboratory testing to field conditions include the disturbed nature of the tested soil (soil is cut to size and rewetted to field specifications), as well as potential changes in the pore network of the soil due to removal from *in situ* stress conditions (Hendry et. al., 2003).

2.4.2 Field Methods

Field studies have been performed to examine *in situ* diffusive transport through low permeability media. Contaminant profiles established from pore water samples from beneath an established contamination source have used to analyze *in situ* diffusion

rates (Goodall and Quigley, 1977; Quigley and Rowe, 1986; Johnson et.al., 1989; King et.al., 1993; Liu and Ball, 1999). The natural diffusion profiles formed by long-term mixing of groundwater with different tracer signatures have been used to study transport in low-permeability media (Desaulniers, et.al., 1981; Remenda et. al., 1994, 1996; Hendry and Wassenaar, 1999). *In situ* tests to examine diffusion in porous rock have also been performed (Phalut et.al., 2003; Vilks et.al., 2003).

Examination of contaminant movement through compacted clay liners at established landfill sites has driven much of the field examination of diffusion (Shackelford, 1991). Most of these studies use laboratory testing to determine values of D_e (i.e. Barone et.al., 1989), though some field profiles have been back-analyzed to determine D_e (Johnson et.al, 1989). The usefulness of these profiles for estimation of D_e is dependent on the accuracy of other system unknowns such as the chronology of source concentrations. Because these profiles examine solute diffusion in response to high ionic strength source leachate, D_e values may reflect electrochemical interactions between dissolved species (Barone et.al., 1989).

Solute profiles through Pleistocene-age aquitards are considered useful for determining D_e values on a field scale (Desaulniers et.al., 1981; Remenda et.al., 1994, 1996; Hendry and Wassenaar, 1999). The groundwater residence times in these deposits is long, preserving the characteristic chemical signature of the water incorporated in the sediments at the time of deposition. The relatively rapid change in climatic conditions that is reported to have occurred at the end of the Pleistocene (10 to 12 ka before present) can be correlated to a change in the isotopic signature of the recharging porewater (i.e. rainwater) to the system (Sauchyn, 1990; Greenland Ice-Core Project

Members, 1993). The mixing of this water with connate water produces characteristic profiles that can be used to infer information on the age and / or transport parameters of the deposit. These profiles are usually used to obtain information on depositional history or advective movement rather than determine diffusive transport rates.

Experiments conducted specifically to obtain field measurements of D_e have been performed to evaluate the suitability of low permeability rock for high-level radioactive waste containment. The performance of both granite (Vilks et.al., 2003) and argillaceous rock (Phalut et.al, 2003) have been considered. Both of these experiments involved the injection of tracers into boreholes. Overcoring of the boreholes was performed after specified time periods and the porewater in the recovered material was analyzed for tracer concentrations. Phalut (2003) also monitored decreasing tracer concentration with time in the borehole source solution.

Evidence of a disturbed zone immediately surrounding the borehole was identified at both sites. Phalut (2003) observed that data from borehole monitoring yielded a greater D_e than those obtained from analysis of the tracer profiles and attributed the difference to the presence of the disturbed zone with a higher D_e close to the borehole wall. Vilks (2003) had to include a zone of decreased D_e adjacent to the borehole wall to produce modelling results that fit measured solute profiles.

Vilks (2003) also observed that laboratory estimates of D_e for a conservative iodide tracer ranged from $2.3 – 2.7 \times 10^{-12}$ m^2/s, greater than those obtained from *in situ* experiments (2.1×10^{-14} to 1.9×10^{-13} m^2/s). The higher values of D_e determined from laboratory experiments were attributed to alteration of the granite rock sample due to removal from high-stress *in situ* conditions.

2.5 Summary

The process of diffusion in geologic material can be described through measurement of the empirical factors of D_e and n_e. These values are dependant both on the material and the solute of interest. Determination of these parameters is typically completed through performance of laboratory tests.

Field studies of ion and isotope profiles have been used to examine the diffusion process. The usefulness of these profiles for determination of D_e is dependent on the accuracy of other unknowns in the system being studied. These include the source concentration or time of development. As these factors often have considerable uncertainty, the focus of these field studies is not typically to estimate D_e

Field experiments designed for the purpose of measuring D_e have been performed in low permeability rock at high stress environments. These experiments have been conducted at highly specialized research facilities and analysis required the destruction of the testing apparatus after completion of the experiment.

CHAPTER 3 MATERIALS AND METHODS

This chapter describes the methodology used for the laboratory and field experiments performed as part of this study. The step-by-step methodology for the spiking and sampling procedure used during the field experiment is included in Appendix A.

3.1 Site Information

The field diffusion testing experiment was performed at the King site, a thick, clay-rich (39% sand, 26% silt, and 35% clay) till aquitard located near Birsay, Saskatchewan, about 140 km south of Saskatoon, Canada (51.05^{o}N latitude, 106.5^{o}W longitude). The aquitard consists of approximately 80m of late Quaternary Battleford till. The clay fraction mainly consists of smectite (50-60%) with lesser amounts of illite (5-15%) (Hendry and Wassenaar, 2000). The till is underlain by 77m of massive, plastic Cretaceous clay (5% sand, 38% silt, and 57% clay), the Snakebite member of the Bearpaw Formation. The clay is in turn underlain by a regionally extensive sand aquifer, the Ardkenneth member of the Bearpaw Formation. The regional direction of groundwater flow in this area is downward through the till and Snakebite Member into the Ardkenneth aquifer (van der Kamp and Jaworski, 1989).

The King site was selected for study because the hydrogeology is well constrained and solute transport in the till has been shown to be dominated by diffusion. Depth to the water table ranges from 2.2 m below ground during the winter to ground surface during spring snowmelt. The upper 3 to 4 m of the till is weathered and

oxidized, creating a dynamic flow environment. Below this, the till is unoxidized and unfractured, resulting in extremely slow water movement. Shaw and Hendry (1998), and Boldt-Leppin and Hendry (2003) performed extensive lab and field hydraulic conductivity (K) testing on the till. They determined that the K of the unoxidized till is 2.7×10^{-11} m/s to 6.0×10^{-11} m/s. Using hydraulic data, Shaw and Hendry (1998) calculated a downward groundwater velocity of 0.5 to 0.8 m per 10ka. Modelling of isotope profiles of the water molecules throughout the thickness of the aquitard also indicated a downward velocity of <1m per 10ka (Hendry and Wassenaar, 2000). These studies, along with examinations of the dissolved chloride (Hendry and Wassenaar, 1999), other solute profiles (Hendry and Wassenaar, 2000), radiogenic carbon analyses of dissolved inorganic carbon (Wassenaar and Hendry, 2000), and radiogenic carbon analyses of dissolved organic carbon (Hendry et al., 2003) clearly showed that solute transport in the unoxidized till is dominated by diffusive transport. Measurements of D_e and n_e for deuterium in the till were determined by Hendry and Wassenaar (1999) using the radial diffusion method of Novakowski and van der Kamp (1996). They reported a D_e of 1.7×10^{-10} m^2 s^{-1} and an n_e equal to the total porosity.

3.2 Laboratory Diffusion Testing

Laboratory diffusion measurements were performed using double-reservoir diffusion cells. This method allows for the simultaneous determination of two independent concentration curves. All equipment required for testing was readily available.

3.2.1 Materials

Six double-reservoir diffusion cell tests were conducted on core samples collected from the intake zones of each diffusion well (two from each of BD45-A, BD45-B, and BD45-C) to determine D_e and n_e of the till with respect to the stable isotopes of water. The diffusion cells were constructed from stainless steel and consisted of two sections (see Figure 3-1). One section contained the source reservoir (volume = 96 cm^3) and the core sample holder (diameter = 64 mm, height = 20 mm). The other section consisted of the collection reservoir (volume = 128 cm^3). Volumes of source and collection reservoirs were decreased to allow quicker equilibration times. To minimize the effects of sampling, the reservoir volumes were maintained such that the total sample volume removed was < 1% of the total reservoir volume. The physical adjustments of the source and collection reservoirs were completed using Teflon plugs and 5mm Pyrex beads (Corning Incorporated).

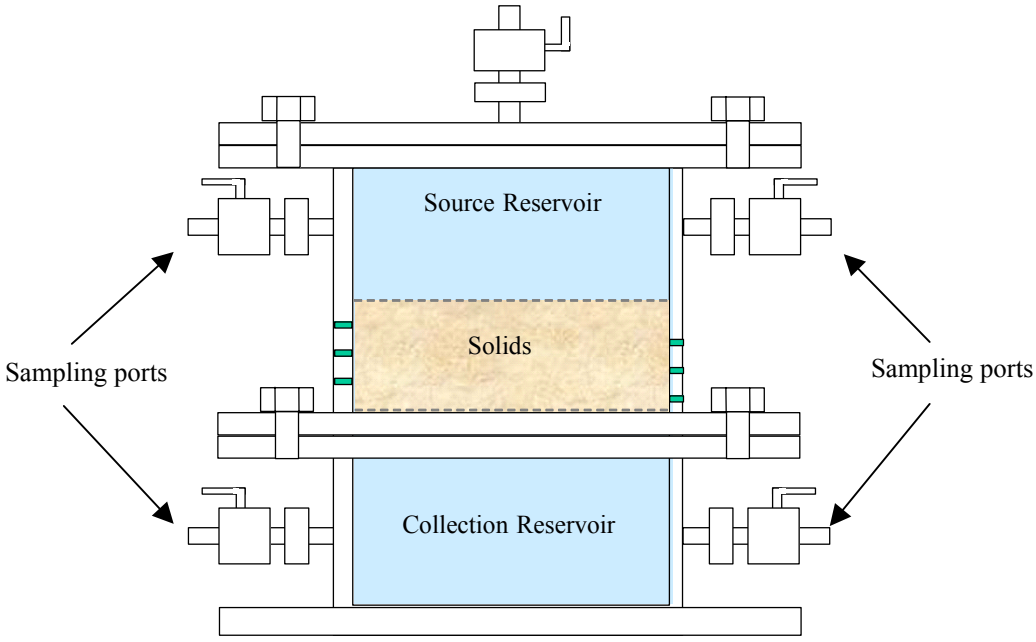

Figure 3-1. Schematic cross-section of double reservoir diffusion cell (adapted from Donahue, 1999).

Oxygen-18 and deuterium ($\delta^{18}O$ and δD) were used as tracers. These are stable isotopes that naturally occur in water. These isotopes are conservative, meaning that their movement is unlikely to be affected by interactions with the soil below approximately 50^{o}C (Lawrence and Taylor, 1972).

3.2.2 Methods

These diffusion cells consist of a reservoir on either side of a soil sample (Figure 3-1). The soil was obtained by taking subcores from the Shelby tube core samples taken at the intake zone of the field wells (described in more detail in Section 3.3.1.1, below). Each subcore sample was saturated with groundwater collected from an onsite piezometer completed at approximately 13.5 m depth. Saturation was performed by first placing the samples in a triaxial permeameter under vacuum (82 kPa) for 4 hours then placing the samples under inflow and outflow pressures of 70 kPa and a confining pressure of 82 kPa for three days. A 20mm thick slice was then removed from the subcore sample and trimmed to a slightly larger diameter than the diffusion cell. The sub-sample was then pushed into place to ensure no preferential pathways existed around the perimeter of the sample.

The diffusion cell reservoirs were filled with the same groundwater used to saturate the soil sample. The source reservoir was then spiked with the same oxygen-18 and deuterium that was used to spike the field diffusion wells.

Testing of all cells commenced on May 16, 2002 at 20:30 (time zero). Immediately after filling and spiking the reservoirs, the cells were placed horizontally to minimize advective movement and ensure good contact between the soil and the

reservoir liquid. All tests were conducted at approximately 5°C to simulate *in situ* groundwater temperatures (Hendry and Wassenaar, 2000).

Sampling was conducted on an increasing time scale (see Appendix B). Reservoir sampling was conducted to minimize the introduction of air into the reservoirs and changing the volume as described by Donahue (1999). Samples were taken through the sampling ports using small volume syringes. A 1mL sample was removed through a port on one side of the cell, while 1mL of the original reservoir solution was simultaneously added through a port on the opposite side. Both source and collection reservoirs were sampled in the same manner.

At the end of the experiment, the diffusion cells were dismantled. The soil cores were retrieved and sectioned into 4 – 5 slices per core. The n of each subsample was calculated based on the measured volume and gravimetric water content of each slice.

An additional test was also conducted using a single reservoir diffusion cell. This cell was set up in the same manner as the double reservoir tests and sampled on the same time scale. The reservoir was filled with the same spiked solution that was used to fill the source reservoirs of the double reservoir diffusion cell tests and functioned as a control sample.

3.3 *In situ* Diffusion Testing

3.3.1 Materials

3.3.1.1 Well Design and Installation

In situ testing to determine D_e and n_e in the unoxidized till was performed on two wells (referred to as BD45-A and BD45-C) that were installed on August 8 and 9, 2001, respectively. A third well (referred to as BD45-B) was also installed at this time

using the same construction methods and materials described above. This well was also used for diffusion testing but used a different methodology (see Appendix D). The three wells were installed in a row, starting with BD45-A and ending with 45-C, each separated by approximately 10 m. To ensure that the solute transport was dominated by diffusion and not impacted by the transition between the oxidized and unoxidized zones, the base of the three piezometers were completed in the unfractured, unoxidized zone of the aquitard at 15.58, 13.30 and 13.43 m below ground surface for the BD45-A, -B, and -C wells.

All boreholes were drilled to 12.0 mbgs using a 0.15 m diameter solid stem auger drill. A 1.5 m long x 76 mm OD Shelby tube was then pushed to the completion depth of each borehole. Once the Shelby tubes were removed from the boreholes, the ends were waxed and they were stored at 15^{o}C and 80% relative humidity until lab testing (about 7 months). All boreholes remained dry during and immediately after drilling, thus underscoring the low K of the formation and indicating that no permeable seams or layers were encountered during drilling.

The construction of all three piezometers was identical. The intake zones were constructed from 0.478 m long x 77 mm OD US Filter / Johnson stainless steel continuous-slot screen (1.02 mm slot size 40% open area). The screen consisted of 24 stainless steel support rods wrapped with triangular wire. The bottoms of the screens were capped with 20 mm thick stainless steel plates and the tops of the screens were attached to a 1.07 m long x 77 mm OD stainless steel riser pipes. The riser pipes were attached to 63.5 mm ID PVC pipes, which extended 0.75 m above ground surface. The tops of the PVC pipes were fitted with vented caps. Once constructed, the piezometers

were pushed into the open boreholes using the drill rig. Because the screen and stainless riser pipe had the same OD as the Shelby tube used to complete the borehole, direct connection between the screen and the stainless riser pipe and the till was ensured. The expanding nature of the clay further ensured a tight seal between the till and the screen and the lower 0.36 – 0.62 m of the stainless steel riser pipes. This was evidenced by the bulging of the till through the open area of the screen, viewed with a downhole camera on November 27, 2002, 475 days after installation (data not presented). To further minimize vertical migration of the conservative tracer along the piezometer, the lower 0.15 m of the annular space between the till and the piezometer was filled with 6 mm diameter bentonite pellets and the remainder of the annular space was then filled with bentonite chips. To complete the installations, the standpipes were topped with vented caps. For protection, steel casings were placed over the piezometers, 1 m x 1 m x 0.15 m thick concrete pads were poured around the steel casings, and they were fitted with locking steel caps.

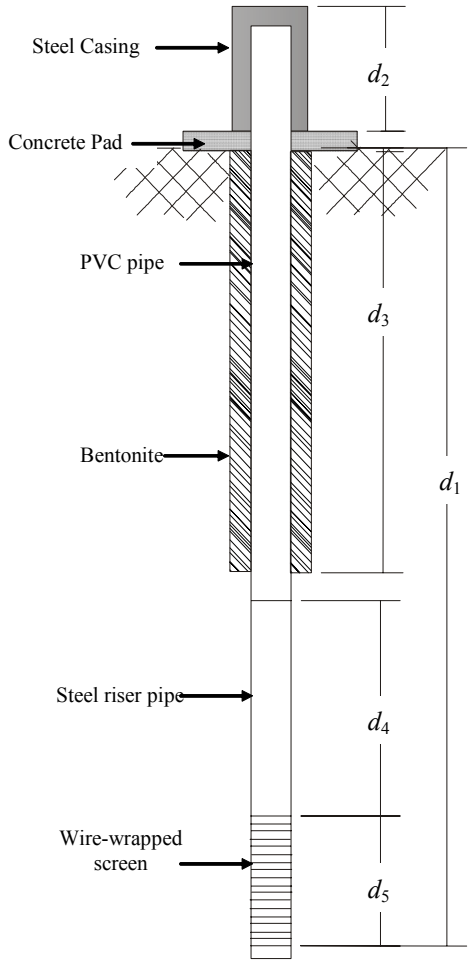

Dimension	Measurement (m)	
	BD45-A	**BD45-C**
d_1	15.44	13.291
d_2	0.963	0.963
d_3	12.0	12.0
d_4	1.07	1.07
d_5	0.478	0.478

Figure 3-2 Schematic of diffusion well installation. Drawing not to scale.

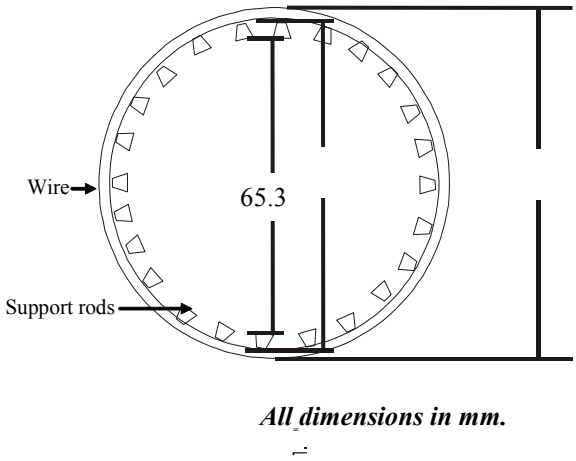

Figure 3-3 Schematic cross-section of well screen. Drawing not to scale.

3.3.1.2 Packer Systems

Purpose-built packer systems were installed in BD45-A and BD45-C to isolate a known volume of groundwater beneath the packer (the reservoir) while allowing for spiking and sampling of this reservoir. Each system consisted of a borehole packer, a pressure transducer, and two water lines. A steel cable was used for lowering the packers into place and a copper tube was used for inflating the packer. The borehole packers (RST Instruments, Model N) were constructed from an inflatable rubber gland with one fixed and one sliding head attached to a hollow stainless steel center shaft. Three stainless steel lines (two 3.175 mm ID and one 1.59 mm ID) ran through the center of the shafts. Pressure transducers (Omega PX437 – 030GI; 0 to 21.09 mH_2O, 0.10% FS accuracy) were attached to the 1.59 mm ID line with stainless steel compression fittings. Pressure measurements from the transducers were stored every hour using a Campbell Scientific CR10X datalogger until July 19, 2002 after which readings were stored every six hours. These readings were used to measure the change in static water level with time for each well. Water lines were constructed by attaching

approximately 14 m of 6.4 mm ID polyethylene tubing to each of the 3.175 mm ID lines using stainless steel compression fittings. The polyethylene tubing was connected to peristaltic pumps to facilitate mixing, spiking and sampling of the isolated reservoir (discussed in Section 3.3.2; Figure 3-5). One water line was extended approximately 38 cm past the bottom of the center shaft of the packer system, while the other was only 5 cm longer than the center shaft (Figure 3-4). This length difference facilitated reservoir mixing in the packed off portion of the wells, decreasing the possibility for short-circuiting within the reservoirs.

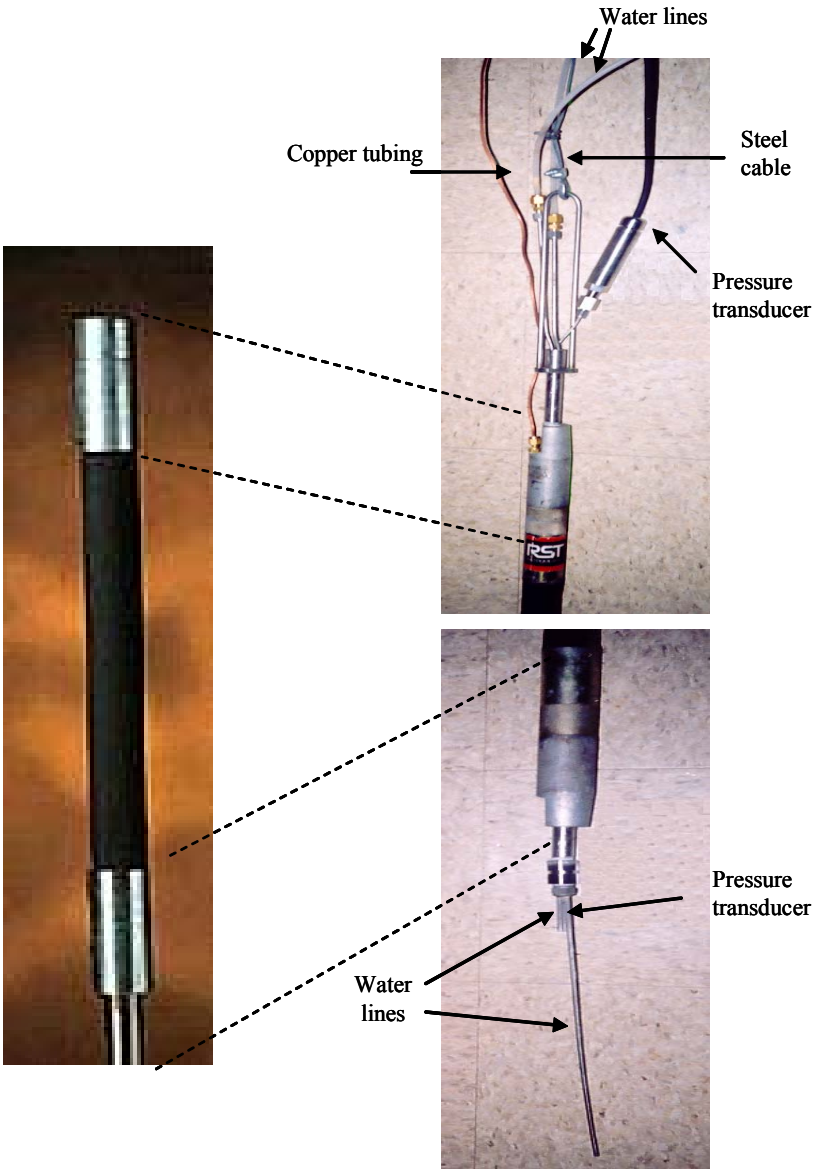

Figure 3-4. Packer system for isolating, spiking and sampling diffusion well reservoirs.

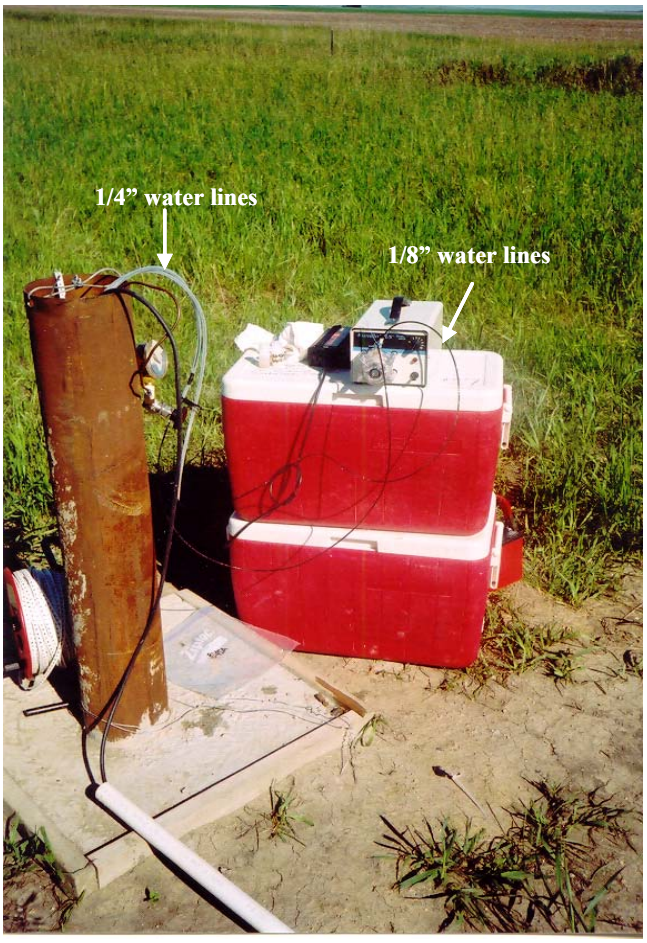

Figure 3-5. Peristaltic pump and water lines used for spiking and sampling diffusion well reservoirs.

3.3.2 Methods

The water levels in the well were allowed to recover for approximately nine months. This ensured enough water was contained in the wells to allow an adequate volume of formation pore water for spiking and monitoring, and to ensure that the packer systems were submerged within the standing water column. During those nine months, monthly water-level recovery measurements were made on all three wells using a downhole water level tape. Water samples were also collected for background isotope analyses on a monthly basis. The monthly water level in BD45-B was monitored for

679 days. Water level data from all wells were used to determine *K* values for the till using the Hvorslev (1951) method.

The packer systems were installed on June 21, 2003 (well BD45-C) and July 3, 2002 (well BD45-A). Both were placed so the longest water lines were positioned approximately 5 cm from the bottom of the wells. This provided the isolation of approximately 2.6 liters of formation water in the reservoirs. The packer systems were lowered on steel cable to the desired depth and inflated with nitrogen gas through a copper tube to a pressure of approximately 1400 kPa, above the minimum pressure required to keep the packer in place (1170 kPa) but below the maximum unconfined working pressure (2448 kPa). This allowed for some loss of pressure in the systems due to settling or possible leakage.

After the packer systems were installed, the systems were allowed to equilibrate for two weeks, allowing water levels to attain static values (verified with the transducer measurements). *In situ* water was added to the polyethylene tubing in well BD45-A to ensure that recovery would be completed as quickly as possible. On July 3, 2002 (well BD45-C) and July 11, 2002 (well BD45-A) the reservoirs were spiked with the conservative tracers $\delta^{18}O$ and δD (time zero). The tracers were incorporated into the packed off reservoirs by mixing the spiking solution into the reservoirs. This solution was created by adding 210 μL (BD45-A) or 200 μL (BD45-C) each of oxygen-18 (95 atom % ^{18}O, Aldrich Chemical Company) and deuterium-enriched water (99.9 atom % D, Aldrich Chemical Company) to 200 mL of groundwater collected from the piezometers. This volume of spiked groundwater was then introduced into the isolated reservoir using the pump system. One of the criteria of the testing was to neither add

nor remove water from the system (and potentially induce advective transport). As a result, 200 mL of water was removed from the systems at the end of the spiking procedure. These samples, which were assumed to be at the same chemical composition as the reservoirs at time zero, served as volume replacement during subsequent sampling episodes.

The reservoirs were sampled on day 1, day 2, day 4, day 8, and day 16, after which sampling was conducted about every 14 days until October 18, 2002. During each sampling episode, reservoir water was first circulated through the tubing with the pump for at least 20 minutes to ensure the collection of a well-mixed sample. Subsequently, 5 mL of porewater was removed from the reservoir and the same volume of original spike solution was introduced. After sampling, the porewater in the reservoirs were again mixed using the pump for approximately 20 minutes. Additional details of the methods used to spike, circulate, and sample the reservoirs are presented in Appendix A.

Isotope composition of the water in samples collected from both the field and laboratory experiments were measured at the National Water Research Institute in Saskatoon, Saskatchewan using standard CO_2-water and H_2-water equilibration techniques. Both ^{18}O and ^{2}H results are expressed using the δ(‰) notation relative to Vienna Standard Mean Ocean Water (VSMOW), calculated as:

$$\delta^{18}O = ((R_{SAMPLE} / R_{VSMOW}) - 1) \times 1000 \qquad [3.1]$$

where R_{SAMPLE} represents the $^{18}O/^{16}O$ ratio of the sample and R_{VSMOW} represents the same ratio for the standard. Error in the measurements is within ±2‰ and ±0.1‰ for δD and $\delta^{18}O$ values respectively.

3.4 Numerical Modelling

Numerical modelling of both the field and laboratory results was performed using the finite element package of SEEP/W and CTRAN/W (GEO-SLOPE, 2004). These programs can be used together to simulate steady-state or transient solute movement in a groundwater system. One-dimensional, two-dimensional and three-dimensional problems that are symmetrical about a vertical axis can be simulated. These axisymmetric problems are defined in two dimensions but are analyzed around a vertical central axis set at x-coordinate equal to zero. The axisymmetric analysis is formulated per unit radian. Steady-state flow conditions for both field and laboratory studies were developed in SEEP/W to establish saturated conditions. The flow system established with SEEP/W was used in CTRAN/W to analyze transient contaminant transport.

For each material type used in the model, SEEP/W requires the input of volumetric water content and hydraulic conductivity functions. Because both the laboratory and field conditions can be represented by saturated conditions, these properties were input as straight-line functions (i.e. invariant with pore water pressure). CTRAN/W allows the input of dispersivity, diffusion, adsorption, and decay properties to quantify material behaviour. These analyses considered only the transport of conservative species therefore D_m and D_e were the only required material properties. Diffusion dominated conditions were established by specifying dispersivity values at the lowest values accepted by the program (1e-30 m) and setting seepage velocities to zero.

Boundary conditions in SEEP/W can be entered as either head or flux values. In CTRAN/W, solute concentration or solute flux values can be specified. The initial conditions of all nodes must be defined in a transient analysis.

A full description of the mesh, material properties, and boundary conditions used to develop both the laboratory and field models in included in Chapter 5.

3.5 Estimation of Best-Fit Diffusion Parameters

The D_e and n_e that best describe the experimental conditions were determined by adjusting D_e and n_e in the numerical model until the model output yielded a visual best fit to the measured data. Subsequently, the goodness-of-fit was determined by calculating the error between simulated and measured diffusion results. The diffusion parameters that minimized the calculated error between measured and modelled data were considered representative of the system under study. Other than D_e and n_e, material parameters were not varied.

The relative error between the measured and simulated diffusion curves was determined using (Phalut et.al., 2003):

$$Error(D_e, n_e) = \sqrt{\frac{1}{N_{\exp}} \sum_{i=1}^{N_{\exp}} \frac{(C_{\exp}(t_i) - C_{num}(t_i, D_e, n_e))^2}{(C_{\exp}(t_i))^2}} \qquad [3.2]$$

where: N_{exp} = number of experimental data points,
C_{exp} = measured concentration in the field well,
C_{num} = numerically modelled concentration in the field well, and
t = time.

Using this equation, the fit of the model becomes more important at later times rather than at the beginning of the experiment when concentrations are greatest. By increasing the relative importance of measurements taken at later times, best-fit

diffusion parameters are more likely to be representative of the soil matrix rather than potentially disturbed areas of soil closer to the screen.

This method of error determination was also used when evaluating the effect of simplifying the finite element mesh used to represent the field system. A description of the procedure used to evaluate the significance of these simplifications is included in Chapter 5.

CHAPTER 4 PRESENTATION OF RESULTS

This chapter presents the results of the field and laboratory experiments. Laboratory data include $\delta^{18}O$ and δD tracer values with time in both source and collection reservoirs. Water level data collected from diffusion wells as well as $\delta^{18}O$ and δD tracer values with time are also presented.

4.1 Laboratory Results

Laboratory diffusion experiments were completed on core samples collected from the field site using six double reservoir diffusion cells. A single reservoir diffusion cell was also used as a control to identify any potential interaction between the tracers and equipment.

All samples collected during laboratory testing (n = 209) were analyzed to determine both $\delta^{18}O$ and δD. These data are presented in Tables B-1 and B-2. A cross plot of the all mean and standard deviations for the $\delta^{18}O$ and δD values for each sampling period yielded a straight-line relationship (Figure 4-1), indicating that the $\delta^{18}O$ and δD trends are a product of mixing between the isotopically-enriched spiked water and the background water and are not the result of isotopic exchange reactions. The similar behavior of $\delta^{18}O$ and δD allows all further discussion to be limited to the δD data. The grouping of collection reservoir data points at the bottom left of the graph (depleted values) are for samples collected from the collection reservoir prior to tracer breakthrough and represent only background (i.e. unspiked) values.

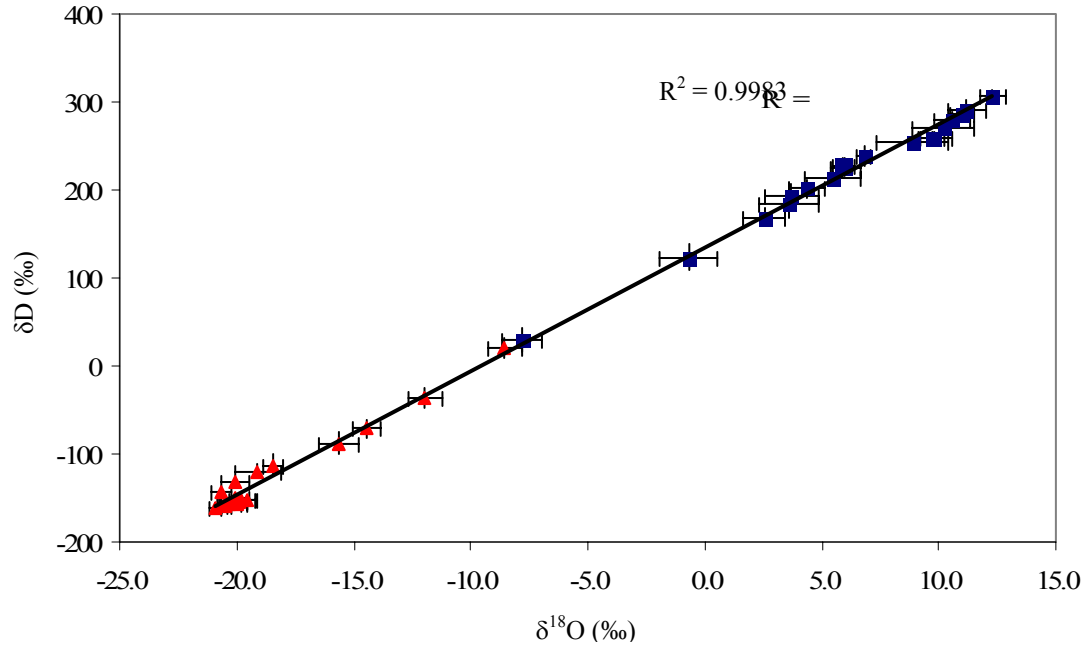

Figure 4-1. Cross plot of $^{18}\delta O$ and δD values of samples taken from double reservoir diffusion cells ($R^2 = 0.9983$). Squares represent values measured in the source reservoir and triangles represent values measured in the collection reservoir.

The data from all six double-cell diffusion cells yielded very similar δD trends with time for both the source and the collection reservoirs, indicating a high level of reproducibility in diffusion tests. The difference between the δD values in the individual sets of data was typically less than 3%. The mean δD values (with associated standard deviations) are plotted in Figure 4-2 and all measured data are presented in Table B-1. Concentrations in the source reservoirs decreased from 306‰ to 30‰ over the course of the experiment (approximately 126 days) while the concentrations in the collection reservoir increased from -162‰ to 21‰ over the same time period.

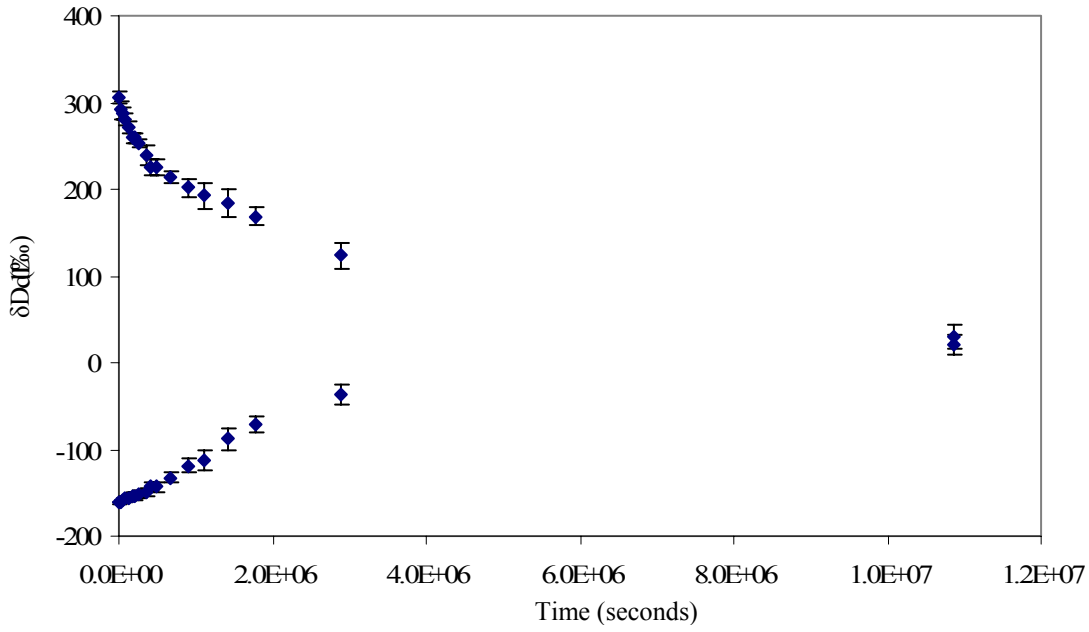

Figure 4-2 Average δD values in the source and collection reservoirs with time. Error bars reflect the standard deviation of samples taken at each time step (n = 6).

In contrast to the test cell data, the δD concentrations in the control cell changed little with time (± 0.5%; data presented in Table B-3) over the sampling period (n = 125 days). The invariant concentrations in these reservoirs suggested that the δD values measured in the test cells were not affected by reactions with the stainless steel of the double reservoir cells or the Teflon and Pyrex used for volume replacement.

After completion of the diffusion cell experiments, *n* was determined on 3 - 7 mm thick slices of the soil cores (4 – 5 slices per core). These data are presented in Table 4-1. Porosities of these samples ranged from 0.34 to 0.41, with a mean of 0.38 ± 0.02 (n = 28). This range is higher than the *n* of 0.31 (standard deviation = 0.01, n = 10) considered representative of field conditions in this till (Shaw and Hendry, 1998), but comparable to porosities determined by Hendry et. al. (2003) of 0.36 to 0.39 on core

samples from this site also using a double reservoir diffusion cell technique. These higher porosities were attributed to the lack of confining pressure in the diffusion cell experiments, which allowed the sample to swell slightly during the test. The lack of a trend in *n* values along the length of the core samples suggests that swelling does not occur evenly throughout the core volume.

Table 4-1 Calculated porosities from core samples used in the double cell diffusion tests.

Cell No.	Mass of Water (g)	Volume of Soil (cm3)	Porosity (*n*)
1	4.83	12.87	0.38
1	4.43	12.87	0.35
1	4.73	12.87	0.37
1	3.40	9.65	0.35
1	6.24	16.09	0.39
2	4.86	12.87	0.38
2	4.19	11.26	0.37
2	3.53	9.65	0.37
2	3.82	11.26	0.34
2	7.71	19.30	0.40
3	6.35	16.09	0.39
3	3.20	8.04	0.40
3	5.78	14.48	0.40
3	3.79	9.65	0.39
3	5.70	16.09	0.35
4	6.43	16.09	0.40
4	4.45	11.26	0.40
4	6.62	16.09	0.41
4	8.73	20.91	0.41
5	4.10	11.26	0.36
5	4.36	12.87	0.34
5	3.66	9.65	0.38
5	5.71	16.09	0.36
5	4.24	11.26	0.38
6	4.29	11.26	0.38
6	3.91	11.26	0.35
6	4.01	11.26	0.36
6	9.16	22.52	0.41

4.2 Field Testing Results

All water level and isotopic data collected from the two test piezometers (BD45-A and BD45-C) are presented and discussed in this section. Water level data collected from the third piezometer (BD45-B) is also presented. Isotopic data collected from BD45-B is not discussed here but is included in Appendix D.

4.2.1 Water Level Data

Figure 4-3 presents water level recovery data for wells BD45-A and BD45-C prior to packer system installation as well as measurements from BD45-B for 679 days of recovery. A comparison between the water level recovery data for the BD45-B and the static values for BD45-A and –C show that even after 679 days of recovery, the water level in this well did not attain steady state conditions, reflecting the extremely low *K* of this till.

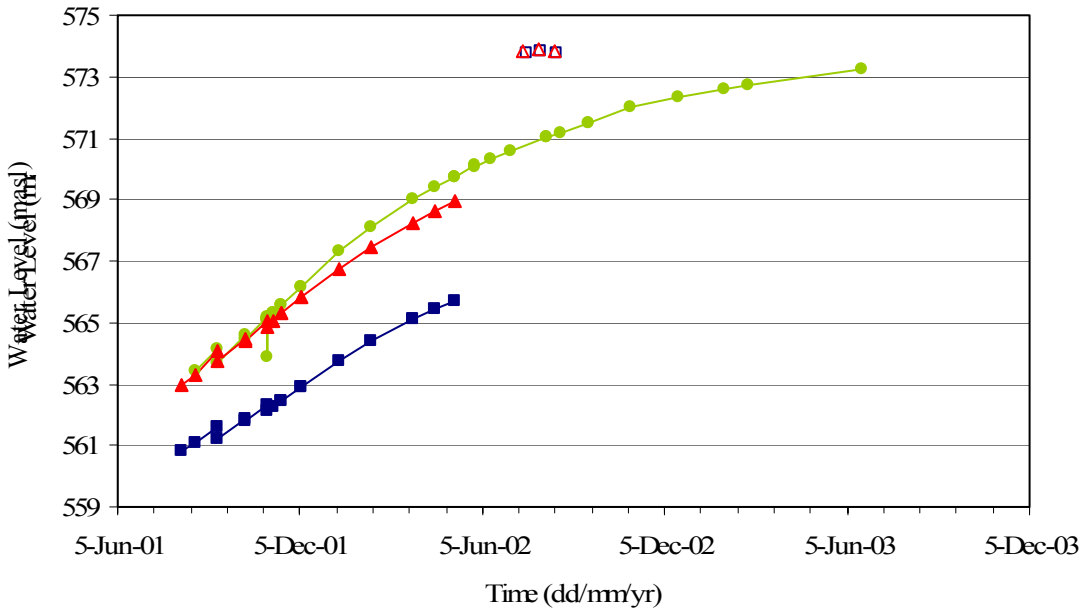

Figure 4-3 Water level recovery data for wells BD45-A, BD45-B, and BD45-C. Solid squares, circles, and triangles represent electric tape water level measurements for wells BD45-A, BD45-B, and BD45-C, respectively. Open squares and triangles represent steady-state water levels for BD45-A and BD45-C measured with the pressure transducers.

After inflation of the packers in wells BD45-A and BD45-C, the water levels in these piezometers were measured using a pressure transducer (Figure 4-4). The pressure measurements showed that static water level conditions in the reservoir were attained within one week of packer inflation and prior to the initiation of *in situ* diffusion testing.

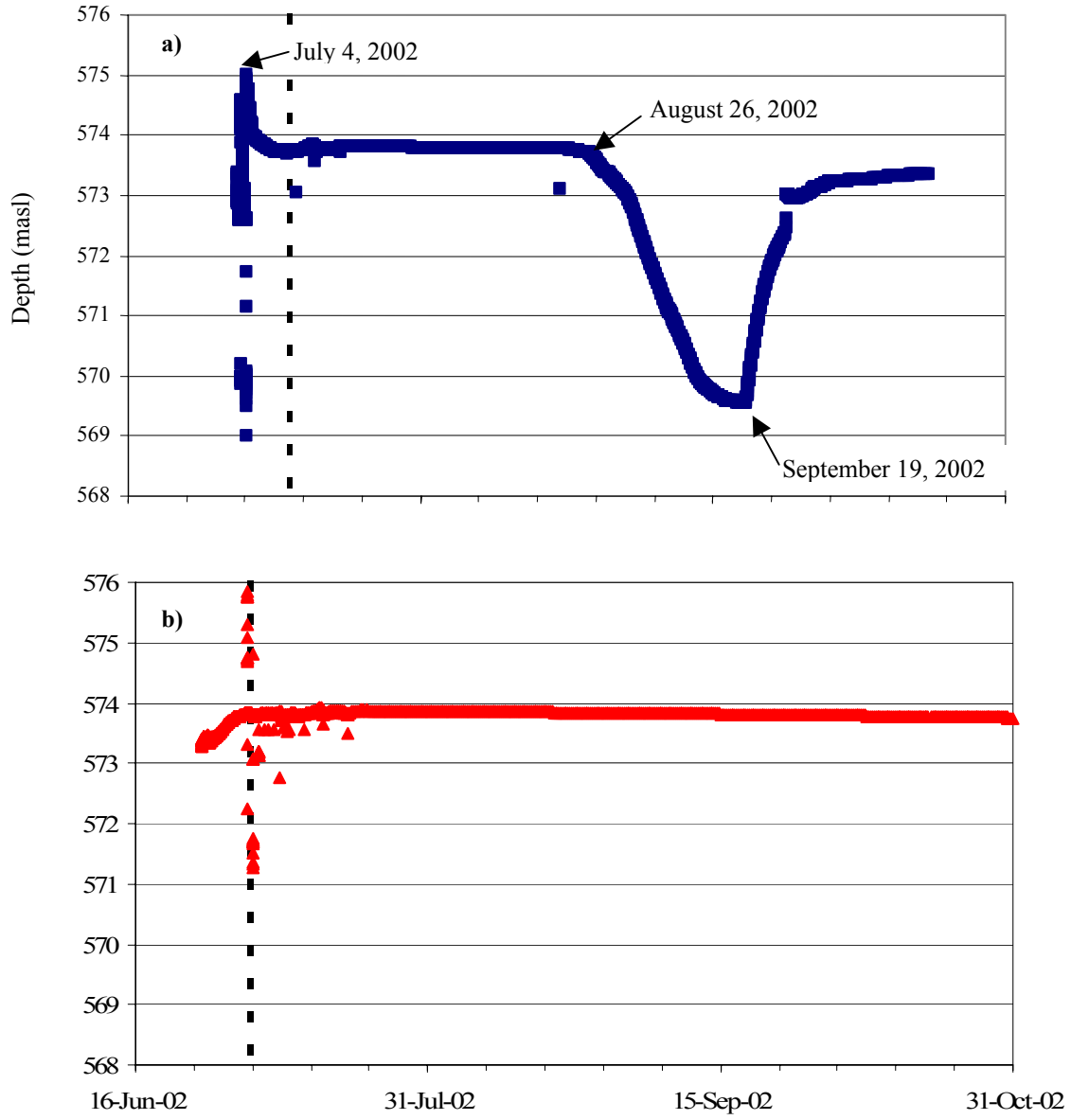

Figure 4-4 Water levels measured with the pressure transducers over the duration of experiment for a) BD45-A, and b) BD45-C. Dotted lines show the start of the diffusion experiments.

Two major water level fluctuations were observed in BD45-A after packer inflation. Immediately after packer inflation and prior to the commencement of the *in situ* diffusion experiment (July 4, 2002), a sharp increase in the water level, followed by a decline to steady state, was observed (Figure 4-4 a). This increase in water level was attributed to the addition of *in situ* groundwater to the tubing to decrease the time required for full water level recovery. In this case, the tubing was filled to about one meter above steady state level and was allowed to recover to steady state conditions prior to commencement of the *in situ* testing (addition of the spike solution; July 11, 2002).

A second pressure fluctuation, a decrease of almost 4 m of head, occurred on August 26, 2002 (Figure 4-4 a). This was followed by a rise to steady state conditions. The decrease was caused by a loss of pressure in the packer system as evidenced by a return to the pre-pressure loss water level after the inflation of the packer at the next sampling period (September 19, 2002). As a result of this loss of pressure, all tracer samples collected after August 25, 2002 in BD45-A were considered to be compromised (discussed in Section 4.2.2) by leakage of water from above the packed off reservoir.

Anomalous outliers in the water levels recorded near the beginning of the diffusion experiments in BD45-A and –C were attributed to the sampling and the transducer measurement protocols used in the experiment. During the early time period, pressure measurements were recorded on 15 minute intervals. As a result, measurements were obtained during reservoir mixing performed for each sampling

incident. These outliers are not evident at later times because the pressure measurement frequency was reduced.

The general decrease in water levels in well BD45-C (573.87 to 573.75 masl; Figure 4-4 b) is believed to reflect the seasonal trend in water level fluctuation as evidenced by similar changes in amplitude in the long-term water levels recorded in a piezometer installed at a depth of 13.3 m at this site (unpublished data). The magnitude of the pressure fluctuations measured in BD45–C corresponds to a change in volume of the reservoir over the course of the experiment of less than 5 mL or less than 0.2% of the total volume of the reservoir isolated by the packer system.

4.2.2 Tracer Concentrations

$\delta^{18}O$ and δD values were determined for water samples collected from the background formation, the spiking solution and during the *in situ* diffusion testing on BD45-A and BD45-C. The background formation values collected from BD45-A and BD45-C prior to commencement of *in situ* testing are presented in Table 4-2. Data from samples collected from BD45-B between September 14 and November 2, 2001 are also included. Because BD45-B was spiked with ^{18}O on November 2, 2001, $\delta^{18}O$ values collected after this date were not considered representative of background values and are not included in this table.

Table 4-2 Background δD and $\delta^{18}O$ values from diffusion wells BD45-A, -B, and -C. Well depth is given in brackets as depth to middle of well screen.

Date	δD (‰)			$\delta^{18}O$ (‰)		
	BD45-A (15.34)	BD45-B (13.058)	BD45-C (13.191)	BD45-A (15.34)	BD45-B (13.058)	BD45-C (13.191)
14-Sep-01				-21.6	-21.2	-21.3
11-Oct-01				-21.6	-20.3	-21.2
11-Oct-01				-21.4		-18.4
11-Oct-01				-20.3		-20.3
2-Nov-01				-21.6	-21.2	-21.2
16-Nov-01				-21.6		-21.3
14-Jan-02	-167.4		-164.6	-21.1		-20.69
15-Feb-02	-166.2			-20.9		
15-Feb-02				-20.8		
28-Mar-02				-21.1		-20.5
8-May-02		-163.4				
29-May-02				-21.2		-20.5
2-Jul-03		-163.8				
10-Jul-03		-165				
31-Jul-03		-162.3				
20-Aug-03		-162.2				
AVERAGE	-166.8	-163.3	-164.6	-21.2	-20.9	-20.6
ST DEV	0.8	1.0		0.4	0.5	0.9

The average and standard deviation of background values obtained from other wells located at the site are consistent with the background values obtained from the diffusion wells. This indicates that δD and $\delta^{18}O$ values are spatially consistent at this depth and do not vary significantly with time. Wells completed at slightly greater depths (B50 and BD45-A) yielded slightly more negative isotope values than those collected from shallower wells, but average values from these depths were not significantly different from the average values determined for the site.

Table 4-3 Background δD and $\delta^{18}O$ values from select piezometers at the King site (from Hendry and Wassenaar, 1999 and unpublished data). Well depth is given in brackets as depth to middle of well screen (mbgs).

Date	δD (‰)					$\delta^{18}O$ (‰)	
	B45 (11.67)	B50 (14.97)	BD45-D (13.39)	BD45-E (13.5)	BD45-F1 (13.35)	B45 (11.67)	B50 (14.97)
7-Nov-95		-164				-21.38	-21.69
1-Jan-96	-163					-21.41	
23-Apr-96	-165	-164				-21.28	-21.59
16-Sep-96	-166	-165				-21.12	-21.46
18-Sep-96	-166	-165					
12-Nov-96	-164	-168				-21.24	-21.3
19-Nov-96	-164	-168					
1-Feb-97	-165	-165					
6-Feb-97	-165	-165				-21.24	-21.51
26-Jun-97	-162	-165					
16-Oct-97	-165	-167					
2-Jul-03			-162	-165	-164.2		
10-Jul-03			-164.5	-165.2	-164.9		
21-Jul-03			-163.1	-163.2			
14-Aug-03			-163.5	-163.9			
MEAN	-164.5	-165.6	-163.3	-164.3	-164.6	-21.3	-21.5
ST DEV	1.3	1.5	1.0	0.9	0.5	0.1	0.1

From the values presented in Table 4-2 and Table 4-3, average background δD and $\delta^{18}O$ values representative of the site can be estimated. These values are presented in Table 4-4.

Table 4-4 Average δD and $\delta^{18}O$ values for King site at completion depth of the diffusion wells.

	δD (‰)	$\delta^{18}O$ (‰)
MEAN	-164.6	-21.1
ST DEV	1.5	0.6

The spiking solutions used in diffusion wells BD45-A and -C were created by adding a known volume of isotopically-enriched solution to a known volume of porewater at background isotopic level (as described in Chapter 3). The δD and $\delta^{18}O$ values for the spiking solutions were calculated using:

$$\delta D\left(\delta^{18}O\right) = \left[\frac{R_{sample} - R_{s\tan dard}}{R_{s\tan dard}}\right] \times 1000 \qquad [4.1]$$

where: R_{sample} = D/H ($^{18}O/^{16}O$) ratio of the sample, and
$R_{standard}$ = D/H ($^{18}O/^{16}O$) ratio of the standard (VSMOW).

The δD and $\delta^{18}O$ values for the spiking solution used in the *in situ* testing at BD45-A and BD45-C are presented in Table 4-5.

Table 4-5 Calculated δD and $\delta^{18}O$ values for diffusion well spiking solutions.

Diffusion Well	δD (‰)	$\delta^{18}O$ (‰)
BD45-A	6570	478
BD45-C	6250	454

The δD and $\delta^{18}O$ values measured on water samples collected during *in situ* diffusion testing in BD45-A and BD45-C are presented in Figure 4-5 and Figure 4-6 and tabulated in Appendix C.

A plot of the two isotopes of water for BD45-A and BD45-C (Figure 4-5 and Figure 4-6) show a well-defined straight-line relationship between the two data sets for both wells. As was the case for the laboratory diffusion tests, the straight lines indicate mixing between two end-points represented by the spike solution and the background solution (groundwater). Samples collected after August 25, 2001 from well BD45-A deviate from this linear relationship. These samples were collected subsequent to deflation of the packer in BD45-A. The deviation suggests that some process is occurring that alters the ratio of these isotopes in the reservoir. This could occur as a result of mixing of the reservoir water with the non-spiked stagnant water above the packer. All data collected from well BD45-A after deflation of the packer are not included in further analyses. The linear correlation between the δD and $\delta^{18}O$ isotopes

allows further discussion to be focused on deuterium, as the findings should also apply to $\delta^{18}O$.

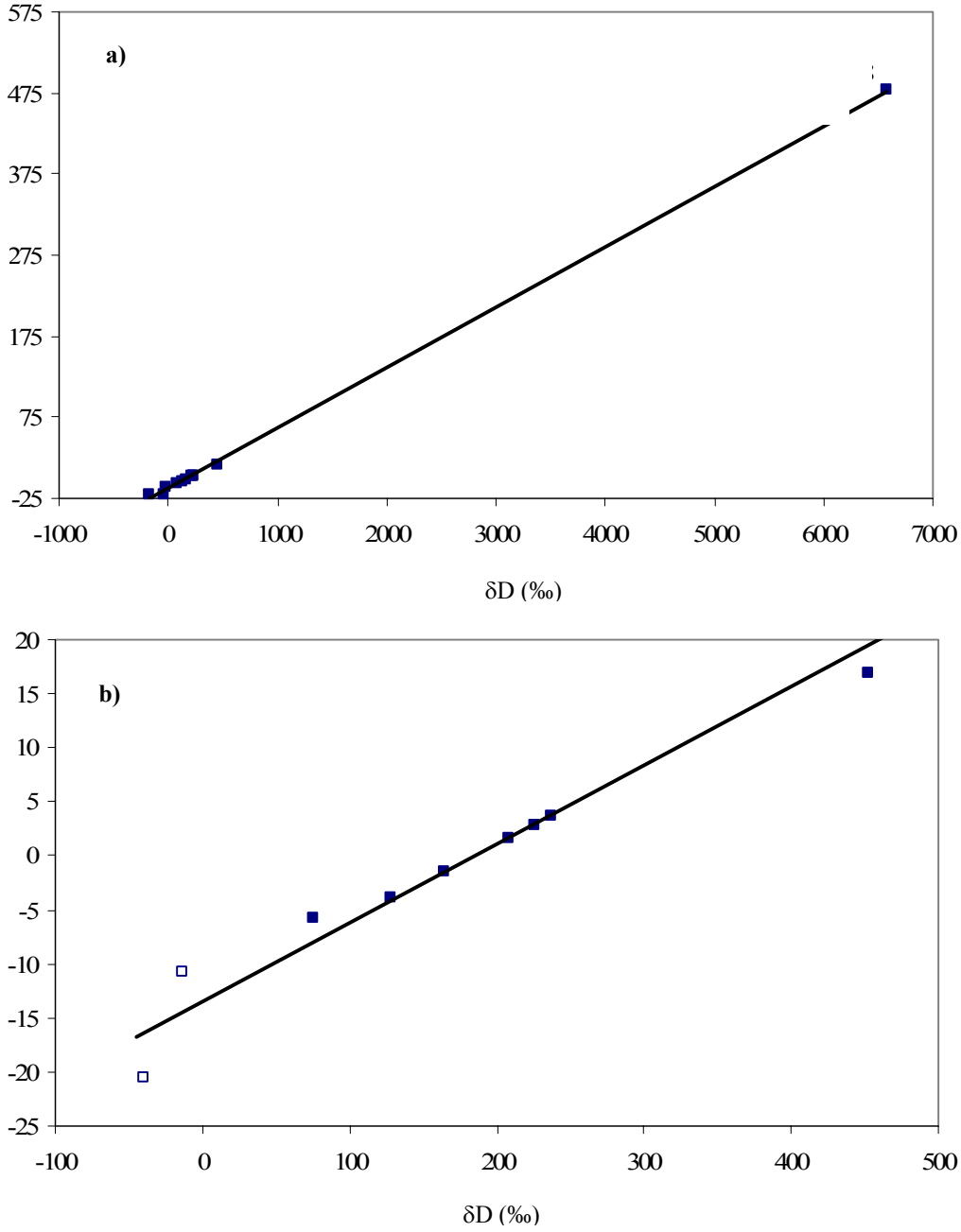

Figure 4-5 Comparison of δD and $\delta^{18}O$ values for samples taken from well BD45-A. Figure a) includes average background values and calculated spiking solution values; b) presents a close-up of trends in $\delta^{18}O$ and δD values of samples collected during the diffusion experiment. Samples collected after August 25 are presented as open squares.

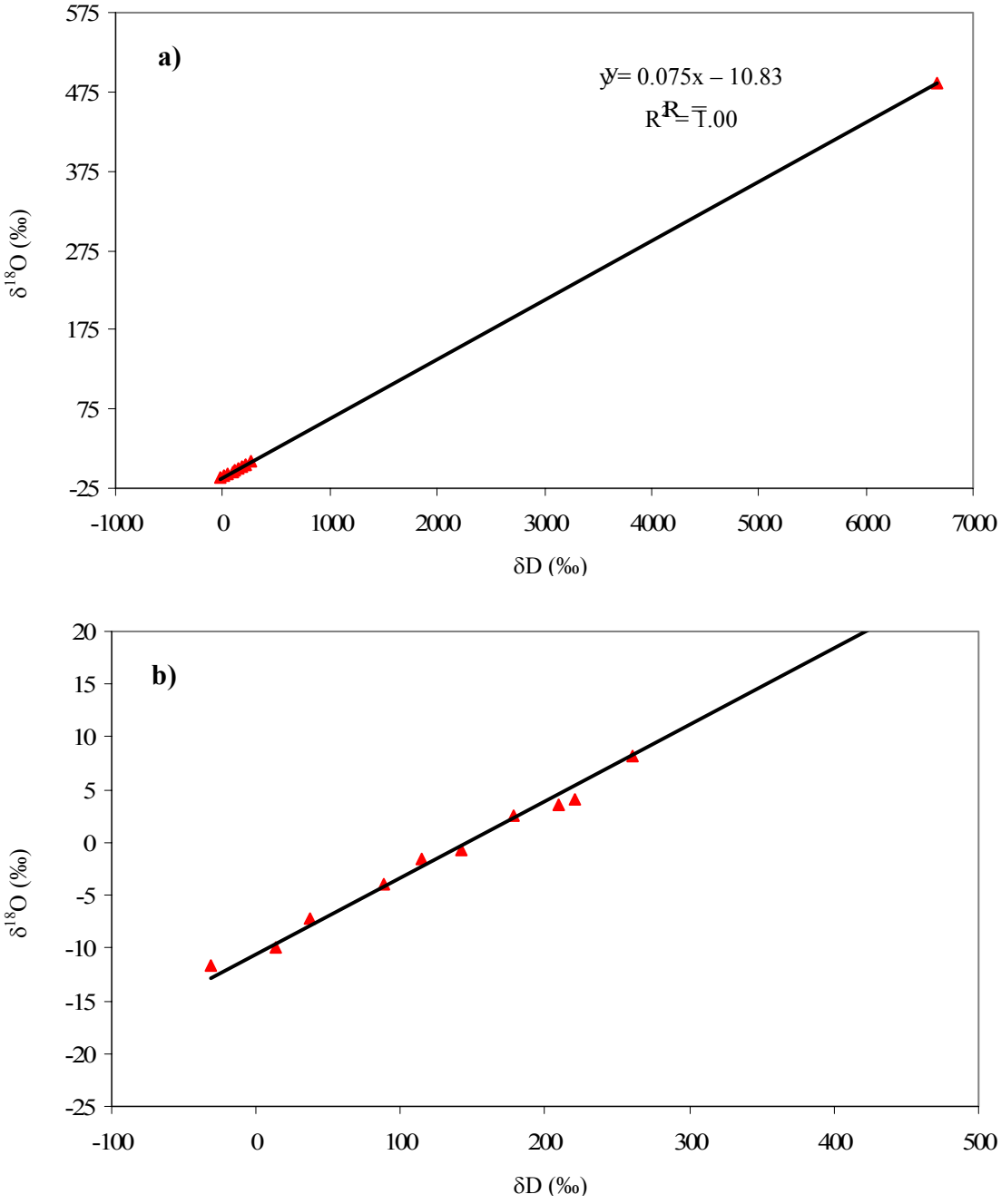

Figure 4-6 Comparison of δD and $\delta^{18}O$ values for samples taken from well BD45-C. Figure a) includes average background values and calculated spiking solution values; b) presents a close-up of trends in $\delta^{18}O$ and δD values of samples collected during the diffusion experiment.

The regression line equations for the diffusion well data are presented in Figure 4-5 a and Figure 4-6 a. The slopes are 0.075 for both BD45-A and BD45-C. The agreement in the slopes indicates that the tracer concentrations are decreasing at approximately the same rate in both wells, which should reflect similar diffusion rates.

δD values in well BD45-A decreased from a high of 452‰ to 75‰ after approximately 42 days. Well BD45-C values decreased from 261‰ to –31‰ after 107 days. δD values in both wells recovered more than 60% towards mean background deuterium values. In both cases, the trends in the data are similar (Figure 4-7), again suggesting similar D_e values.

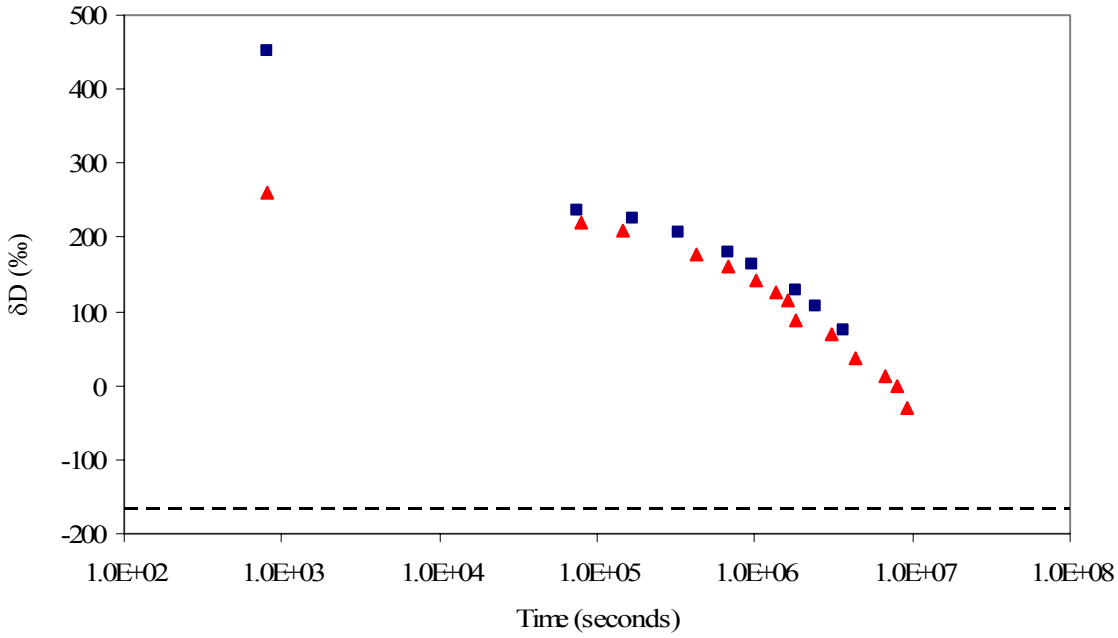

Figure 4-7. Measured δD values in diffusion wells with time. Squares represent measurements from BD45-A, triangles are measurements from BD45-C. The dashed line indicates the average background deuterium value in the formation.

Both isotope values obtained from initial water samples from both BD45-A and BD45-C appear to be high in comparison to the remainder of the curves (Figure 4-7). Pressure data from the transducers do not indicate any changes in water level after the introduction of the spike, ruling out a dilution effect as the cause of the unexpected drop in reservoir concentrations after the onset of the *in situ* testing. Time zero samples were taken directly from replacement solution vessel after mixing in the initial spike solution. If mixing between the spike solution and the well reservoir was incomplete during the spiking procedure (i.e. due to short-circuiting in the replacement solution vessel), these time zero samples would not represent concentrations in the well reservoirs. Subsequent samples were collected directly from the well reservoirs and are therefore considered to be representative of the diffusion process. The estimation of initial concentrations is discussed further in Section 5.2.3.2.

4.3 Summary

The experimental program was designed to measure the diffusion of D and ^{18}O in a clayey aquitard using both field and laboratory methods.

4.3.1 Laboratory Results

Results of the double diffusion cell tests show a high level of reproducibility, with the difference in measurements between the cells typically less than 3%. Control cell measurements indicate that the materials used in the tests did not have an impact on the isotope tracers. δD and $\delta^{18}O$ values plot on a straight line, indicating that the two isotopes behave similarly, consequently further discussion focused on the δD results. Porosity values determined from the diffusion cell tests (n = 0.38, standard deviation = 0.02, n = 28) were greater than typical field results (n = 0.31, standard deviation = 0.01,

n = 10) but within the same range determined from earlier laboratory diffusion experiments (n = 0.36 to 0.39).

4.3.2 Field Results

Monitoring during the field study showed that even after 679 days of recovery, a steady state water level in the BD45-B well was not attained, reflecting the extremely low K of this till. As with the laboratory data, δD and $\delta^{18}O$ values plot on a straight line, allowing further discussion to focus on the δD results. Examination of pressure transducer measurements indicated that samples collected from Well BD45-A after August 26, 2002 (45 days of testing) were suspect because of a packer malfunction. Time zero diffusion concentration results for both wells were anomalous and are considered to be an artifact of the sampling methodology. Estimation of time zero concentrations is discussed in Section 5.2.3.2.

CHAPTER 5 DISCUSSION AND ANALYSIS

Analyses and interpretation of the laboratory and field data are presented in this chapter. Numerical modelling of field and laboratory experiments was conducted to determine the D_e and n_e values that best represent each system. The D_e value was evaluated by modelling a long-term deuterium profile previously established for the King site.

5.1 Analysis of Laboratory Results

The diffusion curves obtained from the laboratory experiments are presented in Chapter 4. A numerical model to simulate laboratory conditions was developed. Best-fit D_e and n_e values were determined by minimizing the error between the measured and simulated data calculated using Eq. [3.2].

5.1.1 Numerical Model Description

The same one-dimensional mesh was used for both the SEEP/W and CTRAN/W simulations of the laboratory results. The mesh was 8.98 cm in length, divided into the source reservoir (3.0cm), the soil (2.0cm), and the collection reservoir (3.98cm) (Figure 5-1). The elements in both the source and collection reservoirs were approximately 0.3cm long. The mesh representing the soil was slightly finer, with elements of 0.2 cm in length. The reservoir porosity was set at 1.0 in the simulations.

An arbitrary total head boundary condition of 1.0 m was set along the left side of the mesh in SEEP/W with zero flux boundaries assigned to all other boundaries. These boundary conditions allowed a saturated, steady-state system to be developed in

which there was zero advection. All seepage velocities were set to zero in CTRAN/W to ensure a diffusion-dominated system. All nodes in the source reservoir were set at an initial concentration of 1.0 mg/L. To compare the modelled concentrations with the measured values, the modeled concentrations were multiplied by the difference in initial δD values measured in the source and collection reservoirs. The initial δD value in the collection reservoir was then added to the modelled values to shift the modelled values into line with the measured δD values. The value of D_e for both reservoirs was set to 1.0 x 10^{-7} m^2/s, about three orders of magnitude greater than that expected of the soil. This high D_e ensured that reservoirs remained fully mixed with respect to concentration.

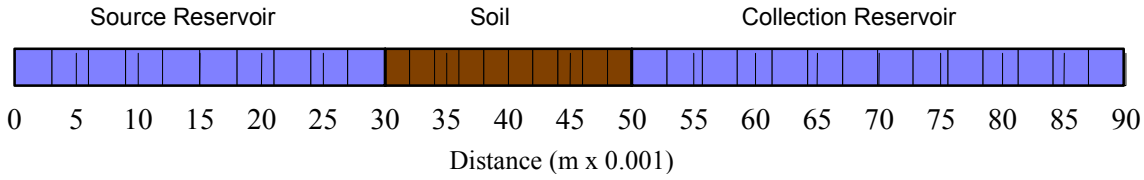

Figure 5-1. Mesh used to simulate the laboratory double-reservoir diffusion experiments.

5.1.2 Best-fit Diffusion Parameters

The n_e for the stable isotopes of water was found to be equal to n by Hendry and Wassenaar (1999) for the till used in this experiment. This is similar to findings for other clayey tills (van der Kamp et.al., 1996).

Measured n values for the laboratory soil samples ranged from 0.34 to 0.40 (Table 4-1). The n was also back calculated from the laboratory tests using the end-point equilibrium range of δD whereby:

$$(\delta D_{initial} V)_{source} = (\delta D_{final} V)_{source} + (\delta D_{final} V)_{collection} + (\delta D_{final} V)_{soil} \quad [5.1]$$

where: δD = deuterium value (‰),
V = volume of liquid (L^3),
initial = value at time zero,
final = value at completion of testing,
source = refers to source reservoir of laboratory cell, and
collection = refers to collection reservoir of laboratory cell.

The measured δD values for the source and collection reservoirs are given in Table B-1. Assuming that the final average δD value for the soil is between the final average δD values measured in the source and collection reservoirs, Eq.[5.1] was used to calculate a range in values for soil water volume. The porosity was then calculated using:

$$n = \frac{V_w}{V_{total}} \quad [5.2]$$

where: n = porosity (L^3L^{-3}),
V_w = volume of water in soil (L^3), and
V_{total} = the total volume of soil sample (L^3).

Using this mass balance approach, the calculated n of the laboratory soil samples ranged between 0.33 and 0.35. These values were at the low end of the values obtained from water contents and core geometries (Table 4-1), but are closer to values considered representative of field conditions in this till (0.31±0.01, Shaw and Hendry, 1998).

The best-fit values of D_e for the laboratory data were determined by minimizing the error between measured and simulated results. Simulations were performed with the soil n_e values ranging from 0.33 to 0.35, encompassing the range of n values determined from mass balance calculations. Porosity values between 0.33 and 0.35

produce similar minimum error values, with best-fit soil D_e ranging from 3.5 x 10^{-10} m^2/s to 4.0 x 10^{-10} m^2/s (Figure 5-2).

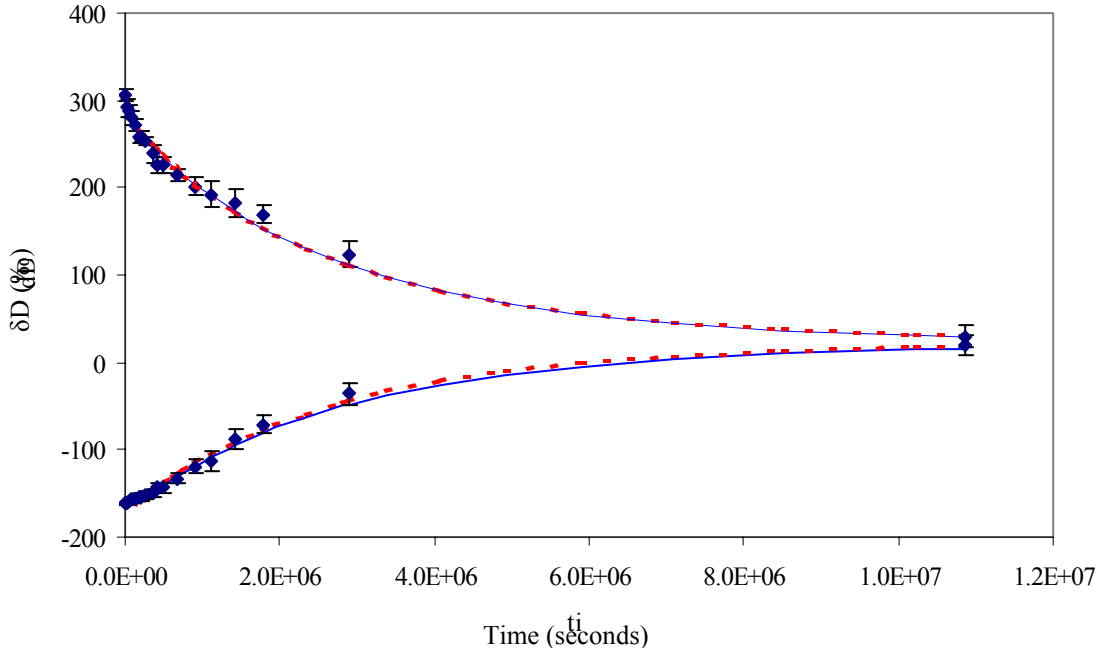

Figure 5-2. Measured and simulated reservoir diffusion concentrations with time. Diamonds represent average measured δD concentrations with standard deviation brackets. Lines represent simulated reservoir concentration values. The dashed line represents a D_e of 4.0 x 10^{-10} m^2/s and n_e of 0.33. The solid line represents a D_e of 3.5 x 10^{-10} m^2/s and an n_e of 0.35.

5.2 Analysis of Field Test Results

5.2.1 Field Hydraulic Conductivity

The *K* of the till was calculated from the water level recovery data collected for the *in situ* diffusion wells. Values of 6.7 x 10^{-11} m/s, 1.6 x 10^{-10} m/s, and 8.4 x 10^{-11} m/s were calculated for wells BD45-A, -B, and –C, respectively. These values were based on water levels recovery data measured using an electric tape and mean static water levels determined from transducer data presented in Figure 4-3. These values are

consistent with previously measured laboratory and field-based *K* values. For example, slug testing conducted in conventional piezometers and laboratory testing of core samples from the unoxidized till at this site were also in the order of 10^{-11}m/s (Shaw and Hendry, 1998). In addition, harmonic analysis of long-term water level responses of piezometers below a depth of 11 m yielded *K* values of 10^{-11}m/s (Boldt-Leppin and Hendry, 2003). The similar values of *K* determined from various methods and directions of testing (i.e. slug tests yielding horizontal *K* values and laboratory testing and analysis of long-term water levels yielding vertical *K* values) suggest that the till is homogeneous and isotropic with respect to *K*.

These low *K* values, along with the fact that wells were installed in 'dry' boreholes, suggested that diffusion, rather than advection, is the dominant transport mechanism in this till. Shaw and Hendry (1998) measured a downward hydraulic gradient of 0.014 m/m through the till at this site. Using this gradient and the *K* values calculated from the diffusion well measurements, Darcy velocities of 3.0×10^{-5} m/a, 7.1×10^{-5} m/a, and 3.7×10^{-5} m/a can be calculated for BD45-A, -B, and –C respectively. From Figure 2-1, these values fall within the range of velocities over which diffusion is dominant. Independent evidence of a diffusion-dominated system is provided by the results of various isotopic and solute transport studies conducted at this site (Hendry and Wassenaar, 1999, 2000; Hendry et.al., 2000; Hendry et. al., 2005).

5.2.2 Numerical Model Description

The simplicity of the mesh layout was an important consideration in developing a representative mesh for field conditions. If the vertical movement of the tracer is small relative to the horizontal movement it is possible to represent the system by

considering only lateral movement, which would only require a one-dimensional axisymmetric simulation. If this is not the case, a larger, more complicated, two-dimensional, axisymmetric simulation is required.

Small geometric details, such as the individual wire wraps that comprise the well screen, can greatly increase the complexity of a finite element mesh. To keep the mesh as simple as possible, it was necessary to understand whether the well screen had a significant effect on the diffusion process or if a representative mesh could be built without including the details of the screen geometry. Understanding the effect of the screen on diffusion may also allow the screen to be represented by some alternate method, such as using a porous layer with an 'equivalent' screen diffusion coefficient.

5.2.2.1 Evaluation of Mesh Design

Optimization of the mesh design was performed by comparing the results from a range in meshes, from simple mesh designs to more detailed configurations. Three basic types of mesh design were considered. These included:

Mesh Design 1: a two-dimensional system,

Mesh Design 2: a two-dimensional system with a line of symmetry taken along a horizontal axis passing through the middle of the well screen, and

Mesh Design 3: a one-dimensional system.

Mesh Designs 2 and 3 were evaluated by comparing the generated results to those obtained with the most complicated mesh design (Mesh Design 1). The material characteristics were held constant for each mesh. Each mesh was solved using an axisymmetric analysis with the center of the well screen set as the vertical axis of symmetry.

Mesh Design 1 is presented in Figure 5-3. Nodal spacing in the well varied from 0.5 cm (x-direction) by 0.33 cm (y-direction) to 0.5 cm by 0.9 cm. The smallest element within the soil was 0.16 cm by 0.4 cm and the largest is 1.7 cm by 2.0 cm. The elements representing the steel plate at the bottom of the well were entered as null elements, or elements without any hydraulic properties, so that no flow or contaminant movement would occur across these elements.

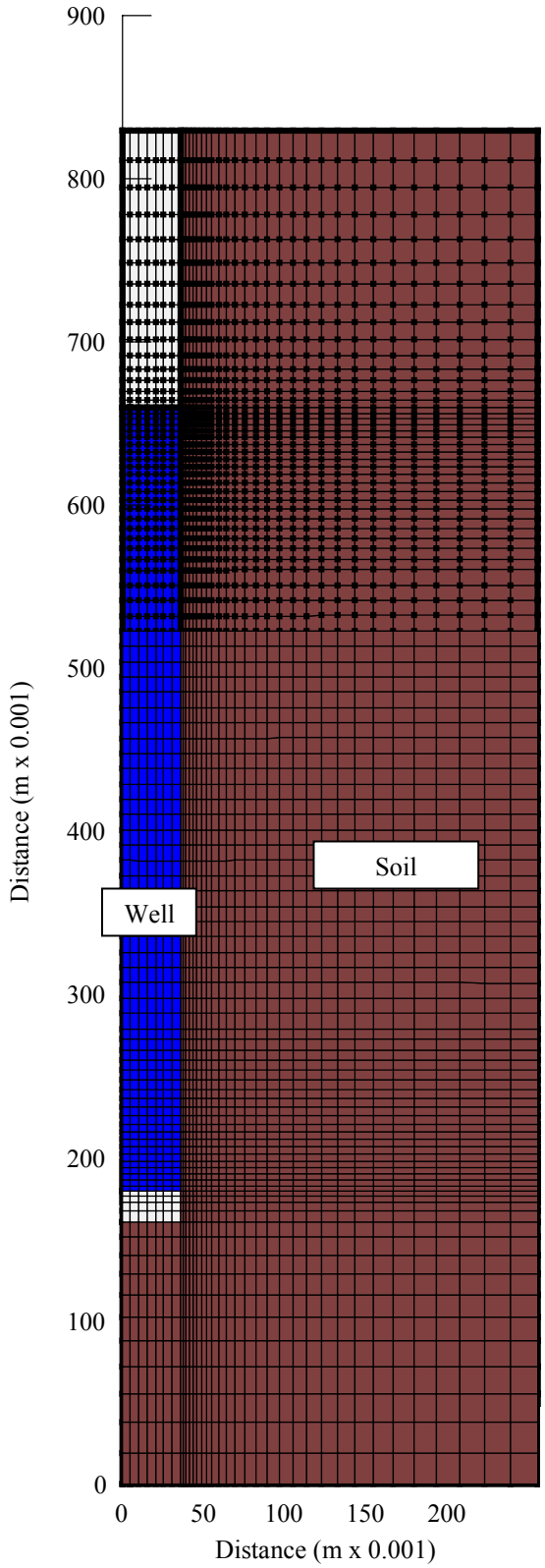

Figure 5-3. Field Mesh Design 1. X-axis is vertical axis of symmetry.

Simulations conducted with Mesh Design 1 were used to define the concept of an 'acceptable error' in D_e. Mesh Design 1 with a soil D_e of 3.0 x 10^{-10} m^2/s was used as the base case. Using this mesh, the soil D_e was increased and the in-well concentrations simulated were compared to in-well concentrations simulated with the base case. The difference between these simulations was quantified by calculating the 'error' between the in-well concentrations for the two simulations using Eq.[3.2]. These error values represent the difference in in-well concentrations produced by changing only the soil D_e.

Table 5-1. Acceptable error in D_e for evaluation of mesh design.

% change in base case De*	Error (%)
2	0.4
5	1
10	2
20	5
25	6
50	11

* refers to the % change from the base case D_e of 3.0 x 10^{-10} m^2/s.

The simulated in-well concentrations determined from the simplified mesh designs with a soil D_e of 3.0 x 10^{-10} m^2/s was then compared to the concentrations determined with the base case using Eq.[3.2]. The error between these simulations was compared to the error values in Table 5-1 to determine the accuracy of the other mesh designs for prediction of D_e.

To develop Mesh Design 2, the size of the mesh was decreased by taking the vertical mid-point of the well screen as a line of symmetry (Figure 5-4). This mesh was 42 cm high by 25.5 cm wide and was divided into the diffusion well, the steel bottom

plate on the well, and the surrounding soil. The same nodal spacing was used in this mesh as in Mesh Design 1 (Figure 5-3).

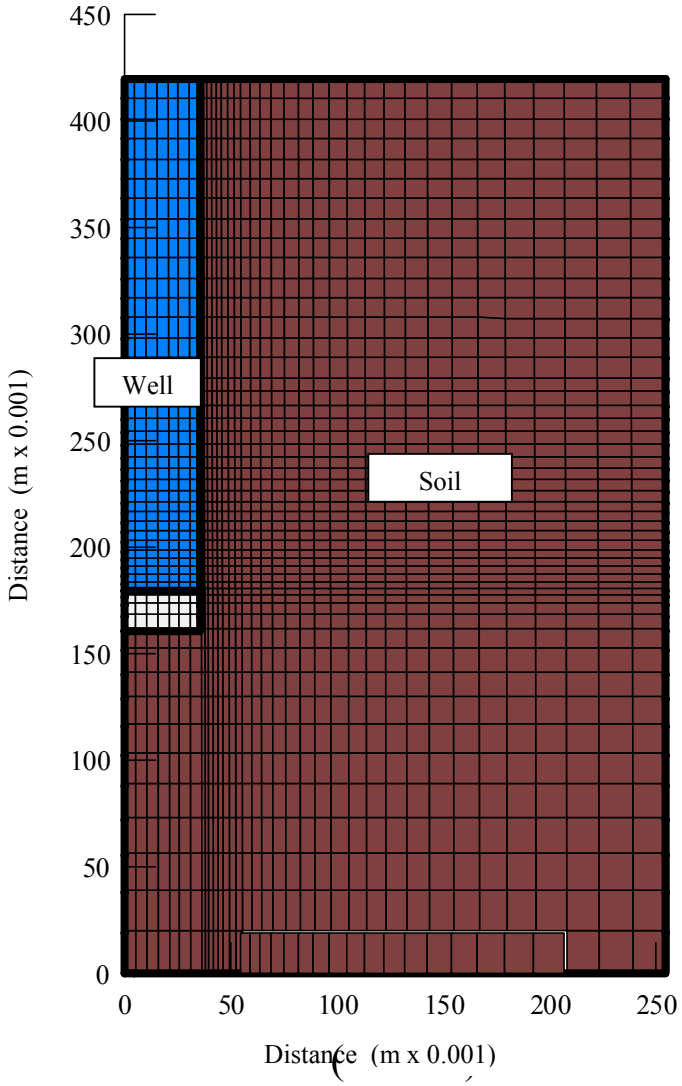

Figure 5-4. Field Mesh Design 2. X-axis is vertical axis of symmetry.

The diffusion curve for a soil D_e of 3.0 x 10^{-10} m^2/s was generated and compared to the results obtained with Mesh Design 1 for the same D_e value. The error produced by this comparison was less than 0.4%. From Table 5-1, this mesh was deemed suitable to predict the D_e to within 2% (approximately 5 x 10^{-12} m^2/s). Therefore, the difference

between Mesh Design 2 and Mesh Design 1 was considered insignificant. Mesh design 2 was deemed to be adequate for the simulations of the field system.

Mesh Design 3 (Figure 5-5) consisted of a single horizontal line of elements representing the spiked solution inside the well and the surrounding soil material. This mesh was 25.5 cm wide, with the horizontal nodal spacing the same as that used in the other two mesh designs.

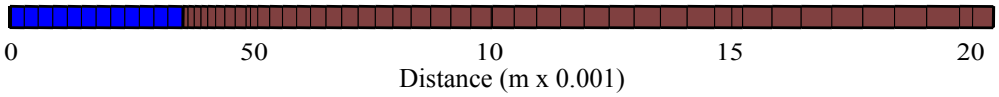

Figure 5-5. Field Mesh Design 3. X-axis is vertical axis of symmetry.

The in-well concentrations with time obtained with this mesh using a soil D_e of 3.0 x 10^{-10}m^2/s were compared to the results obtained from Mesh Design 1 (Figure 5-3) with a soil D_e value of 3.0 x 10^{-10}m^2/s. Using Eq.[3.2], the error between these results was computed to be 5%. From Table 5-1, this shows that the one-dimensional mesh could not accurately predict D_e to within 20% (approximately 5.0 x 10^{-11} m^2/s).

From the results of these analyses, Mesh Design 2 (Figure 5-4) appeared to provide the best balance of accuracy and simplicity for the modelling needs. The limitation of this mesh was that it did not allow incorporation of the detail of the well screen.

5.2.2.2 Effect of Well Screen

To evaluate the effect of the well screen on the determination of D_e for the soil, the mesh in Figure 5-8 was used.

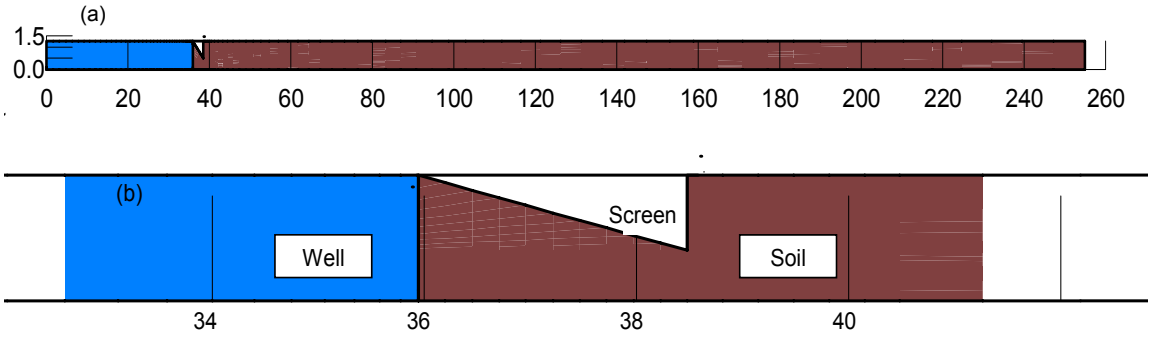

Figure 5-6. Mesh used to simulate the effect of the well screen on determination of soil D_e. The entire mesh (a) is shown at a ratio of 1:0.2 (horizontal:vertical). A close-up of the screen is shown at 1:1 (b). Shown here with 40% open area.

Video photography obtained using a downhole well camera showed soil bulges through the spaces in the well screen. The source of the soil bulges is not known, however, they could be due to shaving of the geologic media during well installation or to swelling of the soil after well installation. Because of the soil bulges, the mesh included soil material in the screen opening. The potential effect of soil bulging into the well volume beyond the well screen was not considered.

This mesh was also a two-dimensional, axisymmetric system. The top of the mesh was taken along a horizontal line of symmetry running through the center of a wire, while the bottom was set at the center of an opening. The nodal spacing in this mesh depended on the configuration of the screen. Spacing generally ranged from 0.0163 cm to 0.800 cm in the x-direction and 0.0021 cm to 0.0127 cm in the y-

direction. As with the mesh used for previous analyses, elements were smaller near the well screen and became progressively larger away from the screen.

In SEEP/W, a total head boundary condition of 1.0 m was applied along the left side of the mesh with all other boundaries set to zero flux. All nodes inside the well were given an initial concentration of 1.0 mg/L in CTRAN/W. The screen was represented by null elements.

To quantify the effect of the well screen on diffusion into the soil, the best-fit D_e was determined for a range in percentages of open area and for two different well screen cross-sections (i.e. triangular, as used in the field test, and rectangular). The model was run for both cross-sectional screen designs for screen open areas ranging from 10% to 90%. A soil D_e of 3.0 x 10^{-10} m^2/s was used in all these simulations. The in-well concentration values with time from each simulation were compared to results of a mesh containing no screen (i.e. 100% open area). The soil D_e of the screenless mesh was altered to minimize the error between the results of this screenless mesh and the results of the screened mesh for each percentage of open area. The value of D_e that produced the minimum error was termed D_{num}, and was considered to be the diffusion coefficient that would be estimated using a mesh that does not include a screen to match results of a screened system.

A summary of the effect of the screen configurations on the best-fit D_e is shown in Figure 5-8. With a triangular screen, the D_{num}/D_e decreases from 1.0 at 100% open area to 0.8 at 10% open area. With a rectangular screen, the D_{num}/D_e is 0.45 for 10% open area. This means that for a screen with 10% open area in a soil with D_e of 3.0 x 10^{-10} m^2/s, a triangular screen would result in a soil D_e estimate of 2.4 x 10^{-10} m^2/s,

while a screen with a rectangular cross-section would produce a soil D_e estimate of approximately 1.4 x 10^{-10} m^2/s. The results of these simulations show that a screen with a rectangular cross-section has a much greater effect on the best-fit D_e than the triangular screen utilized in this study (Figure 5-7).

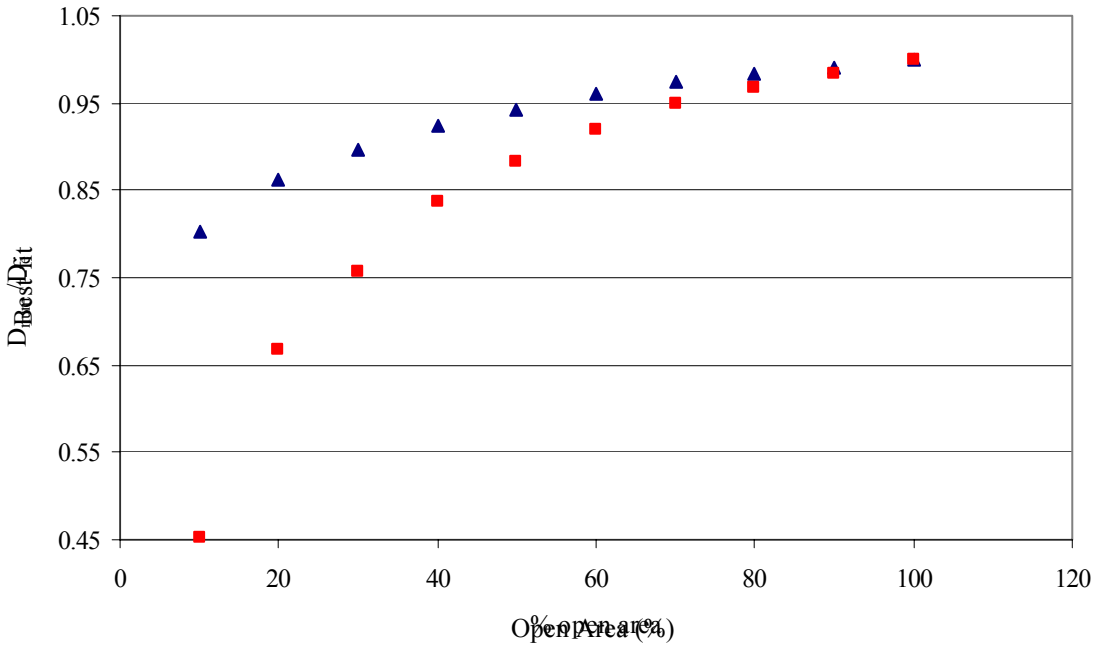

Figure 5-7. The effect of well screen % open area on the estimation of best-fit soil D_e. Triangles represent the effects of a triangular screen, squares represent a rectangular screen.

The effect of incorporating a screen in the mesh has the most impact on the diffusion curve at early times (i.e. prior to 3 x 10^6 seconds or 35 days), when the most rapid decrease in well concentration is occurring. Figure 5-8 demonstrates that the inclusion of a screen results in a sharper curve at this time, with concentrations in the

40% open area system remaining higher inside the screened volume before beginning to decrease when compared to the 100% open area results.

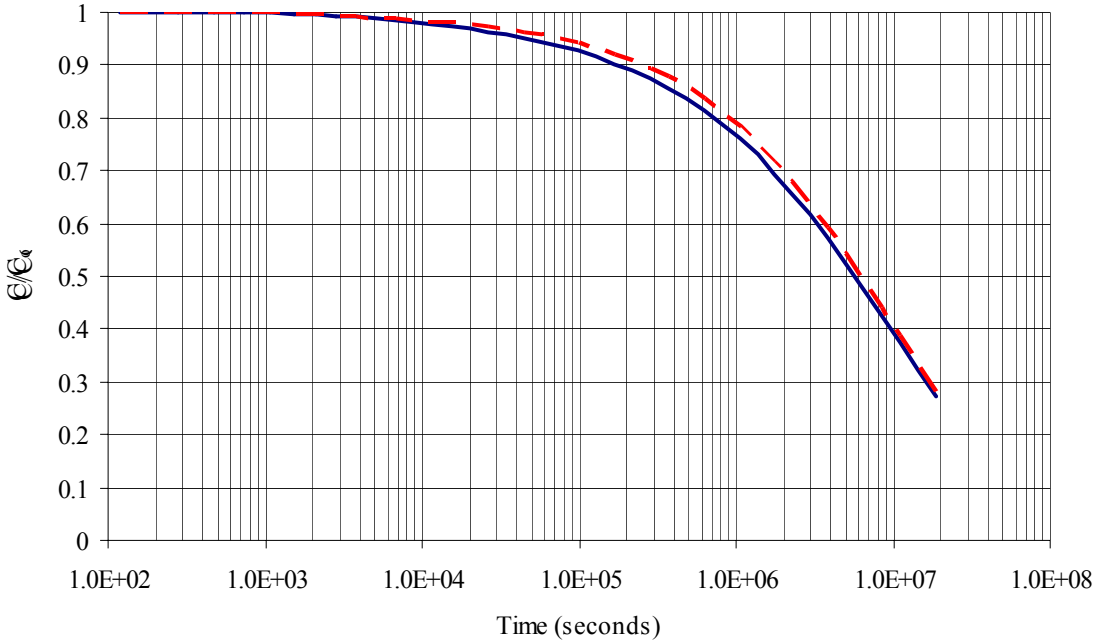

Figure 5-8. Influence of the well screen on the shape of the diffusion curve. The solid line represents an open area of 100%, and the dotted line an open area of 40%. Both simulations were performed with a soil D_e of 3.0 x 10^{-10} m^2/s.

A triangular screen with 40% open area was used for the *in situ* field experiment. For this system, a soil D_e of 3.0 x 10^{-10} m^2/s would be estimated at 2.8 x 10^{-10} m^2/s using a screenless mesh for the simulations (from Figure 5-7). This underestimation (<10%) was not considered significant, therefore it was not deemed necessary to include the screen in the mesh to accurately represent the *in situ* field experiment.

5.2.3 Best-Fit Diffusion Parameters

5.2.3.1 Evaluation of Uncertainty

The accuracy of the best-fit diffusion parameters determined using the numerical model was limited by the accuracy of input parameters used in the formulation of the model. These input parameters include well volume (represented by the well porosity), and well geometry.

The volumes used for the calculation of well porosity (n_{well}) are presented in Table 5-2. Uncertainty in any of these volumes can result in an over or underestimation in the calculation of n_{well}. The estimated uncertainty associated with each of these volumes is also summarized in Table 5-2. Volumes calculated from manufacturer specifications or direct physical measurements were considered to have minimal uncertainty and therefore were not considered to contribute to the overall uncertainty in n_{well}.

The volume of the well screen was calculated using the inner radius of the wire screen. Uncertainty in this value could result from deformation of the screen during installation and from soil pressures, or from sedimentation or swelling of soil into the screened volume. Examination of the screen using a downhole camera confirmed the presence of soil bulges through the screen mesh into the well volume. As noted above, this could have been the result of soil shaving into the screen volume during installation or soil swelling through the well screen after placement. Measurement of the soil volume inside the well screen was not possible. Given that some of the soil swelling was accounted for by assuming the well radius as the inner radius of the wire screen, the influence of additional swelling on the well volume was assumed to be negligible.

Large amounts of sedimentation in the well or screen deformation were not evident using the downhole camera. It was estimated that the decrease in the well volume associated with these factors was < 2% of the screened volume. As a result, the volume of the well screen was estimated to range from 1909mL to 1948mL.

Uncertainty in packer location creates uncertainty in the calculation of the volume contained in the steel riser pipe. Packer location was determined by lowering the packer until the long water tube at the base of the packer (Figure 3-4) touched the bottom of the well, raising the system by the desired distance (5 cm for well BD45-A and 6 cm for well BD45-C), and then securing the steel support cable to hold the packer system in place until the bladders could be inflated. A measurement from the top of the well to the top of the packer system after inflation of the packer system was attempted using an electronic tape. The presence of the water tubing and the transducer line made it difficult to ascertain the top of the packer system with the tape and measurements were unsuccessful.

If the water tube at the bottom of the well was bent, or the uninflated packer system was inclined at the bottom of the well when measuring the desired lift on the support line, the packer could have been located slightly lower in the well than desired. Slight movement of the packer system during securing and inflating could also have occurred. Assuming that the maximum uncertainty in packer placement was one centimeter, the volume of solution contained in the steel riser pipe was estimated to be 664 ± 30mL.

The volume contained in the sample tubing for each well could also be affected by packer placement, and could have an impact on measurements of equilibrium water

levels. The volume of water contained in one centimeter of tubing length was < 0.15 mL. Uncertainty associated with the volume of water contained in all the tubing was considered to be < 5 mL.

Table 5-2. Volumes used in calculation of well porosity for BD45-A (where different, values used for BD45-C calculation contained in brackets).

	Positive Volume (mL)			Negative Volume (mL)	Comments
	minimum	**calculated**	**maximum**		
1. Well screen	1909	1948	1948		Volume of screen calculated from inside wire radius that was determined from manufacturer specifications.
2. Screen support rods				63	From manufacturer specifications
3. Steel riser pipe	634	664	694		Volume in riser pipe below packer before packer inflation. Calculated from packer placement and manufacturer specifications of riser pipe.
4. Packer displacement				300	Volume displaced by packer hardware beneath bladder. Based on measurements of packer system dimensions.
5. Packer shrinkage	335	340	345		Due to packer shrinkage during inflation. Calculation from measured packer shrinkage.
6. Tubing	315 (255)	320 (260)	325 (265)		Volume contained in water sampling lines. Calculated from tubing measurements, packer depth in pipe and equilibrium water level.

From the values presented in Table 5-2, a range of n_{well} values were calculated taking the n_{well} as the total spiked volume contained within the diffusion well system (sum of volumes 1 through 5) divided by the screened volume (sum of volumes 1 and 2). The volume of solution contained in the tubing (volume 6) was not included as part of the total spiked volume in this calculation as mass contained in the tubing was considered to be unavailable for diffusion. The best estimate of n_{well} was determined using the minimum well screen volume and the calculated values for other volumes (Table 5-3).

Uncertainty in the well geometry not only affects the n_{well} calculation but also the surface area over which diffusion is occurring. Variation in the radius of the screen (r_{well}) could be caused by soil from the formation entering the well volume through the openings in the well screen as well as by physical deformation of the well screen, either caused by stress from the surrounding material or stresses during well installation. Soil extending beyond the inner radius of the well screen would cause a decrease in the effective r_{well}. A decrease in the effective r_{well} corresponds to a decrease in screen surface area, slowing the diffusion process. However, the bulges of soil created by the soil swelling or scraping through the screen wires would have greater surface area than a smooth cylinder with the same effective radius. Therefore the smaller effective r_{well} potentially created by soil swelling could be countered by the greater surface area of the soil bulges and, consequently, the change in radius caused by the presence of soil within the inner radius of the well screen was considered negligible. As previously discussed, variations in the r_{well} caused by physical deformation of the well screen were not

evident with the downhole imaging and any potential change in r_{well} was considered to be small. The uncertainty in r_{well} was estimated at one millimeter (Table 5-3).

From this discussion, the uncertainty in the source volume and well geometry of the field system were estimated. The uncertainty in these values is represented by uncertainty in the model input parameters of n_{well} and r_{well}. The range that best represents each of these parameters is summarized in Table 5-3. A best estimate of each parameter is also included in Table 5-3.

Table 5-3. Summary of uncertainty in the input parameters for the numerical model.

Well radius (r_{well}) (mm)			**Well porosity (n_{well})**		
minimum	best	maximum	minimum	best	maximum
34.9	35.9	36.9	1.37	1.38	1.39

5.2.3.2 Estimation of C_o

As discussed in Section 4.2.2, the initial δD values (C_o) measured for both wells appeared anomalous. By establishing the potential range in volume of the well reservoir, a range in theoretical C_o values was determined. The theoretical C_o, or the δD of the total spiked volume, was calculated using:

$$\left(\delta D_{total} \times (V_{total} + V_{spike})\right) = \left(\delta D_{spike} \times V_{spike}\right) + \left(\delta D_{bckgnd} \times V_{total}\right) \quad [5.3]$$

where: V = volume (L^3),
total = refers to the total spiked volume in the diffusion well,
spike = refers to the spiking solution, and
background = refers to *in situ* groundwater.

The δD values of the solutions used to spike each diffusion well were calculated to be 6570‰ and 6250‰ for BD45-A and BD45-C respectively (Table 4-5). Each of these spiking solutions had a volume of 200 mL. From the previous section, the total

spiked volume for well BD45-A was estimated to range between 2832 mL and 2951 mL and between 2772 mL and 2891 mL for well BD45-C.

For well BD45-A, it was necessary to account for the deuterium in the spiking solution that did not enter the diffusion well volume. For example, using the best estimate of the total spiked volume and the calculated δD of the spike solution (6570‰), the theoretical C_o for well BD45-A was calculated to be 273‰ (using Eq.[5.3]). This value was considerably different than the measured C_o value of 452‰, indicating that all of the deuterium contained in the spiking solution was not circulated into the diffusion well volume during the initial mixing. The difference between the measured and calculated C_o values, or the estimated amount of deuterium that did not circulate into the well system but remained in the spike solution, was 179‰. Therefore, the amount of deuterium contained in the spike solution that entered the diffusion well volume was approximated as 6570‰ (the δD of the spike solution) less 179‰, or 6391‰. Using 6391‰ for the δD of the spiking solution, Eq.[5.3] was used to calculate the best-estimate of C_o for BD45-A of 262‰.

Table 5-4. The range in total spiked volumes and the corresponding calculated C_o values for diffusion wells. Note that the maximum theoretical C_o corresponds to the minimum volume estimate.

Diffusion Well	**δD spike solution (‰)**	**Total Spiked Volume (mL)**			**Theoretical C_o (δD ‰)**		
		minimum	best	maximum	minimum	best	maximum
BD45-A	6570	2832	2870	2951	250	262	268
BD45-B	6250	2772	2810	2891	250	261	267

The input parameters used in the numerical model to determine the best-fit diffusion parameters included the well volume (represented by the well porosity) and well geometry, as well as the initial source concentration (C_o). Other than a minimal difference in C_o values, these input parameters are the same for both wells (Table 5-3 and Table 5-4). This information, along with similar rates of change in δD values measured during the diffusion experiment (see Section 4.2.2), suggested that wells BD45-A and BD45-C represent duplicate tests. Therefore, only the results of well BD45-C were used to constrain the range in best-fit diffusion parameters.

5.2.1.1 Determination of Diffusion Parameters

The range of n_{well}, r_{well}, and C_o outlined in the previous section can be used to constrain a range of potential best-fit diffusion parameters. Field n values were measured at 0.31±0.01 (Shaw and Hendry, 1998). Laboratory n values were calculated at 0.34±0.01. Using these measurements, the range in potential n_e values was 0.30 to 0.35. The maximum and minimum estimated n_{well}, r_{well}, and C_o were used to determine the best-fit D_e for the range of n_e values. These parameters are not independent. When

applying the maximum C_o value, the minimum r_{well} and minimum n_{well} must also be used. A best estimate of D_e was also determined using best estimated values for n_{well}, r_{well}, C_o, and n_e. The modelled scenarios and associated best-fit D_e values are presented in Table 5-5.

Table 5-5. Model input parameters and associated best-fit D_e values.

Input Parameters		C_o (δD ‰)	n_e	D_e (x 10^{-10} m^2/s)
r_{well} (mm)	n_{well}			
34.9	1.37	267	0.30	3.6
			0.31	3.3
			0.35	2.8
35.9	1.38	261	0.31	3.5
36.9	1.39	250	0.30	3.5
			0.31	3.2
			0.35	2.8

Estimates of D_e ranged from 2.8 x 10^{-10} m^2/s to 3.6 x 10^{-10} m^2/s. Each combination of n_e and D_e produces a similar minimum error value, indicating that there is no unique solution. Using the best estimates of model input parameters and fixing n_e at 0.31, the best estimate of D_e is 3.5 x 10^{-10} m^2/s.

5.3 Comparison of Diffusion Results

The *in situ* test results are in agreement with diffusion results determined from laboratory testing performed for this experiment. These tests suggest that the D_e for the till material at the King site is 3.5 x 10^{-10} m^2/s. This value is greater than D_e for δD that was determined from previous lab testing (radial diffusion cell tests) with till material from this site. These tests yielded a D_e of 1.7 x 10^{-10} m^2/s (Hendry and Wassenaar, 1999).

A D_e of 2.1 x 10^{-10} m^2/s for Cl^- was also obtained for this till material from radial diffusion cell testing (Hendry et. al., 2000). Their testing was conducted at 5°C on till samples obtained from depths of 16 m, 22 m, and 34 m. The results of this test can be compared to results obtained for δD through calculation of the apparent tortuosity factor (τ_a) for the till material (see Section 2.3.3). The self-diffusion coefficient (D_o) of Cl^- was taken to be 20.3 x 10^{-10} m^2/s at 25°C (Li and Gregory, 1974). This value was corrected to 5°C using the relationship between temperature and viscosity (Li and Gregory, 1974). Applying the corrected D_o and the measured D_e for Cl^- to Eq.[2.9], a value of 0.2 was calculated for τ_a. Table 5-6 summarizes the τ_a calculated for the testing conducted during this experiment as well as results from previous diffusion testing on this till material. The τ_a values calculated from δD diffusion testing were calculated using the D_o of water (26. 6 ± 1.2 x 10^{-10} m^2/s at 25°C (Wang et.al., 1953).

Table 5-6. Summary of τ_a determined from diffusion experiments in Birsay till.

Tracer	D_e **(x 10^{-10} m^2/s)**	τ_a
δD (this experiment)	3.5	0.2
δD (Hendry and Wassennar, 1999)	1.7	0.1
Cl^- (Hendry et.al., 2000)	2.1	0.2

Table 5-6 shows that the τ_a value calculated from the D_e determined for δD during this experiment is the same as the τ_a value determined from previous diffusion testing with

Cl^-. This provides further support to the results of the laboratory and *in situ* diffusion testing conducted during this study.

5.4 Large-Scale Field Comparison

This section includes a summary of the results of the large-scale δD field profile modelling completed at the King site by Hendry and Wassenaar (1999). Subsequently, the modelling conducted during that study was replicated using the till D_e determined during this study.

5.4.1 Aquitard Deuterium Profile

A profile of the δD contained in the pore water at the King site was obtained throughout the depth of the till-clay aquitard system (Hendry and Wassenaar, 1999). Modelling of this δD profile was used to estimate the vertical groundwater velocity through the aquitard system and provide insight into the timing of major geologic and climactic events. In order to use this profile to determine the average advective velocity and the timing of geologic and climatic events, known values of D_e and n_e must be applied. Radial diffusion cell testing was performed to determine the D_e and n_e for the δD in both the till and the clay. For both the materials, a D_e of 1.7 x 10^{-10} m^2/s and a n_e equal to the total porosity of the material were measured.

The δD values with depth were measured from pore water samples obtained from piezometers and radial diffusion cell equilibration of core samples. Well-defined trends were apparent throughout the depth of this aquitard system (Figure 5-9). The low δD values in the till (-178‰) were very similar to the estimated δD of Lake Agassiz (about -180‰) (Remenda et.al., 1994), and therefore were associated with Pleistocene glacial meltwater introduced in the till during deposition. The gradual

decrease in δD from the surface of the unoxidized till (-136‰) to the low of about -178‰ at about 30 m depth was explained by the introduction of precipitation at present day conditions (-136‰ is Saskatoon average). The δD values of -144‰ below about 105 m were associated with postdepositional recharge water that possibly entered the clay during an interglacial period. Development of the δD profile between the till and the clay was attributed to long-term diffusive mixing of the deuterium in the clay and till porewaters.

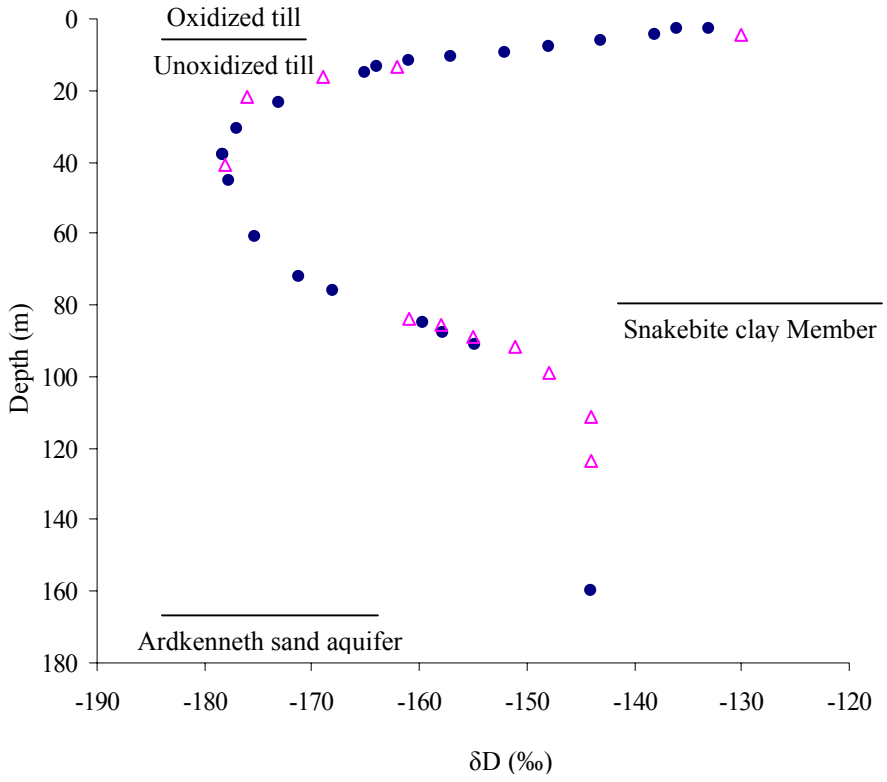

Figure 5-9. Pore water δD values with depth throughout the aquitard system. Circles represent values determined from piezometer samples and triangles represent values determined from radial diffusion cells (adapted from Hendry and Wassenaar, 1999).

Hendry and Wassenaar (1999) performed numerical simulations of the δD profile using POLLUTEv6 (Rowe and Booker, 1997). Groundwater head

measurements at and around the study site indicate mainly vertical flow, therefore a one-dimensional vertical model was applied to the system.

Transport of δD from the upper oxidized till to the underlying unoxidized till was examined separately from the development of the δD profile across the till-clay interface. For the till profile, the upper boundary was set at 4 m below ground surface (the surface of the unoxidized till) with a constant δD of -136‰, and the lower boundary of the model at infinite extent. Initial conditions throughout the depth of the till were set at δD of -178‰. For the simulation of the till-clay interface profile, the till deposited above the clay was assumed to be of infinite extent (initial δD of -178‰), with the lower boundary set at the top of the Ardkenneth aquifer at a fixed δD of -144‰. The initial δD of the clay was set at -144‰.

Assuming a steady-state flow through the till and clay, constant downward flux values ranging from 0.0 to 2.5 m/10ka were applied to the profile for times of 10, 20, and 30 ka. The profile modelling assumed constant hydraulic properties (i.e. gradient and conductivity) throughout the life of the aquitard.

5.4.2 Simulations of Aquitard δD Profile

Simulations were completed using SEEP/W and CTRAN/W to provide consistency with the rest of this document. To ensure the results provided with these programs were the same as results achieved with POLLUTEv6, simulations were performed with the same parameters described in Hendry and Wassenaar (1999) for comparison purposes. The results produced from the two separate modelling programs were in good agreement indicating the program used for this analysis was not an issue.

Using this same conceptual model outlined in the previous sections, simulations of the till-clay profile were performed using the diffusion parameters determined for the till during this study (D_e of 3.5 x 10^{-10} m^2/s, n_e of 0.31). Downward flux values ranging from 0.0 to 1.25 m/10ka were applied to the profile for times of 10, 20, and 30 ka (Figure 5-10).

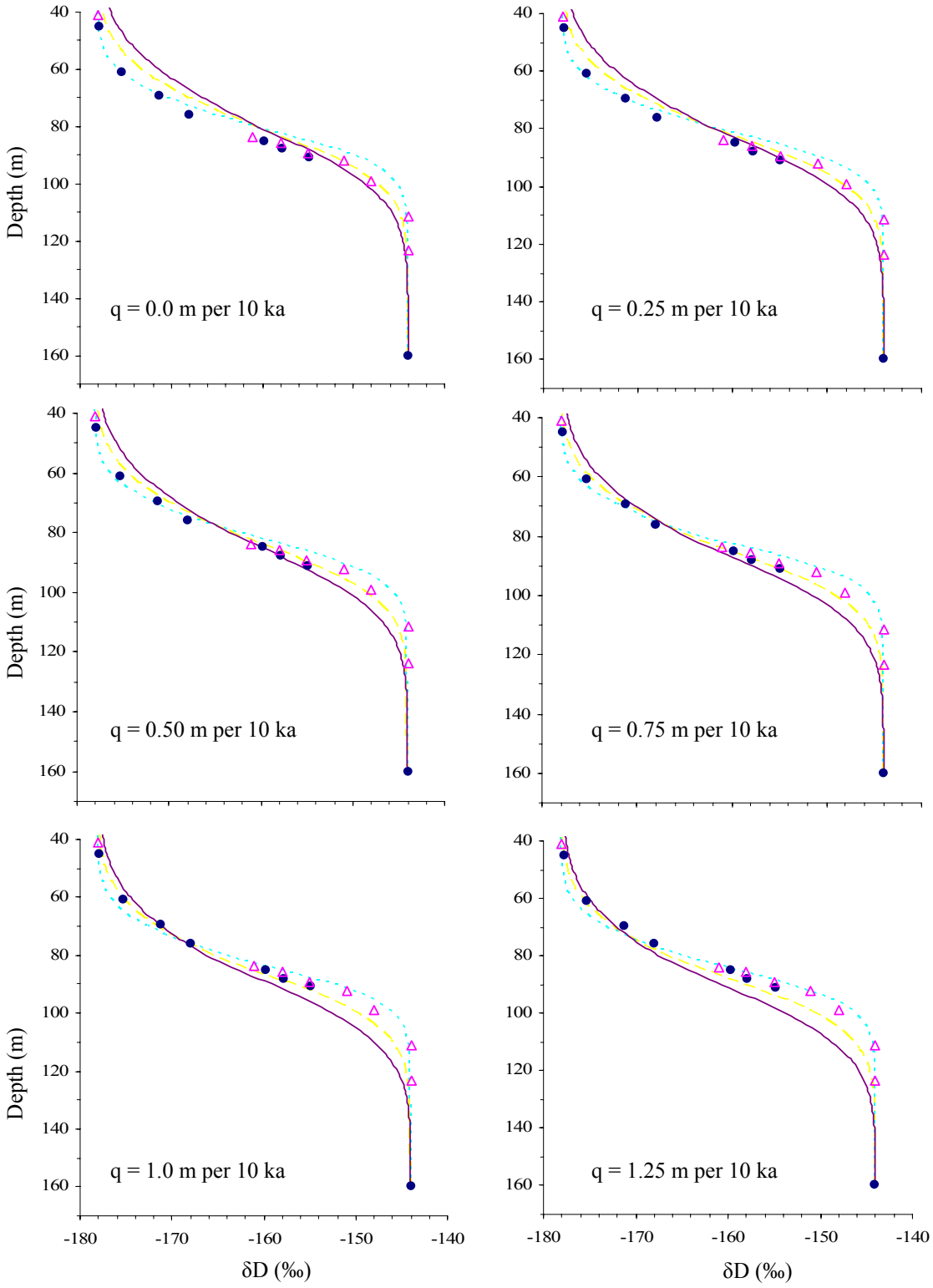

Figure 5-10. Measured and simulated pore water δD values across the till-clay interface for a range in transport times and downward fluxes. Dotted lines indicate a transport time of 10 ka, dashed lines 20 ka, and solid lines 30 ka. The till-clay interface is located at a depth of 80 m.

From visual examination, the best-fit simulation of the measured till-clay profile was obtained with a downward flux between 0.5 and 0.75 m/10ka for a time between 10 ka and 20 ka. Closer examination of these profiles indicates a best-fit time range for this profile between 15 ka and 20 ka (Figure 5-11).

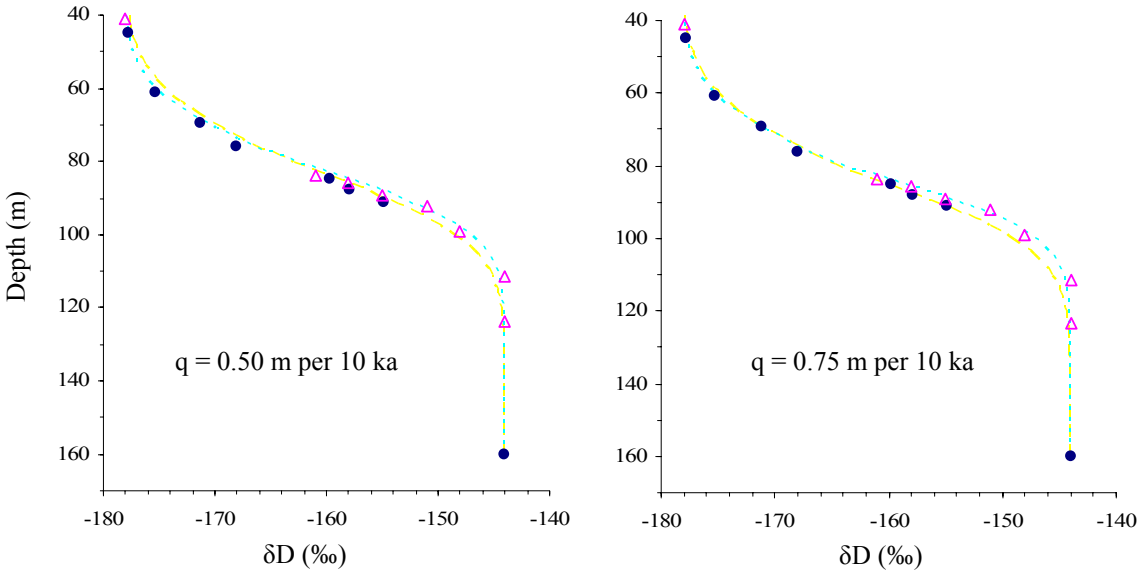

Figure 5-11. Measured and simulated pore water δD values across the till-clay interface for a range in transport times and downward fluxes. Dotted lines indicate a transport time of 15 ka, and dashed lines 20 ka.

Hendry and Wassenaar (1999) found a best-fit profile for the till-clay interface at a downward flux between 0.75 and 1.0 m/10ka and a transport time of 20 to 30 ka. This suggested that the till was deposited between 20 and 30 ka B.P. This time is in agreement with radiocarbon aging performed on organic samples found immediately below the Battleford Formation that suggest the till was deposited between 18 ka and 38 ka B.P. (Christianson, 1971). With a till D_e of 3.5 x 10^{-10} m^2/s, the best fit transport time for the till-clay interface was between 15 and 20 ka B.P. This time also fits within the understanding of the timing of the deposition of the Battleford till.

Applying the best-fit downward fluxes of 0.5 to 0.75 m/10ka to the δD transport from the oxidized to the unoxidized till material produces a best-fit transport time between 5 ka and 7.5 ka (Figure 5-12).

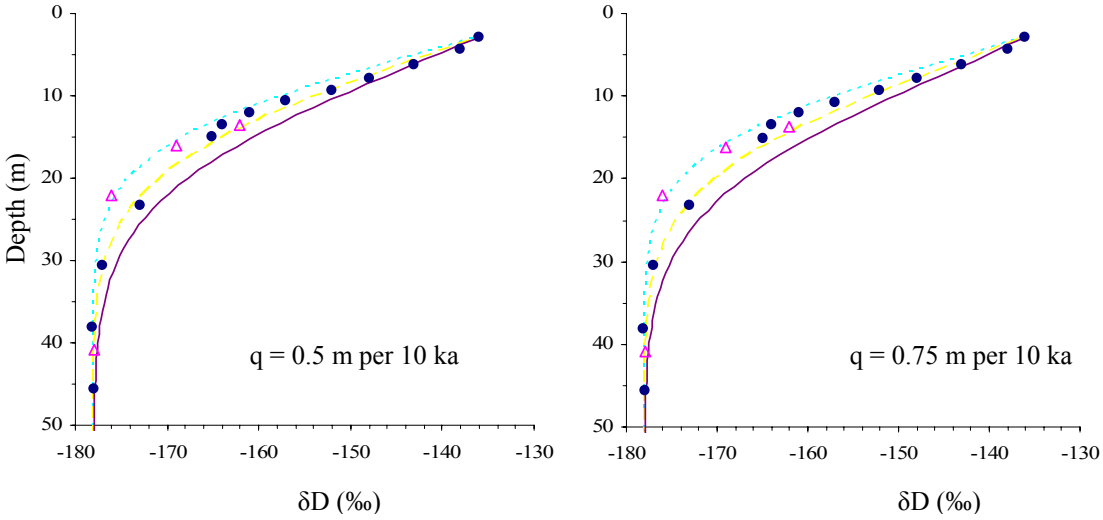

Figure 5-12. Measured and simulated pore water δD values throughout the unoxidized till. The dotted line represents a transport time of 5 ka, the dashed line 7.5 ka and the solid line 10 ka. The interface between the oxidized and unoxidized till is located at approximately 4 m depth.

The time required to develop the δD profile from the oxidized till to the unoxidized till material was associated with the introduction of precipitation with present day δD (-136‰), or the transition to climactic conditions of the Holocene 12 ka B.P. to 10 ka B.P. (Greenland Ice-Core Project Members, 1993). Hendry and Wassenaar (1999) determined a best-fit development time of 7.5 to 10 ka for this profile. Allowing for time required to oxidize the upper 3 to 4 m of till, the time estimate obtained from this profile was determined to be in good agreement with the start of the Holocene.

Assuming the timeline of the till δD profile development corresponds to the on-set of the Holocene, a till D_e of 3.5 x 10^{-10} m^2/s does not produce a fit to measured data using downward flux values of 0.5 to 0.75 m/10 ka. These flux values are higher than values measured for the site. Shaw and Hendry (1998) calculated the downward linear velocity through the till to be between 0.5 and 0.8 m/10ka downward based on measured K values, the measured hydraulic gradient and measured porosity. Using a measured porosity of 0.31 for the till, this corresponds to a calculated flux of 0.16 to 0.25 m/10ka. Applying a downward flux of 0.25 m/10ka to the till-clay profile (using a till D_e of 3.5 x 10^{-10} m^2/s), a range of curves similar to those obtained with a downward flux of 0.5 m/10ka can be simulated by placing the δD interface at approximately 1.5 m below the till-clay interface (Figure 5-13).

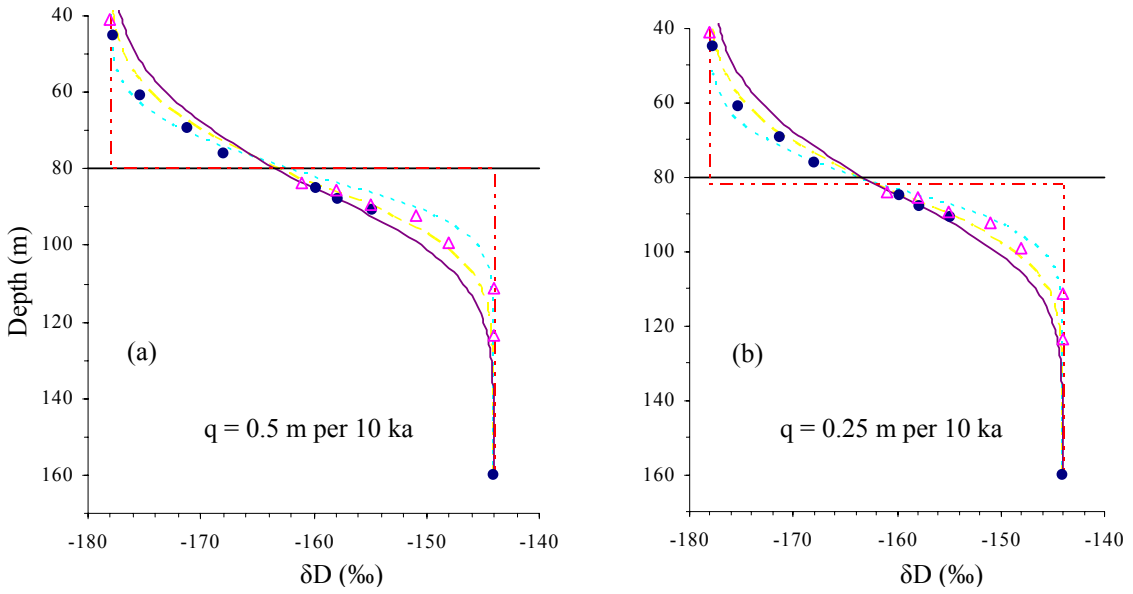

Figure 5-13. Measured and simulated pore water δD values across the till-clay interface for downward flux values of a) 0.5 m/10ka and b) 0.25 m/10ka. The till-clay interface is located at a depth of 80 m and indicated by a solid line. The dash-dotted line represents the initial concentration profiles. Dotted lines indicate a transport time of 10 ka, dashed lines 20 ka, and solid lines 30 ka.

This fit could be explained by the possible presence of a weathered and fractured zone at the top of the clay layer.

A fit to the measured δD profile across the till-clay interface with a flux of 0.25 m/10ka was also obtained by setting the initial δD in the till material to -180‰ . Figure 5-14 shows a fit obtained for a transport times of approximately 20 ka.

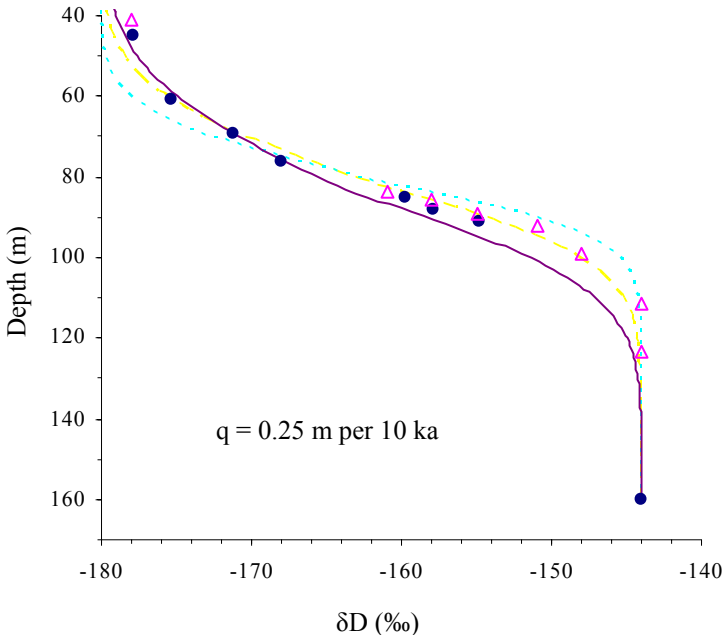

Figure 5-14. Measured and simulated pore water δD values across the till-clay interface for a downward flux of 0.25 m/10ka. The initial concentration profile throughout the till thickness is -180‰. Dotted lines indicate a transport time of 10 ka, dashed lines 20 ka, and solid lines 30 ka.

Applying the lower downward flux value of 0.25 m/10ka to the unoxidized till δD profile, a best-fit transport time of approximately 7.5 ka was determined (Figure 5-15). Allowing approximately 2.5 ka for oxidation of the upper 3 to 4 m of the till (Hendry and Wassenaar, 1999), this estimate agrees well with the timing of the Holocene (12 ka B.P. to 10 ka B.P.).

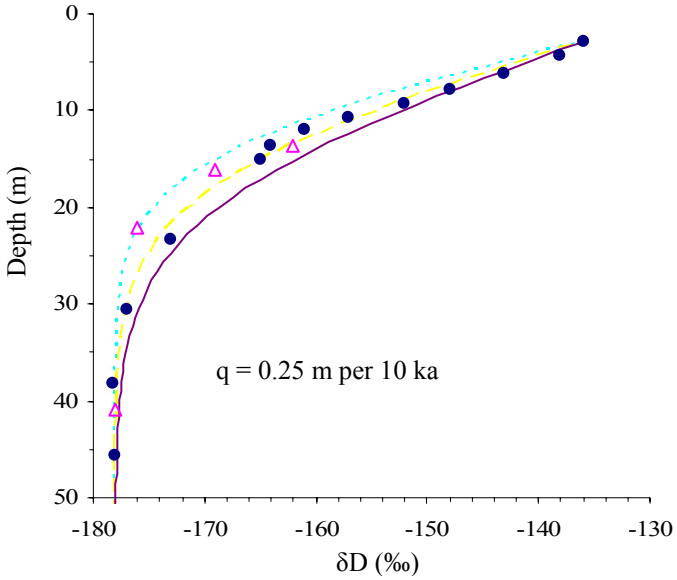

Figure 5-15. Measured and simulated pore water δD values throughout the unoxidized till at a downward flux of 0.25 m/10ka. The dotted line represents a transport time of 5 ka, the dashed line 7.5 ka and the solid line 10 ka. The interface between the oxidized and unoxidized till is located at approximately 4 m depth.

5.4.3 Summary of Large-Scale Field Comparison

To develop the conceptual model of the δD profile through this aquitard system, a number of assumptions were required (i.e. the soil characteristics of the clay-till interface, the initial δD value in the till material). Variations in these assumptions can produce different estimations of the D_e used to best-fit profile development.

The values obtained for transport time and advective flux using the two different D_e values for the till material are different, but both results can be supported. This intimates that even for diffusion-dominated systems, the uncertainty in other factors required for interpretation of naturally occurring, long-term profiles (i.e. geologic time-scale, initial conditions) does not allow or require highly precise D_e measurements.

5.5 Summary

Analysis and interpretation of diffusion testing results from conventional laboratory testing and field testing was performed. Numerical modelling was performed to determine the range in effective diffusion parameters that best represent each test environment (lab and field). Modelling of a long-term δD profile previously reported for the King site was performed to compare the results of the diffusion testing performed here with previous diffusion testing results.

Numerical modelling of the laboratory experiment was performed using SEEP/W and CTRAN/W. The best-fit D_e was determined by minimizing the calculated error between the measured and simulated data as described in Section 3.5. By fixing the n_e equal to the n calculated using a mass balance, a best-fit D_e of 3.5 to 4.0 x 10^{-10} m^2/s was determined for the laboratory experiment.

Field K values ranging from 6.7 x 10^{-11} m/s to 1.6 x 10^{-10} m/s were calculated from water level recovery data. These results, along with support from previous studies, suggest that advection in the till is very slow and solute transport should be dominated by diffusion.

Interpretation of the field experiment results was also completed through numerical modelling using SEEP/W and CTRAN/W. The model was optimized by simplifying the mesh design. Modelling of the fine details of the well screen indicated that the presence of the well screen would have no significant effect on the determination of the best-fit diffusion parameters for this system.

To determine the diffusion parameters that best describe the field system, uncertainty in the model input parameters was quantified. Well volume (represented by

well porosity), well geometry, and the initial δD value in the well were examined for uncertainty. By applying a reasonable range in values for these parameters and fixing appropriate values for n_e, D_e values for the system were predicted to range from 2.8×10^{-10} to 3.6×10^{-10} m^2/s. The best-fit value for the D_e of the field system, determined by applying the most reasonable model input parameters, was 3.5×10^{-10} m^2/s.

Analysis of the field and laboratory experiments shows good agreement in the determination of the D_e. Laboratory results yielded a D_e of between 3.5×10^{-10} and 4.0×10^{-10} m^2/s and field results yielded a D_e of 3.5×10^{-10} m^2/s. These values were greater than results obtained from radial diffusion cell testing performed on the till material from this site, which estimated a D_e of 1.7×10^{-10} m^2/s (Hendry and Wassenaar, 1999). Apparent tortuosity values calculated from radial diffusion cell measurements of the D_e for Cl^- correspond well with the τ_a calculated for the δD D_e determined during this experiment. The D_e determined from the radial diffusion cell testing had previously been applied to analysis of long-term δD profiles established from pore water analysis throughout the depth of the aquitard at this site. The same modelling exercise was performed with the D_e of 3.5×10^{-10} m^2/s determined from this experiment. The values obtained for transport time and advective flux using the two different D_e values for the till material are different, but both results can be supported. This indicates that the development of long-term solute profiles is not overly sensitive to the value of D_e used.

For long-term predictive modelling of a known contaminant source, some of these model conditions may be easier to determine, but similar uncertainties in the

system would exist. For example, the initial contaminant profile may be easier to determine, but uncertainties in changing source characteristics or exact geologic conditions may overshadow some uncertainty in diffusive transport rates. Therefore, very precise measurements of D_e are likely not required for contaminant transport prediction in thick till aquitard systems. More accurate measurement may be more useful in barrier systems such as clay liners or slurry walls, where the characteristics of the diffusion-dominated zone are easier to define and the transport path is shorter relative to the transport time.

CHAPTER 6 SUMMARY AND CONCLUSIONS

This chapter includes a summary of the work presented in this document. Conclusions that can be drawn from this work are presented along with recommendations for future research in this area.

6.1 Summary

In the study of hydrogeology and related disciplines, the greatest challenge is not applying contaminant transport models to field systems but adequate characterization of the appropriate mechanisms and associated material properties.

The purpose of this study was to develop a field-based method to measure the coefficient of molecular diffusion in an aquitard and to evaluate the results obtained from this method by comparing them to the results obtained from conventional lab-scale testing and the back-analysis of a previously obtained field-scale diffusion profile.

The *in situ* experiment consisted of three wells installed at the King site, near Birsay, Saskatchewan. The wells were completed in the unfractured, unoxidized zone of the aquitard. Hydraulic conductivity values calculated from the water level recovery measurements taken after well installation confirmed diffusion-dominated conditions.

Packer systems were placed in two of the wells after the water had reached a sufficient level to allow isolation of an adequate volume for spiking and measuring. The packer systems consisted of a borehole packer, two water lines, and a pressure transducer. The packer isolated the water reservoir at the bottom of the well, while the

water lines allowed for spiking and sampling of that reservoir using a pump system at surface. Pressure transducers were used for monitoring the water levels in the wells.

After installation of the packer systems, the systems were left for two weeks to allow water levels to equilibrate. When static levels had been obtained, the wells were spiked with the conservative tracers oxygen-18 and deuterium. The concentrations of these tracers were monitored with time. Numerical modelling was performed to determine the best-fit diffusion coefficient for the data.

Laboratory diffusion measurements were completed on Shelby tube samples retrieved from the intake zones of wells during installation. Groundwater from the same completion depth as the wells was used to set up six double reservoir diffusion cells. The cells were spiked with the same conservative tracers used for the *in situ* experiments.

Results of the diffusion testing were applied to a previously determined δD field profile and compared to previous diffusion testing performed on this till.

6.2 Conclusions

- Laboratory double reservoir diffusion testing on the Shelby tube samples show a high level of reproducibility, with the difference in measurements between the cells typically less than 3%. Control cell measurements indicate that the materials used to construct the double reservoir cells did not have an impact on the isotope tracers.
- Porosity values determined from the diffusion cell tests were greater those measured previously on field samples but fall in the same range as those from earlier laboratory diffusion experiments. This difference

could be due to swelling of the till material as a result of lack of confining pressure in the diffusion cell experiments. Simulations indicate that slight differences in n_e do not have a great effect on the measured values of D_e, but this effect may be more significant for samples collected at greater depths.

- The hydraulic conductivity determined from the diffusion wells was calculated to range from 6.7×10^{-11} m/s to 1.61×10^{-10} m/s. These values are consistent with previously measured laboratory and field-based K values. These low K values, along with the fact that the BD45-A, -B, and –C piezometers were installed in 'dry' boreholes, indicate that diffusion, rather than advection, is the dominant transport mechanism in this till.
- A two-dimensional mesh with a line of symmetry taken along a horizontal axis passing through the middle of the well screen provided the best balance of simulation accuracy and numerical model simplicity in modelling the *in situ* diffusion experiment.
- The well screen used for this experiment did not have a significant effect on the determination of the D_e.
- A well screen with a rectangular cross-section has a much greater effect on the best-fit soil D_e than the triangular screen utilized in this study.
- The difference in D_e caused by incorporating a screen into the simulation is manifested mainly at the beginning of the diffusion curve where the rapid drop in concentration occurs.

- Uncertainty in system parameters such as well volume and well geometry introduce uncertainty into the determination of D_e. By estimating the range in model input parameters, a range in soil D_e of 2.8 to 3.6 x 10^{-10} m^2/s was estimated.
- The excellent agreement between D_e values determined from laboratory and *in situ* diffusion experiments indicate that a D_e of 3.5 x 10^{-10} m^2/s represents δD diffusion in the till material examined.
- The τ_a value calculated from the D_e determined for δD during this experiment is the same as the τ_a value determined from previous diffusion testing with Cl^-. This is further support for the results of the laboratory and *in situ* diffusion testing conducted during this study.
- Representative results were obtained with this relatively simple method of *in situ* testing.
- The δD D_e determined from the laboratory and *in situ* testing performed for this experiment was higher than D_e values obtained for δD from previous laboratory testing.
- Examination of the naturally occurring long-term δD profile for the Birsay site indicates that even for diffusion-dominated systems, the uncertainty in other factors required for interpretation of naturally occurring, long-term profiles does not allow or require highly precise D_e measurements.

6.3 Application of Research

The method of *in situ* testing described in this document could be applied to other diffusion-dominated systems such as compacted clay liners. The *in situ* testing may be useful in systems where representative sample retrieval may be difficult. Once installed, the *in situ* system could be used for repeated diffusion testing. The diffusion wells are constructed like conventional piezometers and therefore could be used for other types of testing, including sampling and monitoring.

6.4 Recommendations

Additional testing would provide the opportunity to improve and optimize the *in situ* diffusion testing procedure.

The field methodology presented here required the use of a packer system for maintaining the size of the reservoir and controlling the advective movement of water in and/or out of the wells. Information gathered near the completion of the test from BD45-A was compromised due to the failure of the packer system. Other options for this packer system should be investigated.

The initial, or time zero, samples collected from both diffusion wells were retrieved from the replacement solution vessel rather than directly from the well reservoirs. Collection of all samples directly from the well reservoir would ensure representative samples. Sample collection was performed on an increasing time scale. Tightening that time scale during the beginning of the test could provide more definition of the initial the drop-off of the diffusion curve. This would allow more precise fitting of the diffusion curve and help identify any possible outliers in the data.

Varying the size of the diffusion reservoir within the wells may provide additional information on the accuracy of the methods of back-analysis to determine D_e. Increasing the size of the reservoirs would increase the time scale for diffusion, effectively spreading out the diffusion curve, allowing a larger number of samples to be taken during the initial stage of diffusion, and ultimately influencing a greater volume of the aquitard. Comparison of the results obtained by matching these curves with those obtained from smaller, and therefore quicker, diffusion tests would help optimize the time required to perform the diffusion tests.

Two-dimensional modelling was required to accurately represent the diffusion well system. Increasing the relative length of the screened zone would decrease the importance of any vertical diffusion, allowing the system to be represented with a one-dimensional mesh. This would greatly simplify the modelling requirements.

A concern with relying on *in situ* data obtained from wells is the presence of a disturbed zone or "skin" surrounding the well screen caused by stresses induced while boring and installing the well. The presence of this skin can result in parameter estimations that are not representative of the undisturbed soil matrix. D'Astous (1989) performed visual examinations of skins (smearing) produced by different installation methods in clayey glacial deposits. Those wells completed using a Shelby tube (the method employed in this study) resulted in the minimum disturbance, with skins ranging in thickness from 0.10 – 0.15 cm. The presence of a disturbed zone immediately adjacent to borehole walls was also noted during *in situ* diffusion testing performed in low permeability rock (Phalut et.al., 2003; Vilks et.al., 2003). The presence of soil bulges between the wire wraps of the screen was observed during this

study. This indicates altered properties of the material from some distance outside the well screen. The potential effects of a layer of soil with altered transport properties should be investigated. Initially, modelling exercises would help to provide information on the relative importance of such a layer. As previously discussed, performance of a conservative diffusion test using a larger reservoir volume would allow more accuracy near the beginning of the test. This is likely when any potential skin effects are manifested and therefore would help to provide a measurement of diffusion rates across this zone.

This research focused on diffusive transport of the isotopes of water in a naturally occurring aquitard system. Understanding long-term diffusive transport from a waste containment facility requires knowledge of the transport of high ionic strength solutions as well as more reactive molecules.

The ionic strength of the pore water has been correlated to the thickness of the double diffuse layer of clay particles, which has been shown to have an effect on transport properties. This phenomenon has been recognized as having a significant influence on the transport properties of soil (Mitchell, 1976). Van der Kamp et. al. (1996) acknowledges that the presence of the double diffuse layer may influence diffusion rates and the effective porosity for particular ions in some types of geological media. Experimental results agree with this, showing D_e to vary not only with the nature of the solute of interest and the media, but also the electrolyte composition and concentration (Shackelford and Daniel, 1991; Barone, 1989). Practically, this means that long-term estimates of contaminant transport in diffusion-dominated systems should include the effect of increasing ionic strength due to introduction of a

contaminant, as well as the decreasing of this ionic strength with time as mixing with background porewater dilutes the contaminant plume. Studying the effect of increasing the ionic strength of the solution on the movement of conservative ions could provide some insight into the relative importance of the ionic strength of solution on diffusion.

LIST OF REFERENCES

Ball, William P., Chongxuan Liu, Guoshou Xia, and Dirk F. Young. 1997. A diffusion-based interpretation of tetrachloroethene and trichloroethene concentration profiles in a groundwater aquitard. Water Resources Research 33(12):2741 – 2757.

Barone, F.S., E.K. Yanful, R.M. Quigley, and R.K. Rowe. 1989. Effect of multiple contaminant migration on diffusion and adsorption of some domestic waste contaminants in a natural clayey soil. Canadian Geotechnical Journal, 26: 189 – 198.

Boldt-Leppin, B.E.J. and M.J. Hendry. 2003. Application of harmonic analysis of water levels to determine vertical hydraulic conductivities in clay-rich aquitards. Ground Water, 41(4): 514 – 522.

Christiansen, E.A. 1971. Tills in southern Saskatchewan, Canada. In: *Till: a symposium*, R.P. Goldthwait (ed.). Ohio State University Press, Columbus, p.14.

Crank, J. 1975. *The mathematics of diffusion*, 2nd ed., Clarendon Press, Oxford, England.

Crooks, V.E. and R.M. Quigley. 1984. Saline leachate migration through clay: A comparative laboratory and field investigation. Canadian Geotechnical Journal, 21(2): 349-362.

D'Astous, A.Y., W.W. Ruland, J.R.G. Bruce, J.A. Cherry, and R.W. Gillham. 1989. Fracture effects in the shallow groundwater zone in weathered Sarnia-area clay. Canadian Geotechnical Journal, 26: 43-56.

Desaulniers, D.E., J.A. Cherry and P. Fritz. 1981. Origin, age, and movement of pore water in argillaceous Quaternary deposits at four sites in southwestern Ontario. Journal of Hydrology, 50: 231 – 257.

Desaulniers, Donald E., and J.A. Cherry. 1989. Origin and movement of groundwater and major ions in a thick deposit of Champlain Sea clay near Montreal. Canadian Geotechnical Journal, 26: 80-89.

Donahue, R.B., S.L. Barbour, J.V. Headley. 1999. Diffusion and adsorption of benzene in Regina clay. Canadian Geotechnical Journal, 36: 430 – 442.

Freeze, R.A. and J.A. Cherry. *Groundwater*, 604 pp. Prentice-Hall, Inc., Englewood Cliffs, New Jersey, 1979.

GEO-SLOPE, 2004. GeoStudio Users Manual. GEO-SLOPE International Ltd., Calgary, Alberta, Canada.

Goodall, D.C. and R.M. Quigley. 1977. Pollutant migration from two sanitary landfill sites near Sarnia, Ontario. Canadian Geotechnical Journal, 14(2):223-236.

Greenland Ice-Core Project Members. 1993. Climate instability during the last interglacial period recorded in the GRIP ice core. Nature, 364: 203 – 207.

Hendry, M.J., and L.I. Wassenaar. 1999. Implications of the distribution of δD in pore waters for groundwater flow and the timing of geologic events in a thick aquitard system. Water Resources Research, 35(6): 1751 – 1760.

Hendry, M.J. and L.I. Wassenaar. 2000. Controls on the distribution of major ions in pore waters of a thick surficial aquitard. Water Resources Research, 36(2):503-513.

Hendry, M.J., L.I. Wassenaar, and T. Kotzer. 2000. Chloride and chlorine isotopes (^{36}Cl and $\delta^{37}Cl$) as tracers of solute migration in a thick clay-rich aquitard system. Water Resources Research, 36: 285-296.

Hendry, M.J., J.R. Ranville, B.E.J. Boldt-Leppin, and L.I. Wassenaar. 2003. Geochemical and transport properties of dissolved organic carbon in a clay-rich aquitard. Water Resources Research, 39(7):1194.

Hendry, M.J., T.G. Kotzer, and D.K. Solomon. 2005. Sources of radiogenic helium in a clay till aquitard and its use to evaluate the timing of geologic events. Geochimica et Cosmochimica Acta, 69(2): 475 – 483.

Horton, R., M.L. Thompson, and J.F. McBride. 1985. Estimating transit times of non-interacting solutes through compacted soil material. Soil Science Society of America Journal, 51: 48 – 53.

Hvorslev, M.J. 1951. Time lag and soil permeability in groundwater observations. Bulletin No. 36, Waterways Experiment Station Corps of Engineers. U.S. Army, Vicksburg, Mississippi.

Johnson, R.L., J.A. Cherry, and J.F. Pankow. 1989. Diffusive contaminant transport in natural clay: A field example and implications for clay-lined waste disposal sites. Environ. Sci. Technol., 23(3): 340 – 349.

Kemper, W.D. 1960. Water and ion movement in thin films as influenced by the electrostatic charge and diffuse layer of cations associated with clay mineral surfaces. Soil Science Society of America Proceedings, 24:10-16.

King, K.S., R.M. Quigley, F. Fernandez, D.W. Reades and A. Bacopoulos. 1993. Hydraulic conductivity and diffusion monitoring of the Keele Valley Landfill liner, Maple, Ontario. Canadian Geotechnical Journal, 30: 124 – 134.

Lawrence, J.R. and H.P. Taylor, Jr. 1972. Hydrogen and oxygen isotope systematics in weathering profiles. Geochimica et Cosmochimica Acta, 36: 1377 - 1393.

Li, Y.-H., and S. Gregory. 1974. Diffusion of ions in sea water and deep-sea sediments. Geochimica et Cosmochimica Acta, 30: 703 – 714.

Liu, C. and W.P. Ball. 1999. Application of inverse methods to contaminant source identification from aquitard diffusion profiles at Dover AFB, Delaware. Water Resources Research, 35(7): 1975 – 1985.

Meegoda, N.J., and S.D. Gunasekera. 1992. A new method to measure the effective porosity of clays. Geotechnical Testing Journal, 15(4): 340 – 351.

Mitchell, J.K. 1976. *Fundamentals of Soil Behaviour.* John Wiley & Sons, Inc. New York.

Novakowski, K.S. and G. van der Kamp. 1996. The radial diffusion method 2. A semianalytical model for the determination of effective diffusion coefficients, porosity, and adsorption. Water Resources Research, 32: 1823 – 1830.

Pearson, F.J. 1999. What is the porosity of mudrock? In: *Muds and Mudstones: Physical and Fluid Flow Properties*. A.C. Applin, A.J. Fleet and J.H.S. MacQuaker (eds). The Geological Society of London, Special Publication 158: 9-12.

Peyton, G.R., J.P. Gibb, M.H. LeFaivre and J.D. Ritchey. 1985. On the concept of effective porosity and its measurement in saturated fine-grained porous media. Proceedings of the Second Canadian / American Conference on Hydrogeology: Hazardous Wastes in Groundwater: A Soluable Dilemma. Banff, Alberta June 25 – 29. National Water Well Association, pp. 101 – 107.

Phalut, J.-M., Ph. Montarnal, A. Gautschi, E. Tevissen, and E. Mouche. 2003. Characterisation of HTO diffusion properties by an in situ tracer experiment in Opalinus clay at Mont Terri. Journal of Contaminant Hydrology, 61: 203 – 218.

Quigley, R.M., and R.K. Rowe. 1986. Leachate migration through clay below a domestic waste landfill, Sarnia, Ontario, Canada: Chemical interpretation and modeling philosophies. In *Hazardous and Industrial Solid Waste Testing and Disposal* Vol 6 D. Lorenzen et.al.(eds) ASTM STP 933 American Society for Testing and Materials, Philadelphia. pp. 93 – 103.

Quigley, R.M., E.K. Yanful and F. Fernandez. 1987. Ion transfer by diffusion through clayey barriers. *Geotechnical practice for waste disposal, Special Pub. No. 13*, R.C. Woods (ed.), ASCE, New York, N.Y., pp. 137-158.

Robinson, R.A. and R.H. Stokes. 1959. Electrolyte solutions. 2nd ed. Butterworths, London.

Remenda, V.H., J.A. Cherry, and T.W.D. Edwards. 1994. Isotopic composition of old groundwater from Lake Agassiz: Implications for later Pleistocene climate. Science, 266: 1975 – 1978.

Remenda, V.H., G. van der Kamp, and J.A. Cherry. 1996. Use of vertical $\delta^{18}O$ profiles to constrain estimates of hydraulic conductivity in a thick, unfractured aquitard. Water Resources Research 32: 2979 – 2987.

Rowe, K.R. 1987. Pollutant transport through barriers. *Geotechnical Practice for Waste Disposal, Special Pub. No. 13*, R.C. Woods (ed.), ASCE, New York, N.Y. pp. 159-181.

Rowe, K.R., C.J. Caers, and F. Barone. 1988. Laboratory determination of diffusion and distribution coefficients of contaminants using undisturbed clayey soil. Canadian Geotechnical Journal, 25: 108 – 118.

Rowe, K.R. and J.R. Booker. 1997. POLLUTE Users Guide, 6th ed., GAEA Environ. Engin. Ltd., Windsor, Ont., Canada.

Sauchyn, D.J. 1990. A reconstruction of Holocene geomorphology and climate, western Cypress Hills, Alberta and Saskatchewan. Canadian Journal of Earth Sciences, 27: 1504 – 1510.

Shackelford, C.D. 1991. Laboratory diffusion testing for waste disposal – A review. Journal of Contaminant Hydrology, 7: 177 – 217.

Shackelford, C.D. and D.E. Daniel, 1991. Diffusion in saturated soil. I: Background. Journal of Geotechnical Engineering, 117: 467 – 483.

Shaw, R.J. and M.J. Hendry. 1998. Hydrogeology of a thick clay till and Cretaceous clay sequence, Saskatchewan, Canada. Canadian Geotechnical Journal, 35: 1041 – 1052.

Stephens, D.B., K.C. Hsu, M.A. Prieksat, M.D. Ankeny, N. Blandford, T.L. Roth, J.A. Kelsey, and J.R. Whitworth. 1998. A comparison of estimated and calculated effective porosity. Hydrogeology Journal, 6: 156 – 165.

van der Kamp, G., and E.J. Jaworski, 1989. Luck Lake irrigation project: groundwater monitoring to December, 1989. Saskatchewan Research Council, Publication No. R-1220-5-C-89.

van der Kamp, G., D.R. Van Stempvoort, and L.I. Wassenaar. 1996. The radial diffusion method. 1. Using intact core to determine isotopic composition, chemistry, and effective porosities for groundwater in aquitards. Water Resources Research, 32(6): 1815 – 1822.

Van Rees, K.C.J., E.A. Sudicky, P.S.C. Rao, and K.R.Reddy. 1991. Evaluation of laboratory techniques for measuring diffusion coefficients in sediments. Environmental Science and Technology, 25(9): 1605 – 1611.

van Schaik, J.C. and W.D. Kemper. 1966. Chloride diffusion in clay-water systems. Soil Science Society of America Proceedings, 30:22-25.

van Schaik, J.C., W.D. Kemper and S. R. Olsen. 1966. Contribution of adsorbed cations to diffusion in clay-water systems. Soil Science Society of America Journal, 30:17-22.

Vilks, P., J.J. Cramer, M. Jensen, N.H. Miller, H.G. Miller, F.W. Stanchell. 2003. In situ diffusion experiment in granite: Phase I. Journal of Contaminant Hydrology, 61: 191 – 202.

Wang, J.H., C.V. Robinson, and I.S. Edelman. 1953. Self-diffusion and structure of liquid water, III, Measurements of the self-diffusion liquid water with H^2, H^3, and O^{18} as tracers. Journal of the American Chemical Society, 75: 466 – 470.

Wassenaar, L.I. and M.J. Hendry. 2000. Mechanisms controlling the distribution and transport of ^{14}C in a clay-rich till aquitard. Ground Water, 38(3): 343 - 349.

APPENDIX A: FIELD DIFFUSION EXPERIMENTAL PROCEDURES

A1. Procedure for Spiking Diffusion Wells

1. Mark water level on spike container
2. Put on rubber gloves
3. Push black spaghetti tubing down shallow* end of ¼" tubing
4. Install length of flexible tubing from center of 1/8" tubing lengths into pump head
5. Place other end of 1/8" line into spike container
6. On low pump setting (approx. 1 or 2 on Masterflex pump), begin sucking** from spike container.
7. Continue pumping until deep ¼" line is completely filled with water
8. Place deep ¼" line into spike bottle
9. Reverse pump, allowing water to be sucked down deep line
10. Keeping both the 1/8" line and the deep ¼" line in the spike bottle, continue to pump for approximately 40 minutes on a medium high setting (level 6 on Masterflex). Note start time and enter on field data sheet.
11. Remove deep ¼" line from spike container
12. Continue to pump with 1/8" line spitting water into spike container until water level reaches full mark. Note time and enter on field data sheet
13. Stop pump, remove line from spike container. Cap container and set aside.
14. Remove and disassemble pump head
15. Allow water to drain through 1/8" line. Slowly start to pull 1/8" line from shallow ¼"
16. Place 1/8" line in appropriate plastic bag
17. Remove 5mL of solution from spike container and place in 15mL sample jar for time zero sample.

A2. Procedure for Sampling Diffusion Wells

1. Put on rubber gloves
2. Retrieve appropriate 1/8" line for well
3. Push one end of 1/8" down deep ¼" tubing*
4. Place other end in 15mL sample container**.
5. On low pump setting (1 on Masterflex pump), suck** water through 1/8" until it comes out the end at surface. Stop pump. Cap 15mL container.
6. Push end of 1/8" line at surface down shallow ¼" line
7. Reverse pump and let run for 30-40 minutes at medium high setting (6 on Masterflex). Note pumping start time and enter on field data sheet.
8. Use glass container** to measure out 5mL of replacement solution for specific well. Pour replacement solution into 15mL sample container with water removed from well during filling of 1/8" line. Label new 15mL container with well name and date.
9. Stop pump. Note time and mark on field data sheet.
10. Quickly pull out 1/8" line from shallow ¼" and place end of line in 5mL glass container
11. Reverse pump direction and pump on low setting until glass container is filled. Pour contents of glass container into labeled 15mL container
12. Stop pump and place end of 1/8" into 15mL container of replacement solution
13. Reverse pump and run on low until all replacement solution has been pumped down well
14. Reverse pump run on low until a very small amount of water comes out surface end of 1/8" (ensures line is completely filled with water).
15. Push 1/8" line back down shallow end of ¼"
16. Reverse pump and run for 30-40 minutes on medium-high setting. Note start time and mark on data sheet
17. Stop pump. Note time and mark on data sheet. Remove pump head and disassemble
18. Pull out one end of 1/8" line, coiling at the same time.
19. When end is at surface, tie wrap coil and allow line to drain
20. Slowly pull out other end of 1/8", coiling as you pull and tie wrapping when complete
21. Place 1/8" line in dedicated plastic bag for storage

APPENDIX B: RESULTS OF LABORATORY EXPERIMENTS

Table B-1. Measured deuterium values for laboratory cells.

Time	Cell 1		Cell 2		Cell 3		Cell 4		Cell 5		Cell 6	
(hours)	Source	Collection	Source	Collection	Source	Collection	Source	Collection	Source	Collection	Source	Collection
0	313	-163	300	-161	306	-160	309	-164	312	-162	296	-162
6	292	-161	296	-162	300	-158	271	-157	298	-161	290	-161
12	288	-159	285	-164	291	-157	278	-155	298	-159	285	-159
24	278	-159	284		285	-156	266	-152	286	-159	282	-159
36	270	-158	267	-159	276	-155	263	-155	275	-152	280	-158
48	257	-157	257	-150	264	-158	247	-154	263	-151	264	
60	253	-157	255	-158	259	-147	254	-150	267	-152	267	-157
69.5	251	-154	254	-155	258	-143	246	-151	254	-150	259	-156
97.5	235	-149	240	-153	245	-141	219	-149	249	-152	246	-154
117	230			-136	223	-143	237	-142		-142	216	-150
139.5	221	-142	225	-147	230	-134	212	-139	239	-149	229	-147
187.5	207	-130	211	-137	217	-123		-130	225	-137	213	-138
251.5	192	-117	197	-127	207	-112	191	-108	219	-126	204	-126
307.5	181	-105	186	-116	200	-102	172	-103	205	-132	211	-121
396	180	-73	166	-93	192	-82	163	-77	195	-99	202	-104
497	159	-55	157	-80	183	-67	164	-67	178	-80	173	-79
804	109	-22	106	-45	134	-31	115	-25	138	-51	137	-43
3017.5		23	12	6	49	41	32	23	31	16	25	14

Table B-2. Measured oxygen-18 values for laboratory cells.

Time	Cell 1		Cell 2		Cell 3		Cell 4		Cell 5		Cell 6	
(hours)	Source	Collection	Source	Collection	Source	Collection	Source	Collection	Source	Collection	Source	Collection
0	13.0	-20.7	11.9	-20.7	12.2	-20.7	11.9	-21.1	13.0	-21.2	11.8	-21.1
6	10.8	-20.5	11.4	-20.6	11.6	-20.3	9.8	-20.6	12.1	-20.6	11.4	-20.6
12	10.8	-20.6	10.8	-20.7	11.2	-20.1	10.2	-20.4	11.7	-20.5	11.3	-20.4
24	11.2	-20.5	11.4	-21.3	10.5	-19.9	9.3	-19.9	10.8	-20.3	10.1	-20.2
36	7.9	-20.4	10.4	-20.5	11.3	-19.9	9.5	-19.4	11.1	-19.7	11.0	-20.0
48	9.7	-20.2	9.6	-20.1	9.3	-19.6	9.1	-19.9	10.5	-20.0	10.1	-19.4
60	9.0	-19.9	9.6	-20.4	9.6	-18.8	9.4	-19.9	11.1	-19.5	10.4	-20.1
69.5	6.2	-19.4	8.7	-20.0	10.1	-18.8	8.3	-19.4	10.4	-19.6	9.6	-20.0
97.5	11.5	-20.5	2.8	-20.5	4.9	-19.1	5.4		7.8		8.5	-20.1
117	5.9	-20.8		-21.2	5.7	-20.3	5.3	-20.9	6.4	-20.0	6.4	-20.6
139.5	5.7		5.5	-21.8	6.1		5.2		6.9		6.6	
187.5	4.5	-19.9	4.4	-20.8	5.7	-19.6		-19.2	7.3	-20.7	5.6	-20.4
251.5	3.7	-19.2	4.2	-19.8	4.5	-18.0	3.4	-17.8	5.5	-19.6	4.9	-20.2
307.5	2.1	-18.4	4.4	-18.9	3.8	-17.9	2.5	-18.1	4.9	-18.7	4.6	-18.8
396	3.0	-14.8	2.4	-16.0	4.1	-15.0	2.0	-14.9	4.7	-16.3	5.1	-16.8
497	1.5	-13.6	1.8	-15.1	3.5	-14.0	2.0	-14.2	3.5	-15.0	3.0	-15.0
804	-2.0	-11.3	-1.9	-12.6	0.1	-11.5	-1.4	-11.2	0.7	-12.9	0.4	-12.4
3017.5		-9.1	-6.9	-9.5	-7.6	-7.5	-7.3	-8.3	-8.1	-8.5		-8.9

Table B-3. Measured oxygen-18 and deuterium values for laboratory control cell.

Time (hours)	δD (‰)	$\delta^{18}O$ (‰)
0	314	12.9
6	316	12.9
12	313	13.2
24	314	13.1
36		13.8
48	315	14.0
60	313	13.9
69.5		14.0
97.5	312	13.0
117		
139.5		12.0
187.5	312	12.4
251.5	312	12.8
307.5	313	12.3
396		
497	314	13.1
804		
3017.5	313	13.1

APPENDIX C: FIELD DIFFUSION AND WATER LEVEL RESULTS

Table C-1. Measured oxygen-18 and deuterium values for field diffusion well BD45-A.

		BD45-A	
Date	**Time**	**δ18O (‰)**	**δD (‰)**
11-Jul-01	12:45	16.94	452
12-Jul-01	9:55	3.61	238
13-Jul-01	11:30	2.8	226
15-Jul-01	7:40	1.57	208
19-Jul-01	7:45		181
22-Jul-01	12:45	-1.42	164
1-Aug-01	10:45	-3.87	128
8-Aug-01	10:45		107
22-Aug-01	10:15	-5.72	75
19-Sep-01	13:15	-10.66	-14
4-Oct-01	14:15		-32
18-Oct-01	16:10	-18.62	-40

Table C-2. Measured oxygen-18 and deuterium values for field diffusion well BD45-C.

Date	Time	BD45-C δ18O (‰)	BD45-C δD (‰)
3-Jul-01	14:30	8.18	261
4-Jul-01	12:45	4.1	220
5-Jul-01	6:30	3.53	209
8-Jul-01	11:35	2.53	178
11-Jul-01	12:15		160
15-Jul-01	7:30	-0.78	142
19-Jul-01	7:32		126
22-Jul-01	11:30	-1.64	114
1-Aug-01	10:57	-3.94	88
8-Aug-01	10:35		70
22-Aug-01	10:25	-7.25	37
19-Sep-01	14:45	-9.9	14
4-Oct-01	14:30		-2
18-Oct-01	16:30	-11.62	-31

Table C-3. Measured oxygen-18 values for field diffusion well BD45-B.

Date	δ18O (‰)
2-Nov-01	8.18
8-Nov-01	4.1
16-Nov-01	3.53
14-Jan-02	2.53
14-Jan-02	
15-Feb-02	-0.78
15-Feb-02	
2-Mar-02	-1.64
28-Mar-02	-3.94
5-Jun-02	
3-Jul-02	-7.25
8-Aug-02	-9.9
19-Sep-02	
1-Nov-02	-11.62
18-Dec-02	-11.62
3-Feb-03	-11.62
27-Feb-03	-11.62

Table C-4. Water level measurements for field diffusion wells BD45-A and -C prior to installation of packer systems.

Date	BD45A		BD45C	
	Water Depth (mbgs)	Water Elevation (masl)	Water Depth (mbgs)	Water Elevation (masl)
8/8/2001	15.585	560.838	13.443	562.958
8/22/2001	15.315	561.108	13.089	563.312
9/14/2001	14.795	561.628	12.297	564.104
9/14/2001	15.185	561.238	12.674	563.727
10/11/2001	14.53	561.893	11.919	564.482
10/11/2001	14.635	561.788	12.024	564.377
11/2/2001	14.132	562.291	11.377	565.024
11/2/2001	14.287	562.136	11.527	564.874
11/8/2001	14.149	562.274	11.339	565.062
11/16/2001	13.967	562.456	11.098	565.303
11/16/2001	13.973	562.45	11.104	565.297
12/6/2001	13.533	562.89	10.571	565.83
12/6/2001	13.536	562.887	10.581	565.82
1/14/2002	12.693	563.73	9.647	566.754
2/15/2002	12.056	564.367	8.96	567.441
3/28/2002	11.327	565.096	8.163	568.238
4/18/2002	11.008	565.415	7.787	568.614
5/8/2002	11.387	565.036	8.262	568.139
5/8/2002**	10.707	565.716	7.447	568.954

** water level after removing 2L of water.

Table C-5. Water level measurements for field diffusion well BD45-B.

Date	Water Depth (mbgs)	Water Elevation (masl)
8/8/2001	13.328	563056
8/22/2001	12.98	563.404
9/14/2001	12.243	564.141
9/14/2001	12.716	563.668
10/11/2001	11.82	564.564
10/11/2001	11.925	564.459
11/2/2001	11.188	565.196
11/2/2001	11.286	565.098
11/8/2001	11.088	565.296
11/8/2001	11.091	565.293
11/16/2001	10.828	565.556
11/16/2001	10.834	565.55
12/6/2001	10.219	566.165
12/6/2001	10.228	566.156
1/14/2002	9.089	567.295
2/15/2002	8.282	568.102
3/28/2002	7.377	569.007
4/18/2002	6.98	569.404
5/8/2002	6.625	569.759
5/8/2002	6.628	569.756
5/29/2002	6.293	570.091
5/29/2002	6.308	570.076
6/14/2002	6.065	570.309
7/3/2002	5.795	570.589
8/8/2002	5.341	571.043
8/8/2002	5.344	571.04
8/22/2002	5.192	571.192
9/19/2002	4.905	571.479
9/19/2002	4.903	571.481
11/1/2002	4.408	571.976
12/18/2002	4.048	572.336
2/3/2002	3.773	572.611
2/27/2003	3.638	572.746
6/20/2003	3.128	573.256

Table C-7. Transducer water level measurements for diffusion wells BD45-A and BD45-C.

Date	Time	BD45A	BD45C
		Water Level (mbgs)	
26-Jun-02	12:32	6.545	3.281
26-Jun-02	13:32	6.585	3.251
26-Jun-02	14:32	6.615	3.181
26-Jun-02	15:32	15.182	3.141
26-Jun-02	16:32	2.025	3.141
26-Jun-02	17:32	2.055	3.131
26-Jun-02	18:32	2.275	3.151
26-Jun-02	19:32	2.465	3.151
26-Jun-02	20:32	2.665	3.151
26-Jun-02	21:32	2.825	3.151
26-Jun-02	22:32	2.815	3.151
26-Jun-02	23:32	2.805	3.161
27-Jun-02	0:36:00	2.795	3.161
27-Jun-02	3:32	3.505	3.151
27-Jun-02	4:32	3.585	3.141
27-Jun-02	5:32	3.665	3.131
27-Jun-02	6:32	3.735	3.131
27-Jun-02	7:36	3.805	3.121
27-Jun-02	8:36	3.855	3.111
27-Jun-02	9:32	3.915	3.101
27-Jun-02	10:32	15.180	3.111
27-Jun-02	11:35	6.725	3.101
27-Jun-02	12:35	6.545	3.141
27-Jun-02	13:35	1.605	3.211
27-Jun-02	14:35	1.685	3.211
27-Jun-02	15:35	1.745	3.201
27-Jun-02	16:35	1.795	3.201
27-Jun-02	17:35	1.845	3.191
27-Jun-02	18:35	1.885	3.181
27-Jun-02	19:35	1.935	3.171
27-Jun-02	20:35	1.975	3.171
27-Jun-02	21:35	2.025	3.171
27-Jun-02	22:35	2.065	3.161
27-Jun-02	23:35	2.115	3.161
28-Jun-02	0:35:00	2.155	3.151
28-Jun-02	1:35	2.195	3.151
28-Jun-02	2:35	2.225	3.141
28-Jun-02	3:35	2.265	3.131
28-Jun-02	4:35	2.295	3.131
28-Jun-02	5:35	2.335	3.121
28-Jun-02	7:00	2.381	3.121
28-Jun-02	8:00	2.413	3.121
28-Jun-02	9:00	2.441	3.121
28-Jun-02	10:00	2.475	3.121
28-Jun-02	11:00	2.500	3.121
28-Jun-02	12:00	2.527	3.111
28-Jun-02	13:00	2.552	3.111
28-Jun-02	14:00	2.579	3.111

Date	Time	BD45A	BD45C
		Water Level (mbgs)	
28-Jun-02	15:00	2.600	3.111
28-Jun-02	16:00	2.628	3.106
28-Jun-02	17:00	2.648	3.102
28-Jun-02	18:00	2.669	3.098
28-Jun-02	19:00	2.697	3.092
28-Jun-02	20:00	2.714	3.085
28-Jun-02	21:00	2.732	3.082
28-Jun-02	22:00	2.753	3.075
28-Jun-02	23:00	2.770	3.071
29-Jun-02	0:00:00	2.791	3.064
29-Jun-02	1:00	2.808	3.058
29-Jun-02	2:00	2.825	3.060
29-Jun-02	3:00	2.847	3.054
29-Jun-02	4:00	2.862	3.052
29-Jun-02	5:00	2.873	3.045
29-Jun-02	6:00	2.890	3.041
29-Jun-02	7:00	2.904	3.035
29-Jun-02	8:00	2.916	3.030
29-Jun-02	9:00	2.930	3.019
29-Jun-02	10:00	2.936	3.012
29-Jun-02	11:00	2.954	3.005
29-Jun-02	12:00	2.968	3.005
29-Jun-02	13:00	2.972	2.996
29-Jun-02	14:00	2.986	2.993
29-Jun-02	15:00	2.996	2.986
29-Jun-02	16:00	3.006	2.979
29-Jun-02	17:00	3.010	2.975
29-Jun-02	18:00	3.020	2.968
29-Jun-02	19:00	3.027	2.962
29-Jun-02	20:00	3.034	2.958
29-Jun-02	21:00	3.039	2.955
29-Jun-02	22:00	3.054	2.950
29-Jun-02	23:00	3.061	2.947
30-Jun-02	0:00:00	3.065	2.940
30-Jun-02	1:00	3.065	2.940
30-Jun-02	2:00	3.075	2.929
30-Jun-02	3:00	3.082	2.926
30-Jun-02	4:00	3.086	2.923
30-Jun-02	5:00	3.093	2.926
30-Jun-02	6:00	3.102	2.924
30-Jun-02	7:00	3.100	2.920
30-Jun-02	8:00	3.103	2.912
30-Jun-02	9:00	3.113	2.905
30-Jun-02	10:00	3.117	2.902
30-Jun-02	11:00	3.113	2.895
30-Jun-02	12:00	3.121	2.893
30-Jun-02	13:00	3.121	2.889
30-Jun-02	14:00	3.124	2.885
30-Jun-02	15:00	3.128	2.879

Date	Time	BD45A	BD45C
		Water Level (mbgs)	
30-Jun-02	16:00	3.131	2.872
30-Jun-02	17:00	3.135	2.872
30-Jun-02	18:00	3.135	2.865
30-Jun-02	19:00	3.138	2.854
30-Jun-02	20:00	3.138	2.851
30-Jun-02	21:00	3.142	2.847
30-Jun-02	22:00	3.142	2.848
30-Jun-02	23:00	3.155	2.850
1-Jul-02	0:00:00	3.138	2.847
1-Jul-02	1:00	3.141	2.840
1-Jul-02	2:00	3.144	2.840
1-Jul-02	3:00	3.148	2.833
1-Jul-02	4:00	3.151	2.833
1-Jul-02	5:00	3.151	2.836
1-Jul-02	6:00	3.138	2.826
1-Jul-02	7:00	3.138	2.829
1-Jul-02	8:00	3.148	2.829
1-Jul-02	9:00	3.134	2.826
1-Jul-02	10:00	3.141	2.819
1-Jul-02	11:00	3.141	2.796
1-Jul-02	12:00	3.133	2.801
1-Jul-02	13:00	3.131	2.795
1-Jul-02	14:00	3.119	2.794
1-Jul-02	15:00	3.119	2.793
1-Jul-02	16:00	3.112	2.792
1-Jul-02	17:00	3.111	2.792
1-Jul-02	18:00	3.110	2.792
1-Jul-02	19:00	3.100	2.791
1-Jul-02	20:00	3.110	2.789
1-Jul-02	21:00	3.110	2.789
1-Jul-02	22:00	3.103	2.787
1-Jul-02	23:00	3.096	2.787
2-Jul-02	0:00:00	3.092	2.786
2-Jul-02	1:00	3.092	2.786
2-Jul-02	2:00	3.092	2.785
2-Jul-02	3:00	3.086	2.782
2-Jul-02	4:00	3.086	2.783
2-Jul-02	5:00	3.079	2.782
2-Jul-02	6:00	3.079	2.782
2-Jul-02	7:00	3.072	2.782
2-Jul-02	8:00	3.073	2.782
2-Jul-02	9:00	3.075	2.778
2-Jul-02	10:00	3.065	2.775
2-Jul-02	11:00	3.058	2.768
2-Jul-02	12:00	3.054	2.768
2-Jul-02	13:00	3.061	2.754
2-Jul-02	14:00	3.044	2.753
2-Jul-02	15:00	3.044	2.757
2-Jul-02	16:00	3.047	2.757

Date	Time	BD45A	BD45C
		Water Level (mbgs)	
2-Jul-02	17:00	3.040	2.757
2-Jul-02	18:00	3.030	2.750
2-Jul-02	19:00	3.027	2.753
2-Jul-02	20:00	3.027	2.757
2-Jul-02	21:00	3.023	2.757
2-Jul-02	22:00	3.027	2.760
2-Jul-02	23:00	3.013	2.757
3-Jul-02	1:13	3.285	2.756
3-Jul-02	2:38	3.425	2.755
3-Jul-02	4:02	3.545	2.751
3-Jul-02	5:02	3.625	2.743
3-Jul-02	6:02	3.695	2.742
3-Jul-02	7:08	3.775	2.743
3-Jul-02	8:08	3.835	2.741
3-Jul-02	9:08	3.895	2.733
3-Jul-02	10:08	3.945	2.732
3-Jul-02	12:32	6.545	2.738
3-Jul-02	13:32	6.585	0.811
3-Jul-02	14:32	6.615	2.740
3-Jul-02	15:32	15.182	2.737
3-Jul-02	16:32	2.025	2.737
3-Jul-02	17:32	2.055	2.735
3-Jul-02	18:32	2.275	2.737
3-Jul-02	19:32	2.465	2.740
3-Jul-02	20:32	2.665	2.737
3-Jul-02	21:32	2.825	2.737
3-Jul-02	22:32	2.965	2.736
3-Jul-02	23:32	3.095	2.739
4-Jul-02	0:36:00	3.215	2.737
4-Jul-02	1:32	3.285	2.737
4-Jul-02	2:32	3.425	2.736
4-Jul-02	3:32	3.505	2.737
4-Jul-02	4:32	3.585	2.751
4-Jul-02	5:32	3.665	2.753
4-Jul-02	6:32	3.735	2.753
4-Jul-02	7:36	3.805	2.757
4-Jul-02	8:36	3.855	2.756
4-Jul-02	9:32	3.915	2.756
4-Jul-02	10:32	15.180	3.481
4-Jul-02	11:35	6.725	2.755
4-Jul-02	12:35	6.545	4.811
4-Jul-02	13:35	1.605	2.754
4-Jul-02	14:35	1.685	2.761
4-Jul-02	15:35	1.745	2.778
4-Jul-02	16:35	1.795	2.777
4-Jul-02	17:35	1.845	2.777
4-Jul-02	18:35	1.885	2.773
4-Jul-02	19:35	1.935	2.767
4-Jul-02	20:35	1.975	2.758

Date	Time	BD45A	BD45C
		Water Level (mbgs)	
4-Jul-02	21:35	2.025	2.754
4-Jul-02	22:35	2.065	2.754
4-Jul-02	23:35	2.115	2.751
5-Jul-02	0:35:00	2.155	2.754
5-Jul-02	1:35	2.195	2.754
5-Jul-02	2:35	2.225	2.757
5-Jul-02	3:35	2.265	2.757
5-Jul-02	4:35	2.295	2.755
5-Jul-02	5:35	2.335	2.751
5-Jul-02	6:35	2.365	3.381
5-Jul-02	7:00	2.381	3.370
5-Jul-02	8:00	2.413	2.757
5-Jul-02	9:00	2.441	2.760
5-Jul-02	10:00	2.475	2.757
5-Jul-02	11:00	2.500	3.002
5-Jul-02	12:00	2.527	2.762
5-Jul-02	13:00	2.552	2.761
5-Jul-02	14:00	2.553	2.758
5-Jul-02	15:00	2.555	2.753
5-Jul-02	16:00	2.565	2.750
5-Jul-02	17:00	2.565	2.742
5-Jul-02	18:00	2.570	2.742
5-Jul-02	19:00	2.575	2.732
5-Jul-02	20:00	2.579	2.732
5-Jul-02	21:00	2.582	2.728
5-Jul-02	22:00	2.588	2.738
5-Jul-02	23:00	2.593	2.737
6-Jul-02	0:00:00	2.599	2.740
6-Jul-02	1:00	2.604	2.737
6-Jul-02	2:00	2.612	2.736
6-Jul-02	3:00	2.615	2.760
6-Jul-02	4:00	2.618	2.757
6-Jul-02	5:00	2.620	3.002
6-Jul-02	6:00	2.624	2.762
6-Jul-02	7:00	2.632	2.761
6-Jul-02	8:00	2.635	2.758
6-Jul-02	9:00	2.637	2.753
6-Jul-02	10:00	2.643	2.750
6-Jul-02	11:00	2.644	2.742
6-Jul-02	12:00	2.650	2.742
6-Jul-02	13:00	2.652	2.732
6-Jul-02	14:00	2.654	2.732
6-Jul-02	15:00	2.660	2.728
6-Jul-02	16:00	2.662	2.738
6-Jul-02	17:00	2.664	2.737
6-Jul-02	18:00	2.667	2.740
6-Jul-02	19:00	2.669	2.737
6-Jul-02	20:00	2.671	2.736
6-Jul-02	21:00	2.673	2.760

Date	Time	BD45A	BD45C
		Water Level (mbgs)	
6-Jul-02	22:00	2.677	2.757
6-Jul-02	23:00	2.680	3.002
7-Jul-02	0:00:00	2.682	2.762
7-Jul-02	1:00	2.684	2.761
7-Jul-02	2:00	2.686	2.758
7-Jul-02	3:00	2.688	2.753
7-Jul-02	4:00	2.690	2.750
7-Jul-02	5:00	2.695	2.742
7-Jul-02	6:00	2.696	2.742
7-Jul-02	7:00	2.699	2.732
7-Jul-02	8:00	2.702	2.732
7-Jul-02	9:00	2.704	2.728
7-Jul-02	10:00	2.711	2.738
7-Jul-02	11:00	2.715	2.737
7-Jul-02	12:00	2.719	2.740
7-Jul-02	13:00	2.722	2.737
7-Jul-02	14:00	2.726	2.736
7-Jul-02	15:00	2.729	2.760
7-Jul-02	16:00	2.732	2.757
7-Jul-02	17:00	2.735	3.002
7-Jul-02	18:00	2.737	2.762
7-Jul-02	19:00	2.739	2.761
7-Jul-02	20:00	2.742	2.758
7-Jul-02	21:00	2.745	2.753
7-Jul-02	22:00	2.749	2.750
7-Jul-02	23:00	2.751	2.742
8-Jul-02	0:00:00	2.752	2.742
8-Jul-02	1:00	2.755	2.732
8-Jul-02	2:00	2.756	2.732
8-Jul-02	3:00	2.758	2.728
8-Jul-02	4:00	2.760	2.738
8-Jul-02	5:00	2.762	2.737
8-Jul-02	6:00	2.764	2.740
8-Jul-02	7:00	2.768	2.737
8-Jul-02	8:00	2.770	2.736
8-Jul-02	9:00	2.772	2.737
8-Jul-02	10:00	2.775	2.740
8-Jul-02	11:00	2.776	3.801
8-Jul-02	12:00	2.777	2.736
8-Jul-02	13:00	2.778	2.737
8-Jul-02	14:00	2.780	2.731
8-Jul-02	15:00	2.782	2.721
8-Jul-02	16:00	2.785	2.711
8-Jul-02	17:00	2.787	2.692
8-Jul-02	18:00	2.789	2.695
8-Jul-02	19:00	2.791	2.720
8-Jul-02	20:00	2.793	2.757
8-Jul-02	21:00	2.794	2.791
8-Jul-02	22:00	2.797	2.815

Date	Time	BD45A	BD45C
		Water Level (mbgs)	
8-Jul-02	23:00	2.798	2.847
9-Jul-02	0:00:00	2.800	2.850
9-Jul-02	1:00	2.802	2.843
9-Jul-02	2:00	2.801	2.847
9-Jul-02	3:00	2.801	2.843
9-Jul-02	4:00	2.801	2.819
9-Jul-02	5:00	2.800	2.812
9-Jul-02	6:00	2.800	2.972
9-Jul-02	7:00	2.800	2.782
9-Jul-02	8:00	2.799	2.782
9-Jul-02	9:00	2.799	2.778
9-Jul-02	10:00	2.798	2.775
9-Jul-02	11:00	2.798	2.768
9-Jul-02	12:00	2.800	2.768
9-Jul-02	13:00	2.802	2.754
9-Jul-02	14:00	2.801	2.753
9-Jul-02	15:00	2.801	2.757
9-Jul-02	16:00	2.801	2.757
9-Jul-02	17:00	2.800	2.757
9-Jul-02	18:00	2.802	2.750
9-Jul-02	19:00	2.800	2.753
9-Jul-02	20:00	2.799	2.757
9-Jul-02	21:00	2.798	2.757
9-Jul-02	22:00	2.798	3.020
9-Jul-02	23:00	2.798	2.757
10-Jul-02	0:00:00	2.800	3.002
10-Jul-02	1:00	2.802	2.762
10-Jul-02	2:00	2.800	2.761
10-Jul-02	3:00	2.799	2.758
10-Jul-02	4:00	2.798	2.753
10-Jul-02	5:00	2.796	2.750
10-Jul-02	6:00	2.805	2.742
10-Jul-02	7:00	2.802	2.742
10-Jul-02	8:00	2.800	2.732
10-Jul-02	9:00	2.799	2.732
10-Jul-02	10:00	2.798	2.728
10-Jul-02	11:00	2.796	2.738
10-Jul-02	12:00	2.794	2.737
10-Jul-02	13:00	2.792	2.740
10-Jul-02	14:00	2.791	2.737
10-Jul-02	15:00	2.790	2.736
10-Jul-02	16:00	2.788	2.736
10-Jul-02	17:00	2.808	2.737
10-Jul-02	18:00	2.788	2.740
10-Jul-02	19:00	2.820	2.737
10-Jul-02	20:00	2.819	2.736
10-Jul-02	21:00	2.815	2.736
10-Jul-02	22:00	2.843	2.737
10-Jul-02	23:00	2.805	2.740

Date	Time	BD45A	BD45C
		Water Level (mbgs)	
11-Jul-02	0:00:00	2.802	2.737
11-Jul-02	1:00	2.800	2.736
11-Jul-02	2:00	2.799	2.736
11-Jul-02	3:00	2.798	2.754
11-Jul-02	4:00	2.800	2.753
11-Jul-02	5:00	2.800	2.757
11-Jul-02	6:00	2.800	2.757
11-Jul-02	7:00	2.800	2.757
11-Jul-02	8:00	2.799	2.754
11-Jul-02	9:00	2.798	2.753
11-Jul-02	10:00	2.796	2.757
11-Jul-02	11:00	2.811	2.757
11-Jul-02	12:00	2.805	2.757
11-Jul-02	13:00	2.790	2.778
11-Jul-02	14:00	2.788	2.778
11-Jul-02	15:00	2.808	2.778
11-Jul-02	16:00	2.800	2.775
11-Jul-02	17:00	2.799	2.768
11-Jul-02	18:00	2.798	2.761
11-Jul-02	19:00	2.796	2.754
11-Jul-02	20:00	2.805	2.758
11-Jul-02	21:00	2.802	2.747
11-Jul-02	22:00	2.800	2.754
11-Jul-02	23:00	2.799	2.753
12-Jul-02	0:00:00	2.798	2.757
12-Jul-02	1:00	2.796	2.757
12-Jul-02	2:00	2.794	2.757
12-Jul-02	3:00	2.792	2.750
12-Jul-02	4:00	2.791	2.753
12-Jul-02	5:00	2.790	2.757
12-Jul-02	6:00	2.788	2.757
12-Jul-02	7:00	2.808	2.760
12-Jul-02	8:00	2.807	2.757
12-Jul-02	9:00	2.806	3.002
12-Jul-02	10:00	3.493	2.762
12-Jul-02	11:00	2.806	2.761
12-Jul-02	12:00	2.791	2.758
12-Jul-02	13:00	2.791	2.753
12-Jul-02	14:00	2.790	2.750
12-Jul-02	15:00	2.790	2.742
12-Jul-02	16:00	2.789	2.742
12-Jul-02	17:00	2.785	2.732
12-Jul-02	18:00	2.785	2.732
12-Jul-02	19:00	2.782	2.728
12-Jul-02	20:00	2.792	2.738
12-Jul-02	21:00	2.791	2.737
12-Jul-02	22:00	2.794	2.740
12-Jul-02	23:00	2.791	2.737
13-Jul-02	0:00:00	2.790	2.736

Date	Time	BD45A	BD45C
		Water Level (mbgs)	
13-Jul-02	1:00	2.790	2.736
13-Jul-02	2:00	2.787	2.733
13-Jul-02	3:00	2.787	2.733
13-Jul-02	4:00	2.783	2.729
13-Jul-02	5:00	2.783	2.729
13-Jul-02	6:00	2.783	2.729
13-Jul-02	7:00	2.790	2.736
13-Jul-02	8:00	2.790	2.736
13-Jul-02	9:00	2.790	2.736
13-Jul-02	10:00	2.791	2.737
13-Jul-02	11:00	2.787	2.733
13-Jul-02	12:00	2.784	2.730
13-Jul-02	13:00	2.789	2.735
13-Jul-02	14:00	2.780	2.726
13-Jul-02	15:00	2.782	2.728
13-Jul-02	16:00	2.772	2.718
13-Jul-02	17:00	2.769	2.715
13-Jul-02	18:00	2.765	2.711
13-Jul-02	19:00	2.766	2.712
13-Jul-02	20:00	2.766	2.712
13-Jul-02	21:00	2.767	2.713
13-Jul-02	22:00	2.770	2.716
13-Jul-02	23:00	2.763	2.709
14-Jul-02	0:00:00	2.761	2.707
14-Jul-02	1:00	2.762	2.708
14-Jul-02	2:00	2.762	2.708
14-Jul-02	3:00	2.759	2.705
14-Jul-02	4:00	2.755	2.701
14-Jul-02	5:00	2.749	2.695
14-Jul-02	6:00	2.749	2.695
14-Jul-02	7:00	2.742	2.688
14-Jul-02	8:00	2.742	2.688
14-Jul-02	9:00	2.735	2.681
14-Jul-02	10:00	2.735	2.681
14-Jul-02	11:00	2.731	2.677
14-Jul-02	12:00	2.729	2.675
14-Jul-02	13:00	2.725	2.671
14-Jul-02	14:00	2.718	2.664
14-Jul-02	15:00	2.711	2.657
14-Jul-02	16:00	2.716	2.662
14-Jul-02	17:00	2.707	2.653
14-Jul-02	18:00	2.707	2.653
14-Jul-02	19:00	2.701	2.647
14-Jul-02	20:00	2.704	2.650
14-Jul-02	21:00	2.708	2.654
14-Jul-02	22:00	2.705	2.651
14-Jul-02	23:00	2.705	2.651
15-Jul-02	0:00:00	2.706	2.652
15-Jul-02	1:00	2.720	2.666

Date	Time	BD45A	BD45C
		Water Level (mbgs)	
15-Jul-02	2:00	2.731	2.677
15-Jul-02	3:00	2.717	2.663
15-Jul-02	4:00	2.714	2.660
15-Jul-02	5:00	2.724	2.670
15-Jul-02	6:00	2.724	2.670
15-Jul-02	7:00	2.963	2.909
15-Jul-02	8:00	2.811	2.757
15-Jul-02	9:00	2.807	2.753
15-Jul-02	10:00	2.803	2.749
15-Jul-02	11:00	2.801	2.747
15-Jul-02	12:00	2.794	2.740
15-Jul-02	13:00	2.791	2.737
15-Jul-02	14:00	2.791	2.737
15-Jul-02	15:00	2.786	2.732
15-Jul-02	16:00	2.782	2.728
15-Jul-02	17:00	2.780	2.726
15-Jul-02	18:00	2.777	2.723
15-Jul-02	19:00	2.777	2.723
15-Jul-02	20:00	2.775	2.721
15-Jul-02	21:00	2.777	2.723
15-Jul-02	22:00	2.777	2.723
15-Jul-02	23:00	2.774	2.720
16-Jul-02	0:00:00	2.776	2.722
16-Jul-02	1:00	2.776	2.722
16-Jul-02	2:00	2.773	2.719
16-Jul-02	3:00	2.776	2.722
16-Jul-02	4:00	2.776	2.722
16-Jul-02	5:00	2.783	2.729
16-Jul-02	6:00	2.776	2.722
16-Jul-02	7:00	2.776	2.722
16-Jul-02	8:00	2.773	2.719
16-Jul-02	9:00	2.776	2.722
16-Jul-02	10:00	2.767	2.713
16-Jul-02	11:00	2.760	2.706
16-Jul-02	12:00	2.760	2.706
16-Jul-02	13:00	2.752	2.698
16-Jul-02	14:00	2.750	2.696
16-Jul-02	15:00	2.749	2.695
16-Jul-02	16:00	2.744	2.690
16-Jul-02	17:00	2.741	2.687
16-Jul-02	18:00	2.745	2.691
16-Jul-02	19:00	2.746	2.692
16-Jul-02	20:00	2.753	2.699
16-Jul-02	21:00	2.760	2.706
16-Jul-02	22:00	2.756	2.702
16-Jul-02	23:00	2.757	2.703
17-Jul-02	0:00:00	2.754	2.700
17-Jul-02	1:00	2.755	2.701
17-Jul-02	2:00	2.752	2.698

Date	Time	BD45A	BD45C
		Water Level (mbgs)	
17-Jul-02	3:00	2.755	2.701
17-Jul-02	4:00	2.755	2.701
17-Jul-02	5:00	2.759	2.705
17-Jul-02	6:00	2.759	2.705
17-Jul-02	7:00	2.769	2.715
17-Jul-02	8:00	2.762	2.708
17-Jul-02	9:00	2.766	2.712
17-Jul-02	10:00	2.761	2.707
17-Jul-02	11:00	2.767	2.713
17-Jul-02	12:00	2.767	2.713
17-Jul-02	13:00	2.760	2.706
17-Jul-02	14:00	2.760	2.706
17-Jul-02	15:00	2.759	2.705
17-Jul-02	16:00	2.753	2.699
17-Jul-02	17:00	2.759	2.705
17-Jul-02	18:00	2.753	2.699
17-Jul-02	19:00	2.756	2.702
17-Jul-02	20:00	2.753	2.699
17-Jul-02	21:00	2.753	2.699
17-Jul-02	22:00	2.749	2.695
17-Jul-02	23:00	2.746	2.692
18-Jul-02	0:00:00	2.743	2.689
18-Jul-02	1:00	2.749	2.695
18-Jul-02	2:00	2.749	2.695
18-Jul-02	3:00	2.755	2.701
18-Jul-02	4:00	2.762	2.708
18-Jul-02	5:00	2.762	2.708
18-Jul-02	6:00	2.766	2.712
18-Jul-02	7:00	2.776	2.722
18-Jul-02	8:00	2.780	2.726
18-Jul-02	9:00	2.780	2.726
18-Jul-02	10:00	2.767	2.713
18-Jul-02	11:00	2.767	2.713
18-Jul-02	12:00	2.767	2.713
18-Jul-02	13:00	2.760	2.706
18-Jul-02	14:00	2.759	2.705
18-Jul-02	15:00	2.769	2.715
18-Jul-02	16:00	2.780	2.726
18-Jul-02	17:00	2.784	2.730
18-Jul-02	18:00	2.780	2.726
18-Jul-02	19:00	2.777	2.723
18-Jul-02	20:00	2.780	2.726
18-Jul-02	21:00	2.777	2.723
18-Jul-02	22:00	2.781	2.727
18-Jul-02	23:00	2.781	2.727
19-Jul-02	0:00:00	2.785	2.731
19-Jul-02	1:00	2.789	2.735
19-Jul-02	2:00	2.793	2.739
19-Jul-02	3:00	2.797	2.743

Date	Time	BD45A	BD45C
		Water Level (mbgs)	
19-Jul-02	4:00	2.800	2.746
19-Jul-02	5:00	2.800	2.746
19-Jul-02	6:00	2.732	2.750
19-Jul-02	7:00	2.732	3.075
19-Jul-02	8:00	2.732	2.746
19-Jul-02	9:00	2.732	2.750
19-Jul-02	15:00	2.732	2.716
19-Jul-02	21:00	2.732	2.699
20-Jul-02	3:00	2.732	2.691
20-Jul-02	9:00	2.732	2.695
20-Jul-02	15:00	2.732	2.695
20-Jul-02	21:00	2.732	2.695
21-Jul-02	3:00	2.732	2.692
21-Jul-02	9:00	2.732	2.682
21-Jul-02	15:00	2.732	2.670
21-Jul-02	21:00	2.732	2.685
22-Jul-02	3:00	2.732	2.682
22-Jul-02	9:00	2.732	2.690
22-Jul-02	15:00	2.732	2.689
22-Jul-02	21:00	2.732	2.688
23-Jul-02	3:00	2.732	2.688
23-Jul-02	9:00	2.732	2.688
23-Jul-02	15:00	2.732	2.691
23-Jul-02	21:00	2.732	2.688
24-Jul-02	3:00	2.732	2.688
24-Jul-02	9:00	2.732	2.688
24-Jul-02	15:00	2.732	2.691
24-Jul-02	21:00	2.732	2.691
25-Jul-02	3:00	2.732	2.691
25-Jul-02	9:00	2.732	2.691
25-Jul-02	15:00	2.732	2.690
25-Jul-02	21:00	2.732	2.690
26-Jul-02	3:00	2.732	2.691
26-Jul-02	9:00	2.732	2.690
26-Jul-02	15:00	2.732	2.690
26-Jul-02	21:00	2.732	2.690
27-Jul-02	3:00	2.732	2.691
27-Jul-02	9:00	2.732	2.694
27-Jul-02	15:00	2.732	2.694
27-Jul-02	21:00	2.732	2.694
28-Jul-02	3:00	2.732	2.694
28-Jul-02	9:00	2.732	2.694
28-Jul-02	15:00	2.732	2.695
28-Jul-02	21:00	2.732	2.694
29-Jul-02	3:00	2.732	2.695
29-Jul-02	9:00	2.732	2.695
29-Jul-02	15:00	2.732	2.695
29-Jul-02	21:00	2.732	2.694
30-Jul-02	3:00	2.732	2.695

Date	Time	BD45A	BD45C
		Water Level (mbgs)	
30-Jul-02	9:00	2.732	2.695
30-Jul-02	15:00	2.732	2.695
30-Jul-02	21:00	2.732	2.695
31-Jul-02	3:00	2.732	2.695
31-Jul-02	9:00	2.732	2.695
31-Jul-02	15:00	2.732	2.695
31-Jul-02	21:00	2.732	2.695
1-Aug-02	3:00	2.732	2.695
1-Aug-02	9:00	2.732	2.694
1-Aug-02	15:00	2.732	2.694
1-Aug-02	21:00	2.732	2.695
2-Aug-02	3:00	2.732	2.695
2-Aug-02	9:00	2.732	2.695
2-Aug-02	15:00	2.732	2.695
2-Aug-02	21:00	2.732	2.695
3-Aug-02	3:00	2.732	2.695
3-Aug-02	9:00	2.732	2.695
3-Aug-02	15:00	2.732	2.697
3-Aug-02	21:00	2.732	2.697
4-Aug-02	3:00	2.732	2.696
4-Aug-02	9:00	2.732	2.696
4-Aug-02	15:00	2.732	2.697
4-Aug-02	21:00	2.732	2.697
5-Aug-02	3:00	2.732	2.698
5-Aug-02	9:00	2.732	2.698
5-Aug-02	15:00	2.732	2.698
5-Aug-02	21:00	2.732	2.698
6-Aug-02	3:00	2.732	2.699
6-Aug-02	9:00	2.732	2.698
6-Aug-02	15:00	2.732	2.699
6-Aug-02	21:00	2.732	2.699
7-Aug-02	3:00	2.732	2.699
7-Aug-02	9:00	2.732	2.700
7-Aug-02	15:00	2.732	2.698
7-Aug-02	21:00	2.732	2.700
8-Aug-02	3:00	2.732	2.700
8-Aug-02	9:00	2.732	2.700
8-Aug-02	15:00	2.732	2.702
8-Aug-02	21:00	2.732	2.701
9-Aug-02	3:00	2.732	2.701
9-Aug-02	9:00	2.732	2.702
9-Aug-02	15:00	2.732	2.702
9-Aug-02	21:00	2.732	2.703
10-Aug-02	3:00	2.732	2.703
10-Aug-02	9:00	2.732	2.703
10-Aug-02	15:00	2.732	2.704
10-Aug-02	21:00	2.732	2.704
11-Aug-02	3:00	2.732	2.704
11-Aug-02	9:00	2.732	2.705

Date	Time	BD45A	BD45C
		Water Level (mbgs)	
11-Aug-02	15:00	2.732	2.705
11-Aug-02	21:00	2.732	2.705
12-Aug-02	3:00	2.732	2.705
12-Aug-02	9:00	2.732	2.701
12-Aug-02	15:00	2.732	2.705
12-Aug-02	21:00	2.732	2.706
13-Aug-02	3:00	2.732	2.706
13-Aug-02	9:00	2.732	2.706
13-Aug-02	15:00	2.732	2.706
13-Aug-02	21:00	2.732	2.707
14-Aug-02	3:00	2.732	2.706
14-Aug-02	9:00	2.732	2.707
14-Aug-02	15:00	2.732	2.707
14-Aug-02	21:00	2.732	2.707
15-Aug-02	3:00	2.732	2.708
15-Aug-02	9:00	2.732	2.708
15-Aug-02	15:00	2.732	2.709
15-Aug-02	21:00	2.732	2.708
16-Aug-02	3:00	2.732	2.708
16-Aug-02	9:00	2.732	2.709
16-Aug-02	15:00	2.732	2.709
16-Aug-02	21:00	2.732	2.710
17-Aug-02	3:00	2.732	2.710
17-Aug-02	9:00	2.732	2.709
17-Aug-02	15:00	2.732	2.710
17-Aug-02	21:00	2.732	2.711
18-Aug-02	3:00	2.732	2.711
18-Aug-02	9:00	2.732	2.711
18-Aug-02	15:00	2.732	2.710
18-Aug-02	21:00	2.732	2.711
19-Aug-02	3:00	2.732	2.712
19-Aug-02	9:00	2.732	2.712
19-Aug-02	15:00	2.732	2.713
19-Aug-02	21:00	2.732	2.712
20-Aug-02	3:00	2.732	2.713
20-Aug-02	9:00	2.732	2.714
20-Aug-02	15:00	2.732	2.714
20-Aug-02	21:00	2.732	2.714
21-Aug-02	3:00	2.732	2.715
21-Aug-02	9:00	2.732	2.715
21-Aug-02	15:00	2.732	2.715
21-Aug-02	21:00	2.732	2.715
22-Aug-02	3:00	2.732	2.714
22-Aug-02	9:00	2.732	2.714
22-Aug-02	15:00	2.732	2.714
22-Aug-02	21:00	2.732	2.715
23-Aug-02	3:00	2.732	2.716
23-Aug-02	9:00	2.732	2.715
23-Aug-02	15:00	2.732	2.716

Date	Time	BD45A	BD45C
		Water Level (mbgs)	
23-Aug-02	21:00	2.732	2.714
24-Aug-02	3:00	2.732	2.717
24-Aug-02	9:00	2.732	2.716
24-Aug-02	15:00	2.732	2.717
24-Aug-02	21:00	2.732	2.717
25-Aug-02	3:00	2.732	2.718
25-Aug-02	9:00	2.732	2.718
25-Aug-02	15:00	2.732	2.718
25-Aug-02	21:00	2.732	2.719
26-Aug-02	3:00	2.732	2.718
26-Aug-02	9:00	2.732	2.719
26-Aug-02	15:00	2.732	2.719
26-Aug-02	21:00	2.732	2.719
27-Aug-02	3:00	2.732	2.720
27-Aug-02	9:00	2.732	2.720
27-Aug-02	15:00	2.732	2.720
27-Aug-02	21:00	2.732	2.719
28-Aug-02	3:00	2.732	2.720
28-Aug-02	9:00	2.732	2.721
28-Aug-02	15:00	2.732	2.720
28-Aug-02	21:00	2.732	2.721
29-Aug-02	3:00	2.732	2.721
29-Aug-02	9:00	2.732	2.722
29-Aug-02	15:00	2.732	2.722
29-Aug-02	21:00	2.732	2.723
30-Aug-02	3:00	2.732	2.723
30-Aug-02	9:00	2.732	2.724
30-Aug-02	15:00	2.732	2.723
30-Aug-02	21:00	2.732	2.724
31-Aug-02	3:00	2.732	2.725
31-Aug-02	9:00	2.732	2.725
31-Aug-02	15:00	2.732	2.725
31-Aug-02	21:00	2.732	2.726
1-Sep-02	3:00	2.732	2.726
1-Sep-02	9:00	2.732	2.726
1-Sep-02	15:00	2.732	2.727
1-Sep-02	21:00	2.732	2.727
2-Sep-02	3:00	2.732	2.727
2-Sep-02	9:00	2.732	2.728
2-Sep-02	15:00	2.732	2.728
2-Sep-02	21:00	2.732	2.728
3-Sep-02	3:00	2.732	2.727
3-Sep-02	9:00	2.732	2.728
3-Sep-02	15:00	2.732	2.729
3-Sep-02	21:00	2.732	2.728
4-Sep-02	3:00	2.732	2.729
4-Sep-02	9:00	2.732	2.729
4-Sep-02	15:00	2.732	2.730
4-Sep-02	21:00	2.732	2.730

Date	Time	BD45A	BD45C
		Water Level (mbgs)	
5-Sep-02	3:00	2.732	2.731
5-Sep-02	9:00	2.732	2.731
5-Sep-02	15:00	2.732	2.732
5-Sep-02	21:00	2.732	2.732
6-Sep-02	3:00	2.732	2.733
6-Sep-02	9:00	2.732	2.733
6-Sep-02	15:00	2.732	2.733
6-Sep-02	21:00	2.732	2.734
7-Sep-02	3:00	2.732	2.734
7-Sep-02	9:00	2.732	2.734
7-Sep-02	15:00	2.732	2.735
7-Sep-02	21:00	2.732	2.735
8-Sep-02	3:00	2.732	2.735
8-Sep-02	9:00	2.732	2.736
8-Sep-02	15:00	2.732	2.736
8-Sep-02	21:00	2.732	2.736
9-Sep-02	3:00	2.732	2.737
9-Sep-02	9:00	2.732	2.736
9-Sep-02	15:00	2.732	2.738
9-Sep-02	21:00	2.732	2.738
10-Sep-02	3:00	2.732	2.737
10-Sep-02	9:00	2.732	2.738
10-Sep-02	15:00	2.732	2.739
10-Sep-02	21:00	2.732	2.739
11-Sep-02	3:00	2.732	2.739
11-Sep-02	9:00	2.732	2.740
11-Sep-02	15:00	2.732	2.740
11-Sep-02	21:00	2.732	2.739
12-Sep-02	3:00	2.732	2.740
12-Sep-02	9:00	2.732	2.741
12-Sep-02	15:00	2.732	2.741
12-Sep-02	21:00	2.732	2.741
13-Sep-02	3:00	2.732	2.742
13-Sep-02	9:00	2.732	2.741
13-Sep-02	15:00	2.732	2.742
13-Sep-02	21:00	2.732	2.743
14-Sep-02	3:00	2.732	2.743
14-Sep-02	9:00	2.732	2.744
14-Sep-02	15:00	2.732	2.742
14-Sep-02	21:00	2.732	2.744
15-Sep-02	3:00	2.732	2.744
15-Sep-02	9:00	2.732	2.745
15-Sep-02	15:00	2.732	2.745
15-Sep-02	21:00	2.732	2.747
16-Sep-02	3:00	2.732	2.746
16-Sep-02	9:00	2.732	2.747
16-Sep-02	15:00	2.732	2.747
16-Sep-02	21:00	2.732	2.748
17-Sep-02	3:00	2.732	2.748

Date	Time	BD45A	BD45C
		Water Level (mbgs)	
17-Sep-02	9:00	2.732	2.748
17-Sep-02	15:00	2.732	2.749
17-Sep-02	21:00	2.732	2.749
18-Sep-02	3:00	2.732	2.750
18-Sep-02	9:00	2.732	2.749
18-Sep-02	15:00	2.732	2.750
18-Sep-02	21:00	2.732	2.750
19-Sep-02	3:00	2.732	2.751
19-Sep-02	9:00	2.732	2.753
19-Sep-02	15:00	2.732	2.752
19-Sep-02	21:00	2.732	2.752
20-Sep-02	3:00	2.732	2.752
20-Sep-02	9:00	2.732	2.753
20-Sep-02	15:00	2.732	2.754
20-Sep-02	21:00	2.732	2.754
21-Sep-02	3:00	2.732	2.755
21-Sep-02	9:00	2.732	2.754
21-Sep-02	15:00	2.732	2.755
21-Sep-02	21:00	2.732	2.755
22-Sep-02	3:00	2.732	2.755
22-Sep-02	9:00	2.732	2.757
22-Sep-02	15:00	2.732	2.756
22-Sep-02	21:00	2.732	2.756
23-Sep-02	3:00	2.732	2.757
23-Sep-02	9:00	2.732	2.757
23-Sep-02	15:00	2.732	2.758
23-Sep-02	21:00	2.732	2.758
24-Sep-02	3:00	2.732	2.758
24-Sep-02	9:00	2.732	2.758
24-Sep-02	15:00	2.732	2.759
24-Sep-02	21:00	2.732	2.759
25-Sep-02	3:00	2.732	2.759
25-Sep-02	9:00	2.732	2.760
25-Sep-02	15:00	2.732	2.760
25-Sep-02	21:00	2.732	2.760
26-Sep-02	3:00	2.732	2.760
26-Sep-02	9:00	2.732	2.761
26-Sep-02	15:00	2.732	2.760
26-Sep-02	21:00	2.732	2.761
27-Sep-02	3:00	2.732	2.761
27-Sep-02	9:00	2.732	2.762
27-Sep-02	15:00	2.732	2.762
27-Sep-02	21:00	2.732	2.762
28-Sep-02	3:00	2.732	2.763
28-Sep-02	9:00	2.732	2.763
28-Sep-02	15:00	2.732	2.763
28-Sep-02	21:00	2.732	2.764
29-Sep-02	3:00	2.732	2.764
29-Sep-02	9:00	2.732	2.764

Date	Time	BD45A	BD45C
		Water Level (mbgs)	
29-Sep-02	15:00	2.732	2.764
29-Sep-02	21:00	2.732	2.765
30-Sep-02	3:00	2.732	2.765
30-Sep-02	9:00	2.732	2.766
30-Sep-02	15:00	2.732	2.766
30-Sep-02	21:00	2.732	2.765
1-Oct-02	3:00	2.732	2.766
1-Oct-02	9:00	2.732	2.767
1-Oct-02	15:00	2.732	2.767
1-Oct-02	21:00	2.732	2.767
2-Oct-02	3:00	2.732	2.767
2-Oct-02	9:00	2.732	2.767
2-Oct-02	15:00	2.732	2.768
2-Oct-02	21:00	2.732	2.769
3-Oct-02	3:00	2.732	2.769
3-Oct-02	9:00	2.732	2.768
3-Oct-02	15:00	2.732	2.769
3-Oct-02	21:00	2.732	2.769
4-Oct-02	3:00	2.732	2.770
4-Oct-02	9:00	2.732	2.770
4-Oct-02	15:00	2.732	2.770
4-Oct-02	21:00	2.732	2.771
5-Oct-02	3:00	2.732	2.771
5-Oct-02	9:00	2.732	2.772
5-Oct-02	15:00	2.732	2.771
5-Oct-02	21:00	2.732	2.772
6-Oct-02	3:00	2.732	2.773
6-Oct-02	9:00	2.732	2.772
6-Oct-02	15:00	2.732	2.773
6-Oct-02	21:00	2.732	2.773
7-Oct-02	3:00	2.732	2.774
7-Oct-02	9:00	2.732	2.773
7-Oct-02	15:00	2.732	2.774
7-Oct-02	21:00	2.732	2.774
8-Oct-02	3:00	2.732	2.775
8-Oct-02	9:00	2.732	2.775
8-Oct-02	15:00	2.732	2.775
8-Oct-02	21:00	2.732	2.776
9-Oct-02	3:00	2.732	2.776
9-Oct-02	9:00	2.732	2.776
9-Oct-02	15:00	2.732	2.776
9-Oct-02	21:00	2.732	2.777
10-Oct-02	3:00	2.732	2.777
10-Oct-02	9:00	2.732	2.777
10-Oct-02	15:00	2.732	2.778
10-Oct-02	21:00	2.732	2.778
11-Oct-02	3:00	2.732	2.779
11-Oct-02	9:00	2.732	2.779
11-Oct-02	15:00	2.732	2.779

Date	Time	BD45A	BD45C
		Water Level (mbgs)	
11-Oct-02	21:00	2.732	2.779
12-Oct-02	3:00	2.732	2.780
12-Oct-02	9:00	2.732	2.779
12-Oct-02	15:00	2.732	2.780
12-Oct-02	21:00	2.732	2.780
13-Oct-02	3:00	2.732	2.780
13-Oct-02	9:00	2.732	2.781
13-Oct-02	15:00	2.732	2.781
13-Oct-02	21:00	2.732	2.781
14-Oct-02	3:00	2.732	2.782
14-Oct-02	9:00	2.732	2.782
14-Oct-02	15:00	2.732	2.782
14-Oct-02	21:00	2.732	2.783
15-Oct-02	3:00	2.732	2.783
15-Oct-02	9:00	2.732	2.784
15-Oct-02	15:00	2.732	2.784
15-Oct-02	21:00	2.732	2.784
16-Oct-02	3:00	2.732	2.784
16-Oct-02	9:00	2.732	2.785
16-Oct-02	15:00	2.732	2.785
16-Oct-02	21:00	2.732	2.784
17-Oct-02	3:00	2.732	2.785
17-Oct-02	6:15	2.732	2.786
17-Oct-02	12:15	2.732	2.786
17-Oct-02	18:15	2.732	2.787
18-Oct-02	0:15	2.732	2.787
18-Oct-02	6:15	2.732	2.788
18-Oct-02	12:15	2.433	2.787
18-Oct-02	18:15	2.732	2.788
19-Oct-02	0:15	2.732	2.788
19-Oct-02	6:15	2.732	2.789
19-Oct-02	12:15	2.732	2.789
19-Oct-02	18:15	2.732	2.790
20-Oct-02	0:15	2.732	2.790
20-Oct-02	6:15	2.732	2.790
20-Oct-02	12:15	2.732	2.791
20-Oct-02	18:15	2.732	2.791
21-Oct-02	0:15	2.732	2.791
21-Oct-02	6:15	2.732	2.792
21-Oct-02	12:15	2.732	2.793
21-Oct-02	18:15	2.732	2.793
22-Oct-02	0:15	2.732	2.793
22-Oct-02	6:15	2.732	2.794
22-Oct-02	12:15	2.732	2.793
22-Oct-02	18:15	2.732	2.794
23-Oct-02	0:15	2.732	2.794
23-Oct-02	6:15	2.732	2.795
23-Oct-02	12:15	2.732	2.795
23-Oct-02	18:15	2.732	2.796

Date	Time	BD45A	BD45C
		Water Level (mbgs)	
24-Oct-02	0:15	2.732	2.796
24-Oct-02	6:15	2.732	2.797
24-Oct-02	12:15	2.732	2.797
24-Oct-02	18:15	2.732	2.796
25-Oct-02	0:15	2.732	2.797
25-Oct-02	6:15	2.732	2.798
25-Oct-02	12:15	2.732	2.798
25-Oct-02	18:15	2.732	2.799
26-Oct-02	0:15	2.732	2.800
26-Oct-02	6:15	2.732	2.800
26-Oct-02	12:15	2.732	2.800
26-Oct-02	18:15	2.732	2.800
27-Oct-02	0:15	2.732	2.802
27-Oct-02	6:15	2.732	2.801
27-Oct-02	12:15	2.732	2.802
27-Oct-02	18:15	2.732	2.801
28-Oct-02	0:15	2.732	2.802
28-Oct-02	6:15	2.732	2.803
28-Oct-02	12:15	2.732	2.803
28-Oct-02	18:15	2.732	2.803
29-Oct-02	0:15	2.732	2.804
29-Oct-02	6:15	2.732	2.804
29-Oct-02	12:15	2.732	2.805
29-Oct-02	18:15	2.732	2.805
30-Oct-02	0:15	2.732	2.806
30-Oct-02	6:15	2.732	2.806
30-Oct-02	12:15	2.732	2.807
30-Oct-02	18:15	2.732	2.807
31-Oct-02	0:15	2.732	2.808
31-Oct-02	6:15	2.732	2.809
31-Oct-02	12:15	2.732	2.808
31-Oct-02	18:15	2.732	2.809
1-Nov-02	0:15	2.732	2.810
1-Nov-02	6:15	2.732	2.810
1-Nov-02	12:15	2.732	2.810
1-Nov-02	18:15	2.732	2.810
2-Nov-02	0:15	2.732	2.810
2-Nov-02	6:15	2.732	2.811
2-Nov-02	12:15	2.732	2.811
2-Nov-02	18:15	2.732	2.809
3-Nov-02	0:15	2.732	2.809
3-Nov-02	6:15	2.732	2.809
3-Nov-02	12:15	2.732	2.810
3-Nov-02	18:15	2.732	2.809
4-Nov-02	0:15	2.732	2.809
4-Nov-02	6:15	2.732	2.808
4-Nov-02	12:15	2.732	2.808
4-Nov-02	18:15	2.732	2.808
5-Nov-02	0:15	2.732	2.807

Date	Time	BD45A	BD45C
		Water Level (mbgs)	
5-Nov-02	6:15	2.732	2.807
5-Nov-02	12:15	2.732	2.807
5-Nov-02	18:15	2.732	2.805
6-Nov-02	0:15	2.732	2.806
6-Nov-02	6:15	2.732	2.807
6-Nov-02	12:15	2.732	2.806
6-Nov-02	18:15	2.732	2.805
7-Nov-02	0:15	2.732	2.805
7-Nov-02	6:15	2.732	2.804
7-Nov-02	12:15	2.732	2.804
7-Nov-02	18:15	2.732	2.804
8-Nov-02	0:15	2.732	2.803
8-Nov-02	6:15	2.732	2.803
8-Nov-02	12:15	2.732	2.803
8-Nov-02	18:15	2.732	2.802
9-Nov-02	0:15	2.732	2.802
9-Nov-02	6:15	2.732	2.801
9-Nov-02	12:15	2.732	2.801
9-Nov-02	18:15	2.732	2.801
10-Nov-02	0:15	2.732	2.800
10-Nov-02	6:15	2.732	2.800
10-Nov-02	12:15	2.732	2.800
10-Nov-02	18:15	2.732	2.799
11-Nov-02	0:15	2.732	2.799
11-Nov-02	6:15	2.732	2.798
11-Nov-02	12:15	2.732	2.798
11-Nov-02	18:15	2.732	2.797
12-Nov-02	0:15	2.732	2.797
12-Nov-02	6:15	2.732	2.796
12-Nov-02	9:30	13.064	2.796
12-Nov-02	15:00	13.056	2.795
12-Nov-02	21:00	13.052	2.794
13-Nov-02	3:00	13.049	2.795
13-Nov-02	9:00	13.042	2.794
13-Nov-02	15:00	13.038	2.793
13-Nov-02	21:00	13.036	2.793
14-Nov-02	3:00	13.028	10.012
14-Nov-02	9:00	13.024	9.646
14-Nov-02	15:00	13.017	9.325
14-Nov-02	21:00	13.014	9.017
15-Nov-02	3:00	13.011	8.752
15-Nov-02	9:00	13.007	8.517
15-Nov-02	15:00	6.304	8.332
15-Nov-02	21:00	5.990	8.078
16-Nov-02	3:00	5.850	7.831
16-Nov-02	9:00	5.743	7.579
16-Nov-02	3:00	5.650	7.322
16-Nov-02	21:00	5.564	7.070
17-Nov-02	3:00	5.487	6.845

Date	Time	BD45A	BD45C
		Water Level (mbgs)	
17-Nov-02	9:00	5.414	6.647
17-Nov-02	15:00	5.347	6.508
17-Nov-02	21:00	5.278	6.350
18-Nov-02	3:00	5.220	6.181
18-Nov-02	9:00	5.157	6.015
18-Nov-02	15:00	5.101	5.859
18-Nov-02	21:00	5.045	5.710
19-Nov-02	3:00	4.989	5.561
19-Nov-02	9:00	4.943	5.419
19-Nov-02	15:00	4.895	5.291
19-Nov-02	21:00	4.855	5.179
20-Nov-02	3:00	4.815	5.053
20-Nov-02	9:00	4.772	4.930
20-Nov-02	15:00	4.735	4.821
20-Nov-02	21:00	4.704	4.728
21-Nov-02	3:00	4.669	4.624
21-Nov-02	9:00	4.642	4.510
21-Nov-02	15:00	4.607	4.376
21-Nov-02	21:00	4.569	4.241
22-Nov-02	3:00	4.534	4.120
22-Nov-02	9:00	4.509	4.067
22-Nov-02	15:00	4.485	4.029
22-Nov-02	21:00	4.457	3.971
23-Nov-02	3:00	4.433	3.912
23-Nov-02	9:00	4.409	3.867
23-Nov-02	15:00	4.381	3.805
23-Nov-02	21:00	4.356	3.753
24-Nov-02	3:00	4.339	3.694
24-Nov-02	9:00	4.311	3.629
24-Nov-02	15:00	4.291	3.542
24-Nov-02	21:00	4.256	3.439
25-Nov-02	3:00	4.235	3.366
25-Nov-02	9:00	4.225	3.387
25-Nov-02	15:00	4.207	3.390
25-Nov-02	21:00	4.193	3.363
26-Nov-02	3:00	4.180	3.308
26-Nov-02	9:00	4.169	3.245
26-Nov-02	15:00	4.145	3.169
26-Nov-02	21:00	4.131	3.111
27-Nov-02	3:00	4.115	3.067
27-Nov-02	9:00	4.110	3.048

APPENDIX D: ALTERNATE FIELD DIFFUSION EXPERIMENT

D1. Introduction

In the main body of this thesis, field diffusion testing was performed in two specially constructed wells (BD45-A and BD45-C) using packer systems to isolate a known volume of groundwater (reservoir) as well as circulate and sample that reservoir. In addition to these experiments, a second methodology was used to examine diffusion in a third well (BD45-B). This method required less equipment and maintenance than the other diffusion experiments, simply consisting of spiking the well and allowing the water level to recovery naturally.

D2. Materials and Methods

Construction and installation of BD45-B is described in Chapter 3 of the main body of this document. Dimensions are summarized in Figure D-1.

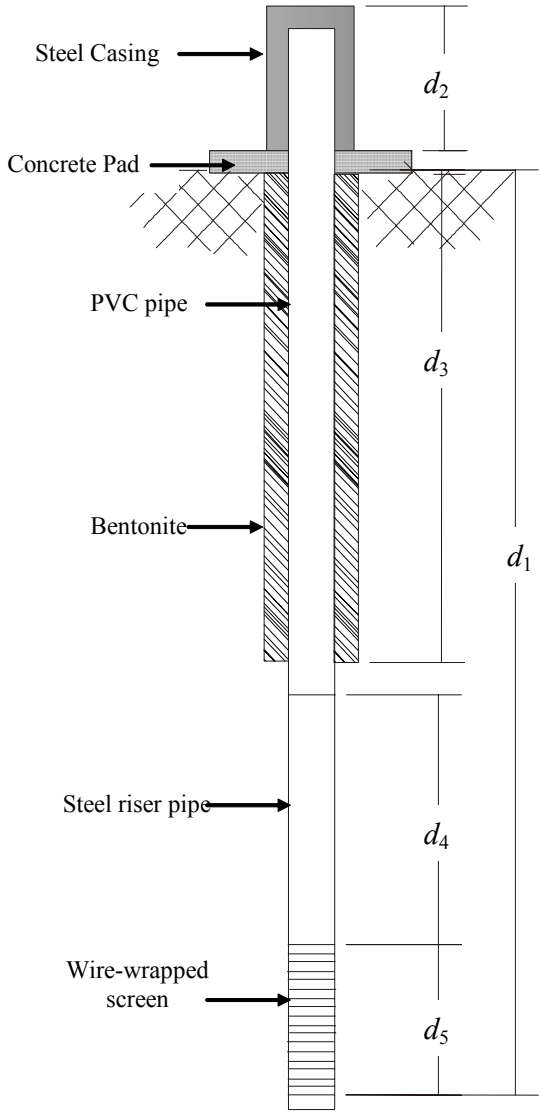

Dimension	Measurement (m) BD45-B
d_1	13.158
d_2	0.967
d_3	12.0
d_4	1.07
d_5	0.478

Figure D-1. Schematic of diffusion well BD45-B. Drawing not to scale.

After installation, monthly water-level recovery measurements were taken in the well using an electronic downhole tape measure. Water samples were also collected for background isotope (δD and $\delta^{18}O$) analyses on a monthly basis. Diffusion well BD45-B was allowed to recover until November 2, 2001. At this time, enough water was contained in the well to allow some water to be removed for use in laboratory diffusion testing while maintaining the groundwater level above the top of the screened intake zone. Approximately 4 L of water was removed and the diffusion well was spiked with ^{18}O (95 atom % ^{18}O, Aldrich Chemical Company).

Water samples were collected weekly for the following two weeks and then on a monthly basis until December of 2002. A final sample was collected in February of 2003. Water level measurements were obtained using an electronic downhole tape measure at each sampling incident.

Wells were sampled by lowering a 2 mL glass sample jar attached to a stiff wire into the standing water column. The jar was lowered to the mid-point of the screened intake zone and then brought up to surface and capped. Prior to sampling, the column of water in the well was mixed by raising and lowering a small fan. This was left at the bottom of the well throughout the experiment to avoid contamination of the water column.

D3. Results

The water level in the well increased approximately 8.9 m throughout the course of the experiment. Using this data, the hydraulic conductivity of the till was calculated to be 1.61×10^{-10} m/s. This value is in good agreement with other hydraulic

conductivity values determined for this site (as discussed in Chapter 5 of the main document).

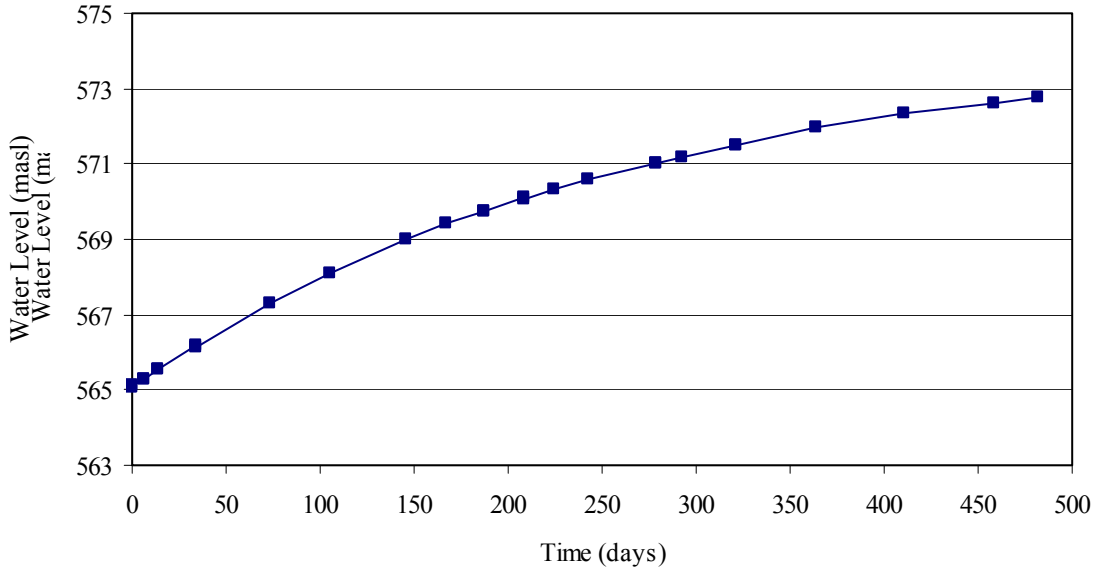

Figure D-2. Water level recovery data for BD45-B obtained using an electronic downhole tape measure.

$\delta^{18}O$ values in BD45-B decreased from a high of 7‰ at the time of spiking to a low of -15.99‰ on December 18, 2002. From this point, $\delta^{18}O$ values in the well began to rise to a high of -9.52‰ on February 27, 2003. Average background $\delta^{18}O$ is approximately -21.1 ± 0.6‰ for the formation (refer to Section 4.3.2 in main document).

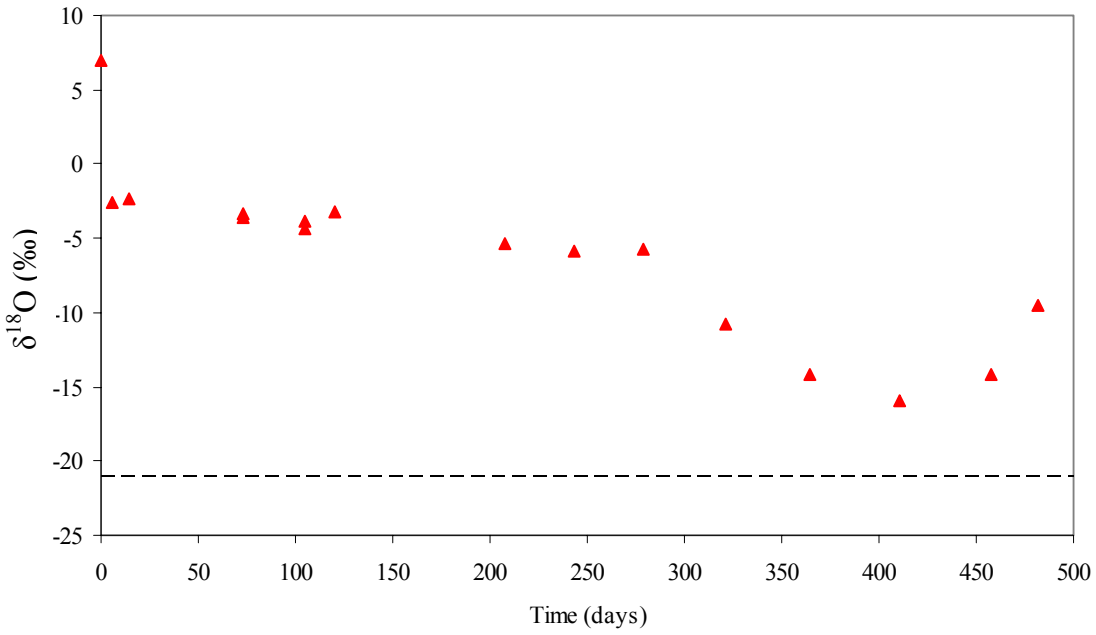

Figure D-3. Measured $\delta^{18}O$ values with time in diffusion well BD45-B. Dotted line indicates average $\delta^{18}O$ background values for the formation.

D4. Analysis and Discussion

Levels of $\delta^{18}O$ in the well were determined by advective movement of water into the well controlled by head gradients and diffusive movement of $\delta^{18}O$ from the well controlled by concentration gradients. The advective movement of water into the well would result in an effective decrease in $\delta^{18}O$ values through dilution of the well reservoir as well as cause $\delta^{18}O$ that has moved out of the well through diffusion to return to the well by the bulk flow of water. Diffusion would result in an effective decrease in $\delta^{18}O$ values through movement from the higher values in the well to lower background values in the surrounding pore water.

If advection of groundwater into the well did not occur, $\delta^{18}O$ values would have decreased at a rate equal to the diffusion rate. The hypothetical effects of dilution due

to advection were calculated by assuming all water entering the well was at the background $\delta^{18}O$ level of -21.1‰. The amount of water that entered the well was calculated from the measured water levels and the known dimensions of the well. Mixing this known amount of pore water at background $\delta^{18}O$ of -21.1‰ with the initial known volume of water spiked to 7‰ reveals $\delta^{18}O$ values that would result if only dilution due to advection was occurring.

The ratio of $^{18}O/^{16}O$ in a water sample can be calculated from the $\delta^{18}O$ of that sample and the $^{18}O/^{16}O$ of the reference standard (VSMOW) using:

$$R_{sample} = \left(\frac{\delta_{sample}}{1000} + 1 \right) R_{VSMOW} \qquad [A.1]$$

where: $R_{sample} = {}^{18}O/{}^{16}O$ in sample
$\delta_{sample} = \delta^{18}O$ for sample (‰)
$R_{VSMOW} = 2.005 \times 10\text{-}3$

The $^{18}O/^{16}O$ ratio of the water in the well that is produced as a result of mixing between the original spiked volume and the new porewater entering the well at background $\delta^{18}O$ can then be calculated using:

$$R_{mix} = \frac{\left(\left(R_{spike} * V_{spike} \right) + \left(R_{background} * V_{dilution} \right) \right)}{\left(V_{spike} + V_{dilution} \right)} \qquad [A.2]$$

This calculated R_{mix} can be expressed as a δ value by rearranging Eq.[A.1].

Values of $\delta^{18}O$ that would have theoretically been measured in the well if only dilution were occurring in the system are compared to the actual measured $\delta^{18}O$ values in Figure D-4. The difference between these two graphs represents the change in the $\delta^{18}O$ that is occurring in the system due to processes other than dilution.

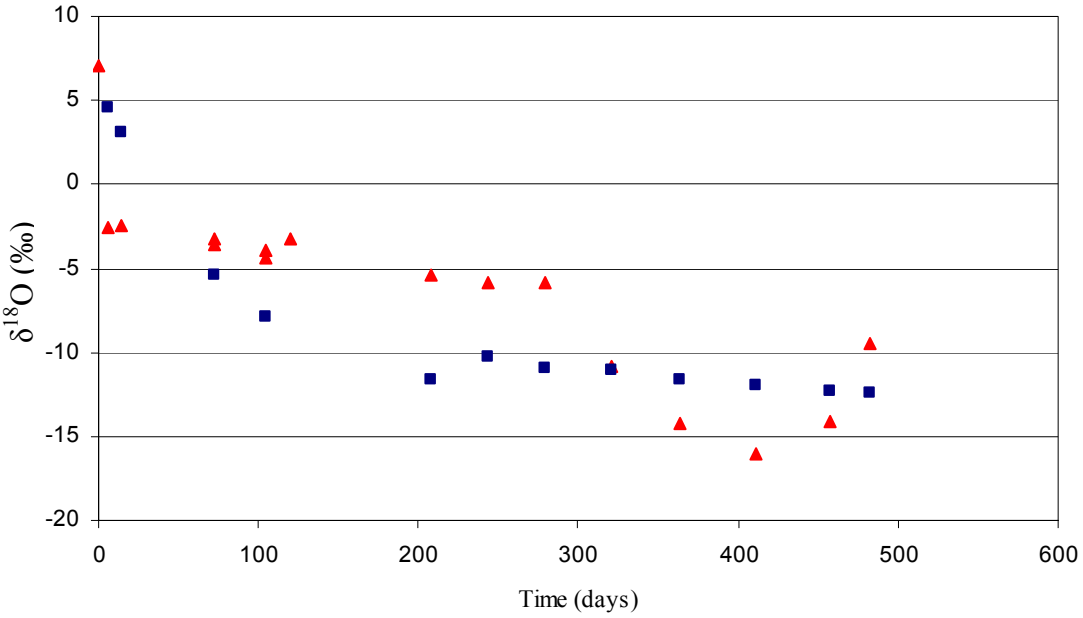

Figure D-4. Comparison of measured $\delta^{18}O$ and hypothetical $\delta^{18}O$ values calculated assuming only dilution due to advection is occurring in the well. Red triangles represent measured $\delta^{18}O$ values, calculated values are represented by blue squares.

Knowing the initial spiked $\delta^{18}O$ value, these calculated changes in $\delta^{18}O$ (see Table D-1) can be used to produce a data set that has been 'corrected' for the effects of dilution due to advection (Figure D-5).

Table D-1. Change in $\delta^{18}O$ values from the original spiked value attributed to processes other than dilution occurring in the system. The original spiked $\delta^{18}O$ value is taken as the value measured on 2 November 2001.

Date	$\delta^{18}O$ (‰ measured)	$\delta^{18}O$ (‰ calculated for dilution-only system)	Change in $\delta^{18}O$ due to other processes (‰)
2-Nov-01	7		
8-Nov-01	-2.6	4.55	5.05
16-Nov-01	-2.4	3.08	6.32
14-Jan-02	-3.3	-5.38	4.92
14-Jan-02	-3.6		
15-Feb-02	-3.9	-7.88	3.98
15-Feb-02	-4.4		
2-Mar-02	-3.2		
28-Mar-02			
29-May-02	-5.4	-11.60	6.20
5-Jun-02			
3-Jul-02	-5.9	-10.28	4.38
8-Aug-02	-5.8	-10.90	5.10
19-Sep-02	-10.8	-11.07	0.27
1-Nov-02	-14.21	-11.63	-2.58
18-Dec-02	-15.99	-12.00	-3.99
3-Feb-03	-14.12	-12.26	-1.86
27-Feb-03	-9.52	-12.38	2.86

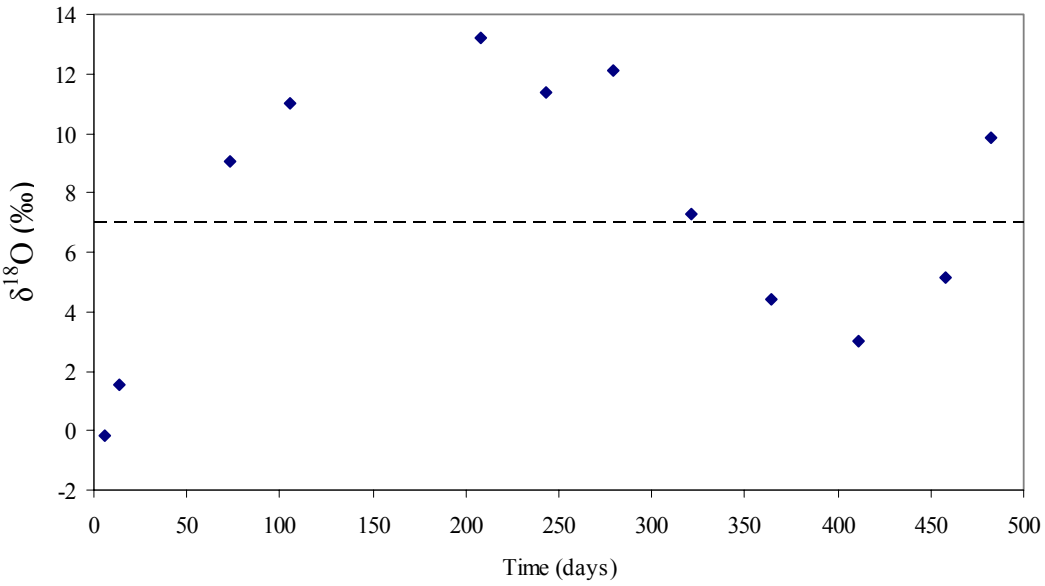

Figure D-5. Measured $\delta^{18}O$ values corrected for the effects of dilution due to advection of pore water into the well. Dotted line indicates initial $\delta^{18}O$ value of spiked reservoir.

Figure D-5 illustrates what the values measured in the diffusion well would be if no dilution was occurring through advection of water into the well. The calculated values increase from the initial spiked value of 7‰ to a high of 13.1‰ after 208 days, after which values display a decreasing trend to a low of 3.0‰ at 411 days. After this point, values again begin to increase.

The process of diffusion causes movement of molecules from an area of high concentration to an area at low concentration, or mixing between the isotopically-enriched spiked water contained in the well and the background pore water. Therefore, all values measured during the process of diffusion should fall between 7‰ and -21.1‰. Advective movement causing ^{18}O that has moved from the well due to diffusion to move back into the well would effectively slow the diffusion process, but this also only a process of mixing between the background groundwater and spiked well water. An increase in $\delta^{18}O$ values above the original spiked value (as shown between days 73 and 321 in Figure D-5) implies an isotopic enrichment process, such as evaporation, is occurring. The initial increase in $\delta^{18}O$ values occurs over a time period from November 2 to May 29, therefore it is unlikely that the increase can be attributed to evaporation. The second increase in $\delta^{18}O$ values that occurs at the end of the experiment (starting at day 411) also takes place during the winter months, beginning in December.

Another mechanism that could affect the isotopic signature of the water in the well would be the introduction of another water source. The most likely source of water would be leakage from the ground surface. The mean annual $\delta^{18}O$ of precipitation in the Saskatoon area is approximately -17‰. To explain the increase in

$\delta^{18}O$ above initial spiked values, this water source would have to have a $\delta^{18}O$ level above the highest level determined in the well (13.2‰), therefore leakage from surface is not a probable explanation.

Over-estimating the amount of dilution occurring in the well could also result in a perceived enrichment in ^{18}O caused by other transport and/ or mixing processes. Water level measurements (Figure D-2) do not show any obvious anomalies, indicating this is an unlikely explanation.

D5. Summary and Conclusions

A simple field test to measure the diffusion of a conservative isotope of water in till was attempted. Well BD45-A was allowed to recover until the water level was above the screened intake zone. The well was then spiked with water isotopically enriched with respect to ^{18}O. Water levels and samples for isotopic analysis were obtained periodically to monitor the water level recovery and the change in $\delta^{18}O$ with time in the well.

Water level measurements were used to calculate the change in volume in the well with time. From this, the effect of dilution due to advective groundwater movement into the well on the $\delta^{18}O$ level in the well could be determined. Hypothetically, any change in $\delta^{18}O$ that could not be attributed to dilution should be due to other transport processes, such as diffusion, occurring.

Correction of the $\delta^{18}O$ results for the effects of dilution revealed fluctuations in the $\delta^{18}O$ values in the well rather than a decrease in values that could be attributed to a transport or mixing process. Values of $\delta^{18}O$ greater than the initial spiked level of 7‰ were calculated. These values could not be attributed to evaporative enrichment or

mixing with more enriched waters. An overestimation of the effects of dilution was also considered to be an unlikely explanation.

This method of diffusion testing required a minimal amount of equipment. Results indicate the system was not constrained well enough to provide an estimate of the diffusion rate.